The Gimballed Helicopter Testbed: Design, Build and Validation

by

Charles Lidstone

A thesis submitted in conformity with the requirements
for the degree of Master of Applied Science
Department of Electrical and Computer Engineering
University of Toronto

© Copyright Charles Lidstone 2003

Abstract

To facilitate the development of an autonomous robot helicopter, an indoor helicopter flight test apparatus has been designed, built and validated. The design is motivated by a brief discussion of helicopter dynamics. Several options for the apparatus are considered and a detailed specification is laid out. Key design considerations are discussed in detail and the final design for the gimbal test stand is presented. Associated equipment is described and a manual for the operation of the stand is appended. To validate the capabilities of the test stand a system identification experiment was performed repeatedly. The consistency of the model extracted indicates that the entire system is reliable and accurate.

Acknowledgements

I must acknowledge the help of many people who contributed to this work.

I would like to extend my thanks to Prof. Ted Davison who has given me much encouragement and guidance, to Dr. Scott Bortoff who formulated the initial plan, to Prof. Bruce Francis who provided help at an important time and to the Electrical Engineering department for its support.

I need to especially thank Cameron Kerr who contributed great practical insight and drafting skill. Without his help, this project would not have been possible.

I would also like to express my gratitude to the Machine Tool Lab in the Department of Mechanical Engineering and ISO-Lux Manufacturing Co. for their quality workmanship.

Finally, I must convey my appreciation to Atsuhiko Sakurai, Suneil Sastri and all of the students at the Systems Control Group.

Table of Content

List of Figures

List of Tables

List of Symbols

a	Control pitch mixing coefficient
b	Flybar mixing coefficient
c	Blade cord length
c_d	Blade drag coefficient
c_l	Blade lift coefficient
$\mathbf{f}_{body}$	Total aerodynamic force on the fuselage
F_T	Blade element aerodynamic force tangent to blade rotation
F_z	Blade element vertical aerodynamic force
g	Acceleration of gravity
$\mathbf{g}_{body}$	Total aerodynamic torque on the fuselage
h	Mast height (from centre of gravity to main rotor hub)
H	Forward force developed by the main rotor and applied to the helicopter at the hub
$\hat{\hat{I}}$	Helicopter's moment of inertia
I_b	Blade moment of inertia about the flap hinge
l_{tr}	Boom length (from centre of gravity to tail rotor hub)
M	Helicopter mass
$M_{\dot{\beta}}$	Flap moment due to flapping velocity
M_θ	Flap moment due to control pitch
M_λ	Flap moment due to inflow
M_y	Pitch moment developed by the main rotor and applied to the helicopter at the hub
M_x	Roll moment developed by the main rotor and applied to the helicopter at the hub
N	Number of rotor blades
Q	Torque required to rotate the main rotor
R	Rotor radius, or blade length
r_{cg}	Distance from centre of gravity to axis of rotation
${}^W R_B$	The rotation matrix, which transforms a vector in the Body CS to the World CS
T	Vertical force developed by the main rotor and applied to the helicopter at the main rotor hub, or main rotor thrust
T_{tr}	Tail rotor thrust
$\mathbf{v}_{air}$	Total air velocity in the plane of the blade cross section
x_B	Helicopter position, x-coordinate in Body CS
$\dot{\mathbf{x}}_B$	Helicopter velocity
$\ddot{\mathbf{x}}_B$	Helicopter acceleration
${}^B\mathbf{x}_B$	Helicopter position expressed in the Body CS
y_B	Helicopter position, y-coordinate in Body CS
${}^P\hat{\mathbf{y}}_P$	Pitch CS y-axis unit vector, expressed in the Pitch CS

Y	Lateral force developed by the main rotor and applied to the helicopter at the main rotor hub
z_B	Helicopter position, z-coordinate in Body CS
${}^{Y}\hat{\mathbf{z}}_{Y}$	Yaw CS z-axis unit vector, expressed in the Yaw CS
α	Blade angle of attack
β	Blade flap angle
$\dot{\beta}$	Blade flap rate
$\ddot{\beta}$	Blade flap acceleration
β_0	Blade conning angle
β_{1c}	Peak longitudinal blade flap angle
β_{1s}	Peak lateral blade flap angle
β^{fly}	Flybar flap angle
β_{1c}^{fly}	Peak longitudinal flybar flap angle
β_{1s}^{fly}	Peak lateral flybar flap angle
θ	Control pitch angle
θ_0	Collective pitch control
θ_{1c}	Longitudinal cyclic pitch control
θ_{1s}	Lateral cyclic pitch control
θ_B	Pitch of the Body CS relative to the World CS
θ_P	Pitch joint angle
$\dot{\theta}_P$	Pitch joint rate
θ_R	Roll joint angle
$\dot{\theta}_R$	Roll joint rate
θ_Y	Yaw joint angle
$\dot{\theta}_Y$	Yaw joint rate
ρ	Air density
λ	Rotor inflow ratio
ϕ_B	Roll of the Body CS relative to the World CS
τ_b	Torque due to imbalance
ψ	Blade azimuth
ψ_B	Yaw of the Body CS relative to the World CS
$\boldsymbol{\omega}_B$	Helicopter attitude rate
$\dot{\boldsymbol{\omega}}_B$	Helicopter attitude acceleration
${}^{B}\boldsymbol{\omega}_B$	Helicopter attitude rate
${}^{B}\omega_x$	Helicopter roll rate
${}^{B}\omega_y$	Helicopter pitch rate
${}^{B}\omega_z$	Helicopter yaw rate
Ω	Rate of rotation of the rotor

Chapter 1

Introduction

Full authority autopilots for fixed wing aircraft have been in use for decades but few, if any, exist for helicopters. Helicopters are complex dynamic systems, which exhibit a high degree of non-linearity and strong coupling between states. These properties have precluded the development of a full authority autopilot. However, with modern control and modelling techniques, a safe and effective autopilot for helicopters should soon be within reach.

Remote control (RC) helicopters from the hobby industry have become highly sophisticated since their beginning 20 years ago. Their low cost, small size and relatively easy maintenance make them the ideal vehicles for developing and testing control strategies. While there are some significant differences between RC helicopters and their full size counterparts [1] [2], modelling and control of RC helicopters should provide significant insight to the full size helicopter control problem. Regardless of the applicability to full sized helicopters, RC helicopters are a particularly challenging plant for control systems design. To this end, RC helicopters have been the subject of substantial interest from research groups around the world [2]-[7].

For the last few years, the Systems Control Group at the University of Toronto has been developing an autonomous robot helicopter. The robot is based on a TSK MyStar60 helicopter from the RC hobby industry. The purpose of the project is to research applied nonlinear control and trajectory planning/tracking [1]. To support these goals, significant effort will be required in many related areas. In particular, position sensing and system integration will be key to the robot's performance. Each of these areas requires extensive research and many hours of experimentation.

It is possible to carry out experiments on a RC helicopter in free flight. However, free flight operation has several limitations. First, free flight operation must take place outdoors because of safety considerations. This significantly limits operation time due to weather conditions. Second, free flight operation requires a skilled pilot at all times. However, even with a skilled pilot, crashes in free flight are unavoidable. This causes significant down time for maintenance. In addition, nitro-methane engines, normally used on RC helicopters in free flight, require more maintenance than electric motors. Electric motors are practical only in constrained flight. Clearly, free flight operation poses several problems for an intensive research effort.

The alternative is to carry out experiments on a RC helicopter constrained to a test stand. This method of operation specifically addresses all of the problems mentioned above. Constrained operation also has significant advantages. First, a test stand can be used for the development of position sensors. Position sensing capability is needed for both free flight and constrained operation. Free flight operation requires sophisticated wireless position sensing capability. The development of suitable position sensors for the autonomous robot helicopter is an ongoing area of research [8]. However, in constrained operation, position sensing can be provided through direct mechanical measurement.

Hence, a test stand can also facilitate the development, calibration and performance evaluation of sophisticated position sensors for use in free flight. Finally, a test stand is also an excellent verification tool to ensure that all onboard systems are robust to the harsh, vibrating and accelerating environment of the helicopter.

This work documents the development, construction and validation of the Gimbal Test Stand and its associated hardware. The Gimbal Test Stand constrains the motion of an RC helicopter to attitude degrees of freedom only, allowing safe indoor operation. This eliminates dependence on weather conditions and pilot skill. The Gimbal Test Stand also provides optical encoders to directly measure the helicopters attitude.

In order to clearly understand the physical requirements for the test stand, an introduction to helicopter flight dynamics is given in Chapter 2. In Chapter 3, several test stand configurations are considered. The physical interaction of the Gimbal Test Stand with a helicopter is studied, and a candidate design is selected. Chapter 3 concludes with a detailed specification for the completion of the candidate design. Chapter 4 is a brief review of key design decisions made during the stands construction. Chapter 4 also includes some information about additional components that may add useful functionality to the stand. All of the systems associated with operation of the test stand are described in Chapter 5. This includes the helicopter, its onboard power plant and actuation system, and the data acquisition system, which reads the sensors and transmits commands to the helicopter. Chapter 6 documents some simple identification experiments performed to demonstrate the capabilities of the system as a whole. The consistent results show that the system will provide reliable data for a wide range of possible experiments. Finally, Chapter 7 suggests some experiments, which may be of interest along with many possible improvements to the test stand.

Chapter 2

Background

This chapter gives a qualitative introduction to the very intricate field of helicopter theory. Most of the dominant control systems related effects will be reviewed, but this is in no way a complete discussion. This section is designed to be an aid when first reviewing any of the standard texts on helicopter flight, [9] [10].

The chapter begins with an introduction to helicopters, how they fly, and how they are controlled. Next, a sketch of the development of the helicopter equations of motion is presented and discussed. The chapter concludes with a discussion of the major differences between RC helicopters and their full sized helicopters.

2.1 Rotor Configuration

Helicopters are aircraft, which use rotating wings to provide lift, directional control, and propulsion. The rotating wings, or blades, are arranged in rotors. Traditional helicopters use a single main rotor and a smaller tail rotor.

The main rotor is powered by an engine, which imparts torque to the rotors hub. Torque applied in this way must be countered, or the entire vehicle would rotate under the imbalance. In the traditional helicopter configuration the tail rotor provides the counter torque. Occasionally two counter rotating rotors are used to balance torque, and even more exotic configurations exist. Only the traditional configuration will be considered here.

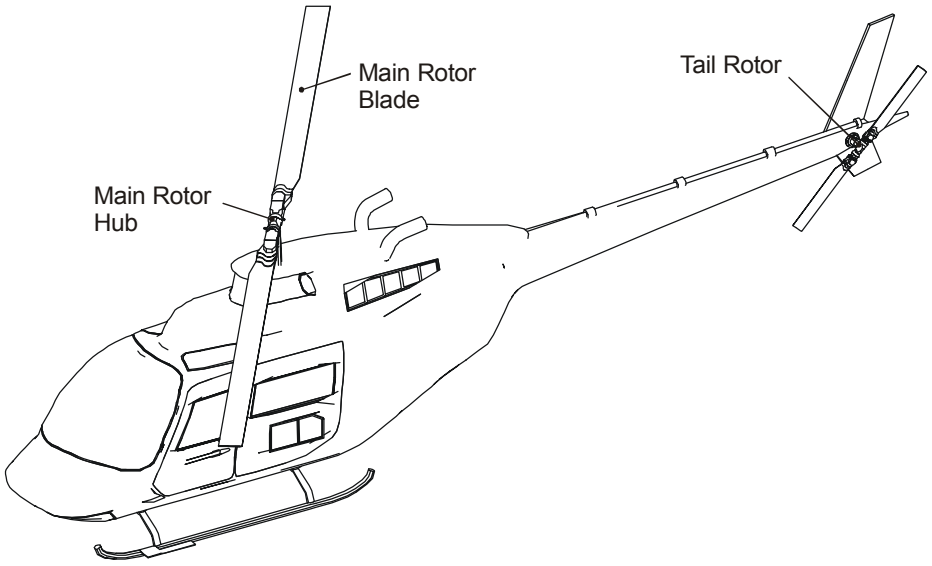

Figure 1: Traditional helicopter configuration

The traditional configuration is further subdivided based on the structure of the main rotor. Rotor blades are subject to large structural stresses due to the lift they generate. Blades are either hinged, or are designed to be flexible, to reduce the stresses. This results in three categories of traditional helicopter. Articulated rotor helicopters with independent flap and lag hinges on each blade. Teetering rotor helicopters with two blades rigidly connected to each other, and connected to the hub through a shared flap hinge. And hingeless rotor helicopters with flexible blades. All three types of rotor have feathering hinges, which allow the pitch of the blades to be varied.

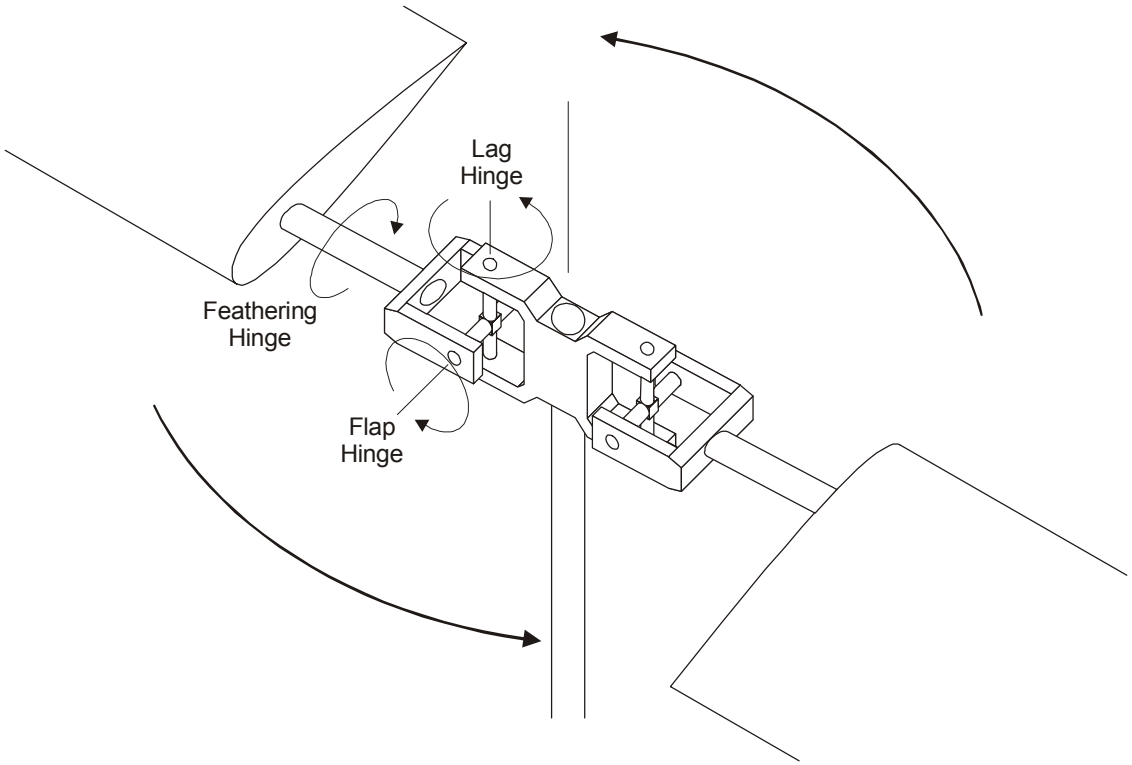

Figure 2: Rotor with flap feathering and lag hinges

While the controls on these three types are the same, the flight characteristics can vary significantly. The discussion that follows will focus on the articulated rotor; key characteristics of the hingeless rotor will also be mentioned.

2.2 Mode of Flight

Helicopters fly by balancing on the thrust of the main rotor. If the thrust vector is tilted, the helicopter will accelerate in the opposite direction. If the magnitude is increased, the acceleration will increase.

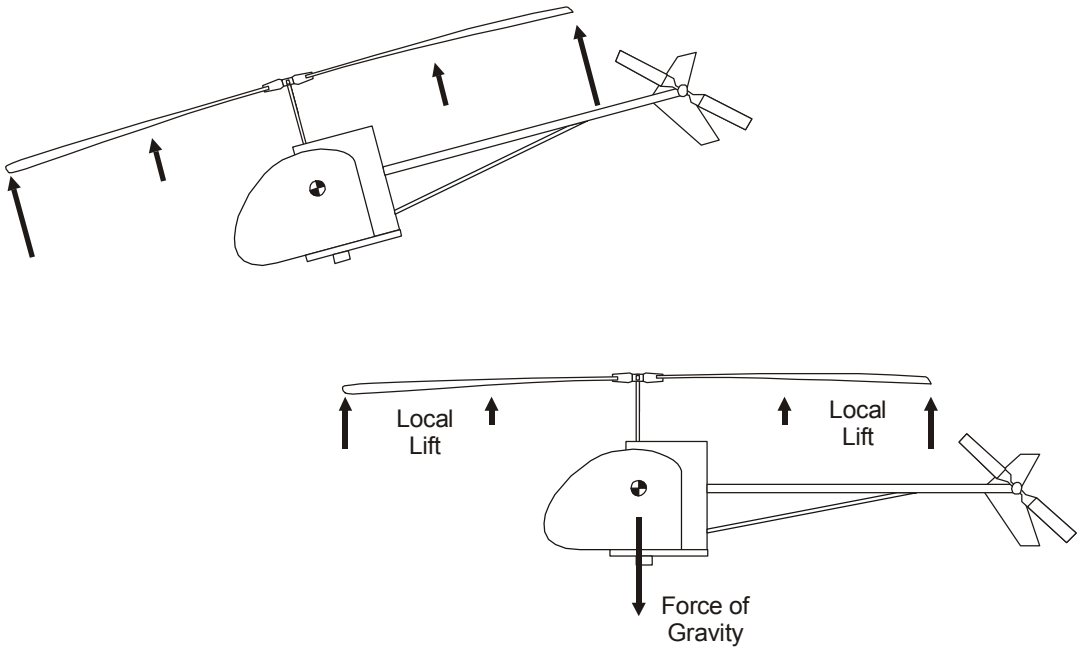

Figure 3: Helicopter balancing on thrust vector

In this way a helicopter can maintain a fixed position in the air opposing gravity with its thrust, or accelerate to fairly high-speed forward flight by tilting the thrust vector back.

The thrust vector is essentially perpendicular to the plane of the main rotor disc[1,2], so flight can be controlled by tilting the main rotor. Rotor tilt is brought about by allowing the blades to flap in a periodic motion about their flap hinges, with a frequency of one cycle per revolution.

[1] The path traced out by the blade tips defines the plane of the main rotor disc.

[2] In forward flight, main rotor thrust is deflected ½° to 1° from perpendicular; the tilt is proportional to forward speed. Pg. 178, [9]

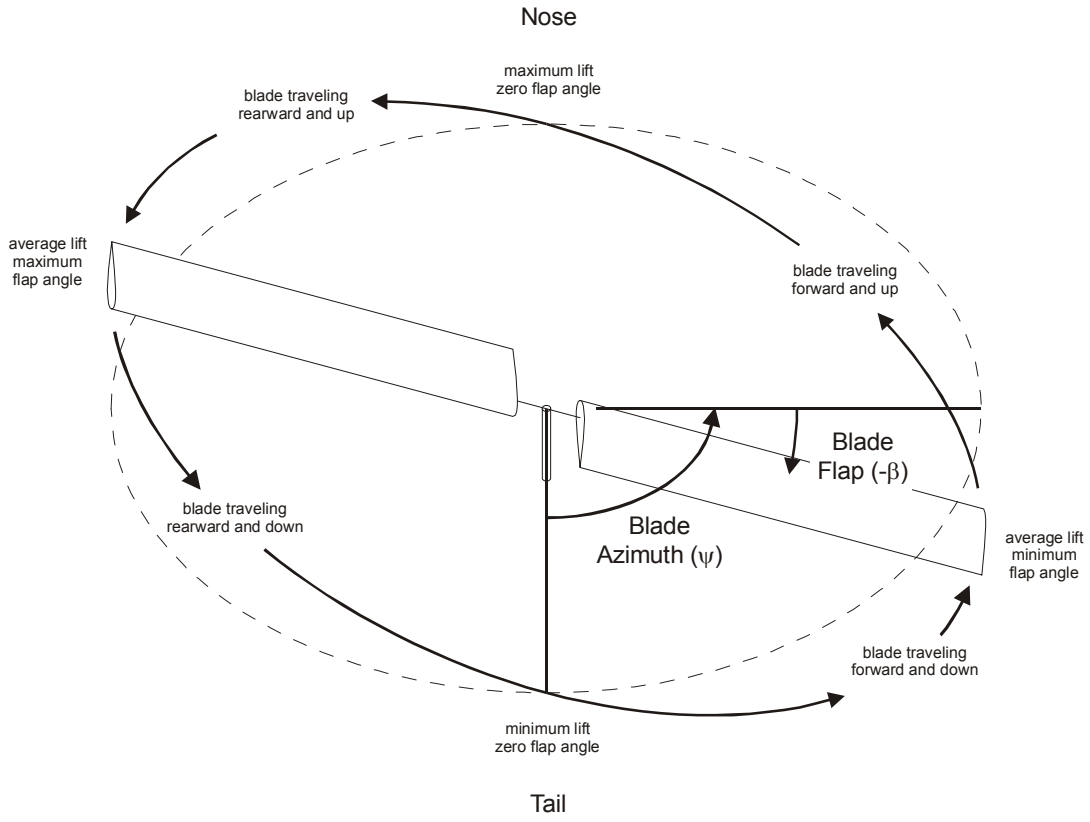

Figure 4: Periodic blade flapping due to longitudinal cyclic pitch input

Flapping can be induced by periodic variation in lift as a function of azimuth. The mechanism for controlling blade lift, and inducing flapping, will be discussed in Section 2.3. Flapping is also caused by local variation in airspeed, and hence lift, which occurs in forward flight. The airspeed of a blade approaching the direction of travel is increased by the helicopter's speed. The airspeed of a blade retreating from the direction of travel is decreased by the helicopter's speed.

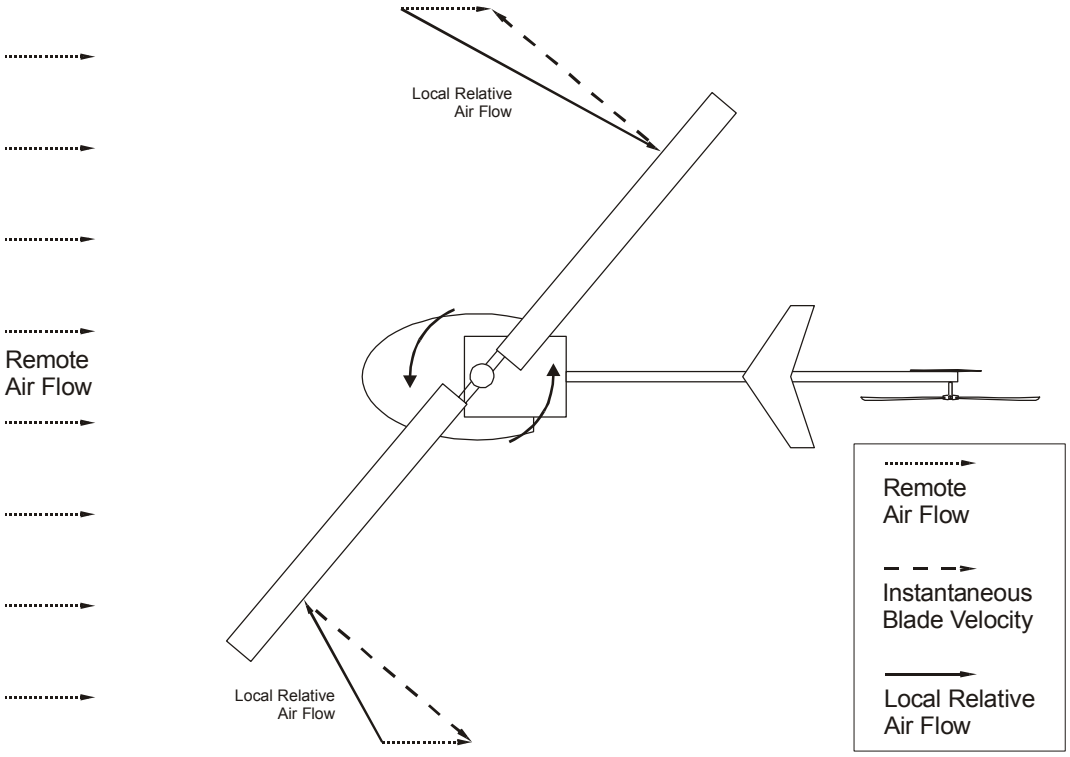

Figure 5: Asymmetric forward flight

The top speed of a helicopter is limited in part by the stall airspeed of the retreating blade.

2.3 Control

Typically a helicopter has 5 controls. The first three controls adjust the pitch of the main rotor blades as a function of their position around the rotor disc. They are collective pitch, longitudinal cyclic pitch and lateral cyclic pitch, and together they control the magnitude and tilt of the main rotor thrust respectively. The fourth control is tail rotor pitch. It adjusts the magnitude of the tail rotor thrust. Finally, the helicopters rotor speed is controlled with the engine's throttle.

Collective and Cyclic Pitch act on the main rotor through a mechanism known as a swashplate, which allows the pitch of the rotating blades to be actuated from the fixed fuselage of the helicopter.

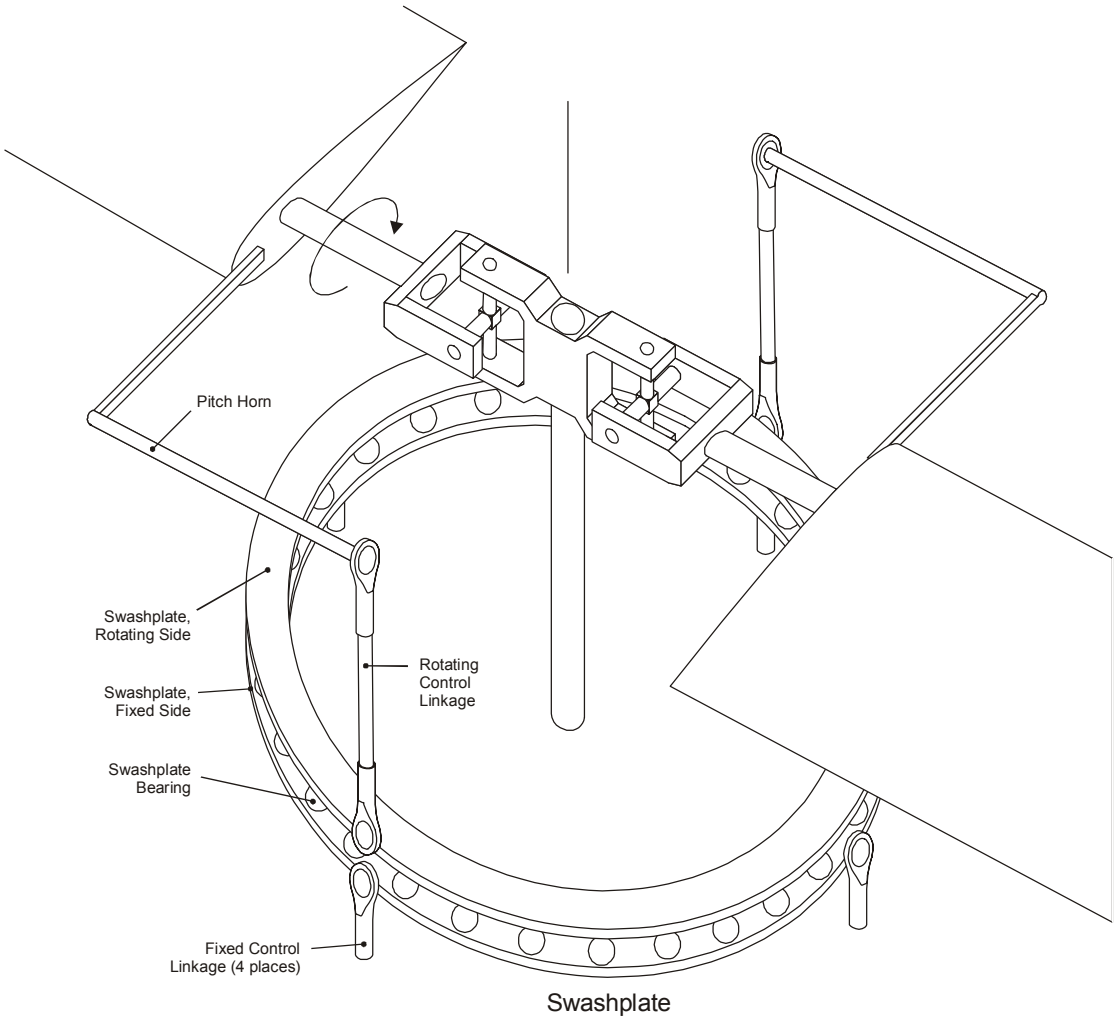

Figure 6: Swashplate

The swashplate provides thrust magnitude control, or collective pitch, by varying the thrust generated by the rotor disc symmetrically. Control linkages on the fixed fuselage are extended to raise the fixed side of the swashplate. This raises the rotating side of the swashplate and extends the blades' pitch horns. Extending the pitch horns forces the

blades to rotate about their feathering bearings, changing their angle of attack, and consequently their lift.

The swashplate also provides control over rotor tilt, or cyclic pitch, by varying the distribution of lift as a periodic function of position around the rotor disc. In Figure 6 it can be seen that each pitch horn connects to the swashplate 90° forward of the blade it is attached to in the direction of rotation. Extending the rear fixed control linkage while retracting the front fixed linkage tilts the swashplate forward. The tilted swashplate causes sinusoidal variation of the blade pitch as the blade travels around the rotor disc. The pitch reaches a maximum on the left, and a minimum on the right, resulting in a positive roll, or lateral torque, on the rotor disc. Because flapping of an articulated rotor is a harmonic oscillation driven at resonant frequency, the flapping induced will lag the torque applied by 90° in the direction of rotation. The thrust tilt follows the flapping, also lagging the torque by 90°. The result is that with this swashplate configuration the mechanical lead cancels the dynamic lag, and a forward tilt of the swashplate results in a forward tilt of the rotor. The dynamics of blade flapping are discussed further in 2.4.2. Swashplate tilt has two degrees of freedom, which provides longitudinal and lateral cyclic pitch control.

Due to the flap hinges on an articulated rotor no moment can be directly transferred between the rotor disc and the helicopter's fuselage. Instead, pitch and roll moments on the helicopter are the result of thrust tilt in conjunction with the vertical separation of the main rotor from the helicopter's centre of gravity. The moment resulting from thrust tilt is large enough to bring the helicopter into alignment with the rotor disc quickly[3].

[3] Pg. 446 [10].

However, thrust magnitude varies with the vehicle's weight. This creates an undesirable coupling between a helicopter's weight and its control response. In hingeless rotor designs directly coupled moment creates 4-5 times the moment thrust tilt alone provides. This allows significantly stronger pitch and roll response, and the load coupling is largely eliminated.

The tail rotor pitch is varied with a tail rotor swashplate. The mechanism is similar to the main rotor, however there are no cyclic pitch controls on the tail rotor. Varying the thrust of the tail rotor provides heading, or yaw, control.

Finally, rotor thrust is also affected by the engine speed. Increasing the rate of rotation will increase the aerodynamic lift of the blades. Because the engine reacts slowly, the engine's throttle is not used to control main rotor thrust. Throttle is only used to regulate rotor speed. Keeping rotor speed constant improves control linearity and simplifies analysis [2].

2.4 Dynamics

A helicopter can be modelled as a rigid body in free space. Helicopter dynamics will be developed in the body fixed coordinate system, "Body CS". The Body CS is a right orthogonal coordinate system with the origin attached to the centre of mass of the helicopter, the x-axis points forward, the y-axis points to the right, and the z-axis points down. Helicopters are normally designed so that the principal axes of the helicopter's moment of inertia are aligned with the Body CS axes, alignment will be assumed here. An inertial coordinate system, the "World CS", will also be used. The World CS will coincide with the Body CS when the helicopter is hovering at an equilibrium point at

some arbitrary location in space. The position of the helicopter relative to the World CS expressed in the Body CS is ${}^{B}\mathbf{x}_{B} = \begin{bmatrix} x_B, & y_B, & z_B \end{bmatrix}^T$. The prefix indicates the coordinate system used to describe the quantity, the subscript indicates the nature of the quantity. The development of helicopter dynamics will be in the Body CS, so the prefix will be dropped in most of this chapter. The orientation of the Body CS relative to the World CS will be represented in x-y-z- Euler angles. The rotation matrix, which transforms a vector in the Body CS to the World CS, is ${}^{W}R_{B}$.

$$ {}^{W}R_{B} = \begin{bmatrix} \mathrm{c}\psi_B \mathrm{c}\theta_B & \mathrm{c}\psi_B \mathrm{s}\theta_B \mathrm{s}\phi_B - \mathrm{s}\psi_B \mathrm{c}\phi_B & \mathrm{c}\psi_B \mathrm{s}\theta_B \mathrm{c}\phi_B + \mathrm{s}\psi_B \mathrm{s}\phi_B \\ \mathrm{s}\psi_B \mathrm{c}\theta_B & \mathrm{s}\psi_B \mathrm{s}\theta_B \mathrm{s}\phi_B + \mathrm{c}\psi_B \mathrm{c}\phi_B & \mathrm{s}\psi_B \mathrm{s}\theta_B \mathrm{c}\phi_B - \mathrm{c}\psi_B \mathrm{s}\phi_B \\ -\mathrm{s}\theta_B & \mathrm{c}\theta_B \mathrm{s}\phi_B & \mathrm{c}\theta_B \mathrm{c}\phi_B \end{bmatrix} \qquad (2.1) $$

where ψ_B, θ_B, ϕ_B are rotations about the axes of the Body CS, as displayed in Figure 7.

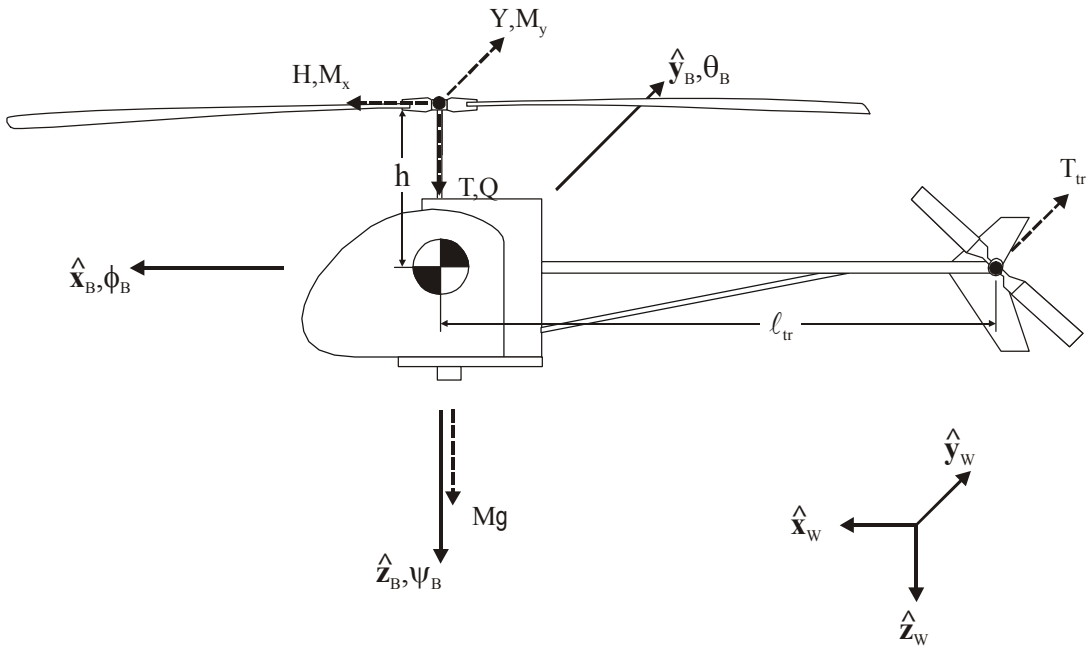

Figure 7: Helicopter forces and coordinate systems

The development of helicopter equations of motion will be sketched here, beginning with blade aerodynamics, and blade flapping behaviour. With the blade flapping behaviour defined, the forces and moments at the rotor hub can be found. It will then be possible to write the equations of motion for the helicopter moving in free space. With suitable approximations it is possible to solve the equations of motion, but no attempt at a solution will be made here.

2.4.1 Blade Aerodynamics

The first step in developing the helicopter equations of motion is determining the aerodynamic forces generated by the rotor. Consider a 2-dimensional slice of a rotor blade.

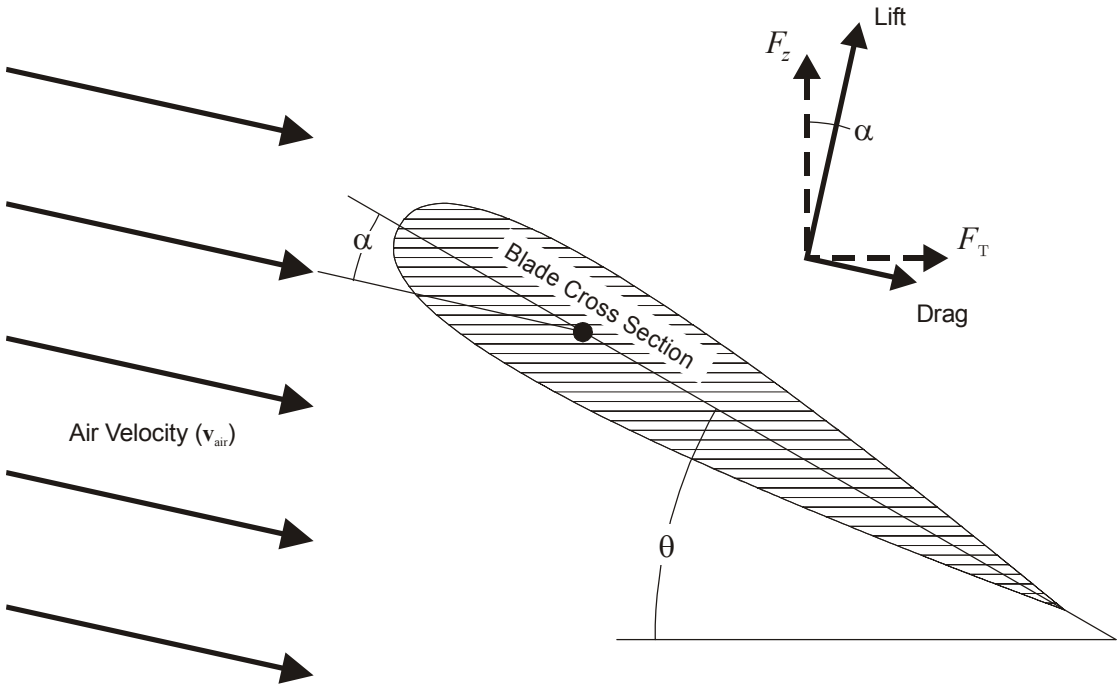

Figure 8: Aerodynamic forces on blade cross-section

The air velocity shown in Figure 8 is the projection of the total air velocity seen by the rotor disc into the plane of the blade cross-section; in general there is a radial component as well. The lift of the blade cross section is directed perpendicular to the angle of the in plane air velocity, and the drag of the cross section is directed parallel to the in plane air velocity. The magnitude of lift and drag can be calculated with Bernoulli's equations.

$$\begin{aligned} \left|\text{Lift}\right| &= \tfrac{1}{2}\,\rho c c_l \left|\mathbf{v}_{air}^2\right| \alpha \\ \left|\text{Drag}\right| &= \tfrac{1}{2}\,\rho c c_d \left|\mathbf{v}_{air}^2\right| \alpha \end{aligned} \tag{2.2}$$

where

ρ	is the air density,
c	is the blade cord length,
c_l	is the blade lift coefficient,
c_d	is the blade drag coefficient,
α	is the blade angle of attack,
$\mathbf{v}_{air}$	is the local in plane air velocity.

The blade angle of attack, α, is the angle between the blade centreline and the direction of the in plane component of air velocity. The local in plane air velocity, $\mathbf{v}_{air}$, is the combination of the helicopter's wind speed and fuselage rotation, the blade's rotation and flapping, and a local airflow called induced velocity. Induced velocity is an airflow resulting from the rotor's lift generation. It is normally approximated a priori by equating rotor thrust with the mass flow of air moving through the rotor disk.

The lift and drag forces in Figure 8 can be resolved as F_z, the total aerodynamic force along the z-axis of the Body CS, and F_T, the total aerodynamic force tangent to the rotor blade rotation. There is also a force due to friction between the blade and radial airflow, F_r, perpendicular to the plane of Figure 8.

2.4.2 Blade Flapping

The flap angle, β, of an articulated rotor can be expressed as a moment balance about the flap hinge.

$$I_b\ddot{\beta} \quad + \quad \Omega^2 I_b\beta \quad = \quad \int_0^R rF_z\left(\theta, \mathbf{v}_{air}, r\right)dr \tag{2.3}$$

where

I_b	is the blade moment of inertia about the flap hinge,
Ω	is the rate of rotation of the rotor,
R	is the rotor radius,
θ	is the commanded pitch angle of the blade, the control pitch,
$\mathbf{v}_{air}$	is the air velocity in the plane of the blade cross-section.

In hover the remote air velocity is zero, and (2.3) can be simplified as follows:

$$\begin{array}{ccccc} I_b\ddot{\beta} & + & \Omega^2 I_b\beta & = & M_\theta\theta + M_{\dot{\beta}}\dot{\beta} + M_\lambda\lambda \\ \left(Inertia\right) & & \left(Centripital\ Force\right) & & \left(Aerodynamic\ Force\right) \end{array} \tag{2.4}$$

where

M_θ	is the flap moment due to blade pitch angle,
$M_{\dot{\beta}}$	is the flap moment due to flapping velocity,
M_λ	is the flap moment due to inflow,
λ	is the rotor inflow ratio.

This is essentially a simple harmonic oscillation where the centripetal force term provides the restoring force and the aerodynamic force provides damping and driving force, via the $\dot{\beta}$ term, and the θ term respectively.

The control pitch, θ, represents the three control inputs which effect the main rotor. Cyclic pitch is a function of azimuth, which implies that the driving force is periodic with frequency equal to the rotors rate of rotation, or 1 cycle per revolution. θ can be expressed as the combination of the three main rotor controls.

$$\theta = \theta_0 + \theta_{1c}\cos(\psi) + \theta_{1s}\sin(\psi) \tag{2.5}$$

where

θ_0 is the collective pitch control,
θ_{1c} is the longitudinal cyclic pitch control,
θ_{1s} is the lateral cyclic pitch control.

To solve (2.4) rotor azimuth is used in place of time, this is possible because the rotor's rate of rotation is taken to be constant. Also, it is assumed that the rate of rotation is high, and that the transients in the flap response will have negligible effect on the dynamics of the helicopter[4]. In this way only the steady state solution for β is needed. The form of the steady state solution will be a harmonic series.

$$\underset{\left(\begin{matrix}Flap\\Angle\end{matrix}\right)}{\beta} = \underset{\left(\begin{matrix}Conning\\Angle\end{matrix}\right)}{\beta_0} + \underset{\left(\begin{matrix}Longitudinal\\Flapping\end{matrix}\right)}{\beta_{1c}\cos(\psi)} + \underset{\left(\begin{matrix}Lateral\\Flapping\end{matrix}\right)}{\beta_{1s}\sin(\psi)} + HHT \tag{2.6}$$

Only the mean and first fundamental terms are required for performance and control analysis[5].

The blade flapping behaviour determines many critical aspects of helicopter flight; it will be useful to explore two areas before moving on. The fundamental frequency of the oscillation in (2.4) is $\sqrt{\frac{I_b\Omega^2}{I_b}} = \Omega$, exactly equal to the rate of rotation of the main rotor, or 1 cycle per revolution. The fundamental frequency of the driving force is also 1 cycle per revolution. As with any simple harmonic oscillator driven at resonant frequency the motion lags the driving force by 90°. Hence, an articulated rotor helicopter responds to longitudinal cyclic pitch variation with a roll, as mentioned in Section 2.3.

[4] Sometime known as the quasi-static representation. Flap transients normally die off in about ¼ of a rotation, see pg. 622 [9]. This is equivalent to about 0.05s for a full sized helicopter, and 0.01s for an RC helicopter.

[5] Pg. 212 [9].

The coefficients $M_{\dot{\beta}}$ and M_{θ} are equal for an articulated rotor. In this way 1° of cyclic pitch input is equivalent to 1° of blade flap amplitude. This so-called pitch flap equivalence leads to an interpretation of a rotor as a rigid rotating system experiencing gyroscopic precession[6].

The equations of blade flapping developed here do not take fuselage motion into account. In general, (2.3) must be extended to include terms due to angular and vertical acceleration of the fuselage, and the coriolis acceleration, which results from the coupled fuselage and blade rotations[7].

2.4.3 Rotor Forces

The rotor forces and moments seen by the helicopter can be developed from the aerodynamic forces on the blade cross-section as discussed in 2.4.1, and the steady state solution to blade flapping from 2.4.2. The forces on the blade cross-section are first integrated along the length of the blade to form the blade force as a function of azimuth. This force is then averaged over one rotation and multiplied by the number of blades, N.

[6] Pg. 191 [9].

[7] For blade flapping equations that take fuselage motion into account, see pg. 436 [9].

$$T = N\frac{1}{2\pi}\int_0^{2\pi}\int_0^R F_z\,dr\,d\psi \tag{2.7}$$

$$H = N\frac{1}{2\pi}\int_0^{2\pi}\int_0^R \left(F_T\sin\psi + F_r\cos\psi\right)dr\,d\psi \tag{2.8}$$

$$Y = N\frac{1}{2\pi}\int_0^{2\pi}\int_0^R \left(-F_T\cos\psi + F_r\sin\psi\right)dr\,d\psi \tag{2.9}$$

$$Q = N\frac{1}{2\pi}\int_0^{2\pi}\int_0^R rF_T\,dr\,d\psi \tag{2.10}$$

$$M_y = -N\frac{1}{2\pi}\int_0^{2\pi}\int_0^R rF_z\cos\psi\,dr\,d\psi \tag{2.11}$$

$$M_x = N\frac{1}{2\pi}\int_0^{2\pi}\int_0^R rF_z\sin\psi\,dr\,d\psi \tag{2.12}$$

H , Y , and T are the aerodynamic forces developed by the main rotor and applied to the helicopter at the main rotor hub. Q is the torque required to rotate the main rotor. M_x and M_y are moments developed by the main rotor and applied to the helicopter at the hub. Because of the flap hinge, M_x and M_y are zero for articulated rotor helicopters. All of these forces and moments are displayed in Figure 7.

2.4.4 Equations of Motion

The Newton-Euler equations of rigid body motion for the helicopter are:

$$M\ddot{\mathbf{x}}_B + M\boldsymbol{\omega}_B \times \dot{\mathbf{x}}_B = \begin{bmatrix} -H \\ Y + T_{tr} \\ -T \end{bmatrix} + {}^{W}R_B^T \begin{bmatrix} 0 \\ 0 \\ M\mathsf{g} \end{bmatrix} + \mathbf{f}_{body} \tag{2.13}$$

$$\hat{\hat{I}}\dot{\boldsymbol{\omega}}_B + \boldsymbol{\omega}_B \times \hat{\hat{I}}\boldsymbol{\omega}_B = \begin{bmatrix} -M_x + hY \\ M_y + hH \\ Q - l_{tr}T_{tr} \end{bmatrix} + \mathbf{g}_{body} \tag{2.14}$$

where

M is the mass of the helicopter,
g is the acceleration of gravity,
T_{tr} is the tail rotor thrust,
$\hat{\hat{I}}$ is the moment of inertia of the helicopter,
h is the distance from the helicopter's centre of mass to the main rotor hub,
l_{tr} is the distance from the helicopter's centre of mass to the tail rotor hub.

$\mathbf{f}_{body}$ and $\mathbf{g}_{body}$ represent the aerodynamic forces and moments developed by the helicopter fuselage and fixed lift generating surfaces.

2.4.5 Hingeless Rotor

In addition to the effect of directly coupled moments, discussed in Section 2.3, the dynamics of blade flapping for a hingeless rotor differ somewhat from the articulated rotor case. In (2.4) the restoring force proportional to flap angle is due entirely to centripetal acceleration. The restoring force due to flap angle for a hingeless rotor has an additional term due to blade stiffness, which increases the resonant frequency of blade flapping. The resonant frequency of a typical full sized hingeless rotor is 1.10-1.15 cycles per revolution. Cyclic pitch excites flapping at exactly 1 cycle per revolution, which is below the resonant frequency, so the rotor tilt lags cyclic pitch input by less than 90°. This leads to coupling between the lateral and longitudinal cyclic pitch inputs, which the pilot must take into account.

2.5 RC Helicopter Configuration

Modern remote control helicopters are very similar to their full size counterparts. However, there are several important differences. Model helicopters have much faster dynamics due to their small size. Also, the stiffness of their rotor blades is very high compared to full size hingeless rotors.

A model helicopter is typically too fast for a human to control without special stability augmentation. The required stability augmentation is provided by a bell-hiller mechanism, commonly known as a flybar.

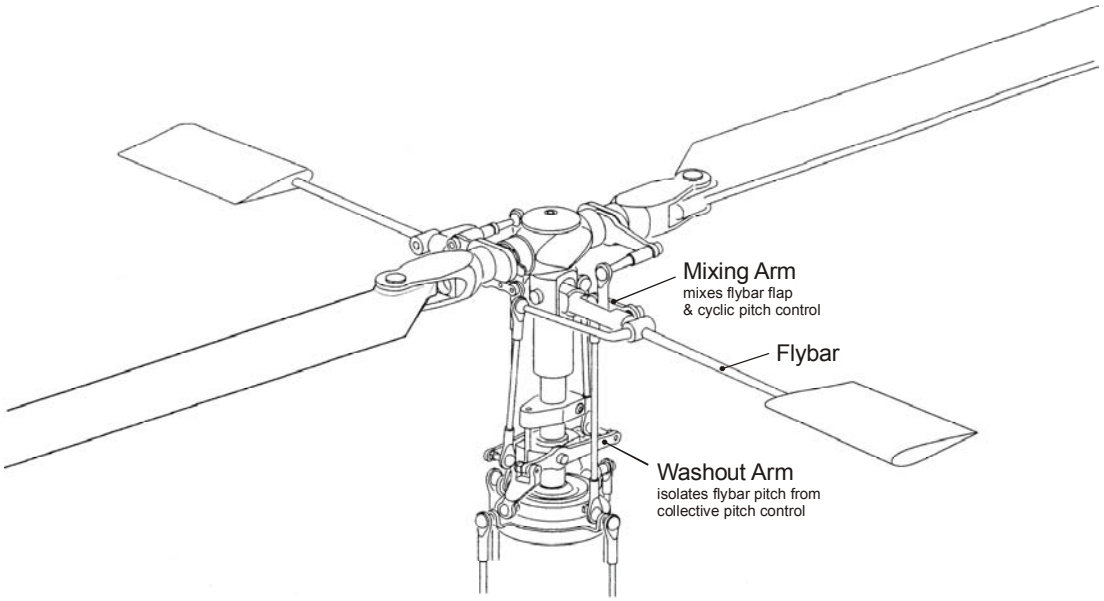

Figure 9: Rotor with flybar[8]

The flybar rotates with the main rotor, but it is allowed to flap, or teeter, independently. Control linkages mix the flybar's flap angle with the pilot's cyclic pitch input to form the

[8] Figure 9 derived from figure 47 on pg. 30 of [11]

cyclic pitch seen by the main rotor. When the helicopter experiences a disturbance, the flybar continues to rotate in its original plane. Relative to the helicopter the flybar tilts, which applies cyclic pitch to oppose the disturbance.

The lift generated by the flybar is too small to have a significant effect on the dynamics of the helicopter as a whole; however, the flybar's lift is substantially larger than reaction forces in the control linkages [2]. Using these approximations, the flapping equations for a flybar are essentially identical to the equations for an articulated rotor presented in Section 2.4.2. Given the control pitch as stated in (2.5), a solution for flybar flap angle, β^{fly}, can be found. Because the flybar is a teetering rotor there will be no β_0^{fly} term, otherwise the solution will be similar to (2.6):

$$\beta^{fly} = \beta_{1c}^{fly}\cos(\psi) + \beta_{1s}^{fly}\sin(\psi) \tag{2.15}$$

The main rotor pitch for a rotor with a flybar is a linear combination of the control pitch from (2.5) with the control pitch due to flybar flap.

$$\theta = \theta_0 + \left(a\theta_{1c} + b\beta_{1s}^{fly}\right)\cos(\psi) + \left(a\theta_{1s} + b\beta_{1c}^{fly}\right)\sin(\psi) \tag{2.16}$$

a and *b* are derived from the control linkage geometry. Development of the equations of motion for a helicopter with a flybar follows from the development of Section 2.4, with (2.16) replacing (2.5). It is sometimes assumed that the main rotor of an RC helicopter is rigid enough to neglect main rotor flapping altogether [2].

Chapter 3

Concept and Requirements

An ideal test stand will allow the helicopter to move as it does in free flight without significantly increasing inertia, mass, and friction. These requirements cannot be met because of the physical limitations of construction material and work area. However, a good design can be achieved by balancing these four basic requirements:

1. The stand must operate within a small room without compromising the safety of the operator or allowing damage to the helicopter.
2. Motion of the helicopter on the stand must be a close analogue of a helicopter in hover.
3. The stand must provide sensors to monitor the motion of the helicopter.
4. The stand must allow for whatever electrical connections the sensors and helicopter require for in lab operation.

In Section 3.1 several approaches for meeting the four requirements are discussed. In Section 3.2 the preliminary design for a gimbal test stand is presented. An analysis of how motion on the test stand compares to helicopter flight in free space is presented in Section 3.3. Next, Section 3.4 addresses how the stand meets the remaining basic

requirements. Finally, Section 3.5 presents an improved gimbal test stand concept, and a detailed list of specifications required for the final stand design.

3.1 Basic Configurations Considered

Three basic types of test stand were considered: a flexible stand, a rigid stand with sliding and rotating joints, and a rigid stand with only rotating joints.

3.1.1 Flexible Stand

It is possible to design a flexible stand, which consists of rope-like constraints. The constraints would allow the helicopter to move freely within a small sphere and protect the operator and helicopter from collisions and damage. This type of system can be very inexpensive and provides a good representation of free flight near hover. However, the system does not offer any position sensing capability. Also, to provide sufficient protection and eliminate any possible interference with the rotors, the range of free motion may be very limited. This type of stand was rejected.

3.1.2 Sliding and Rotating Joints Stand

It may be possible to design a stand that allows as much free motion as rope constraints by using both linear joints and rotating joints. Linear joints and associated linear sensors are highly specialized and require expensive parts. Also, to make effective use of the linear joints, the kinematic design would be very time consuming. This type of stand was rejected.

3.1.3 Rotating Joints

Rotating joints and the required Sensors for them are readily available, inexpensive, and easy to work with. Also, as discussed in Section 2.2, helicopter controls actuate the three attitude degrees of freedom and vertical thrust only. Reproducing attitude motion will capture most of the hovering dynamics of a helicopter. Additionally, rotating joints can be configured to allow continuous motion with no hard end-stops. Finally, the kinematic design of a test stand that reproduces attitude motion is straightforward.

3.2 Gimbal Test Stand

Given the considerations outlined in Section 3.1, the preliminary design concept for a 3 degree of freedom (DOF) gimbal test stand was developed.

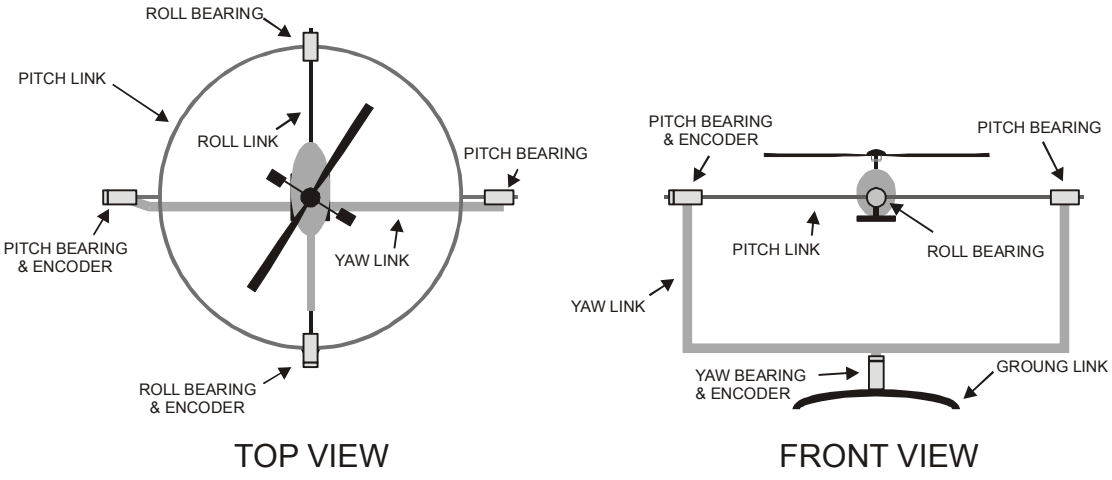

Figure 10: Gimbal Test Stand as originally conceived

The preliminary design consisted of four nested links connected with three orthogonal joint axes. The innermost link, the roll link, is rigidly attached to the helicopter, rotating in every direction with the helicopter. The pitch link is next, connected to the roll link with roll bearings. The pitch link follows the helicopter in both pitch and yaw motion, but

it is isolated from the helicopter's roll motion. The Yaw link is connected to the pitch link with the pitch bearings. The Yaw link is only able to yaw, it is isolated from the helicopter's pitch and roll. Finally, there is a stationary ground link to support the yaw bearing. It was an initial assumption that the joint axes would meet at a common intersection that would coincide with the helicopter's centre of mass.

3.3 Gimbal Test Stand Kinematics & Dynamics

In order to determine how the helicopter's motion on the test stand relates to its motion in free flight, the kinematics and dynamics of the stand plus helicopter must be considered. In Section 3.3.1 joint angles will be related to helicopter attitude. The relationship between joint angular rate and helicopter attitude rate will be developed in Section 3.3.2. Finally, Section 3.3.3 - Section 3.3.5 discusses how the test stand will affect forces and inertial effects of the helicopter's dynamics.

3.3.1 Kinematics

To express the helicopter's attitude as a function of joint angles coordinate systems are attached to each link of the stand, the Roll CS, Pitch CS and Yaw CS, respectively. Each will be orthogonal and right-handed, and they will be identical to the Body CS when all of the joint angles are zero.

The yaw joint angle, θ_Y, measures the relative attitude of the Yaw CS with respect to the World CS. To express the transformation as a rotation matrix, the Yaw CS axes are written as a combination of World CS axes. So a rotation of θ_Y about the z-axis of the World CS gives the attitude of the Yaw CS.

$$ {}^{W}\mathbf{R}_{Y} = \begin{bmatrix} \cos\theta_{Y} & -\sin\theta_{Y} & 0 \\ \sin\theta_{Y} & \cos\theta_{Y} & 0 \\ 0 & 0 & 1 \end{bmatrix} \tag{3.1} $$

The pitch joint angle, θ_P, specifies the relative attitude of the Pitch CS with respect to the Yaw CS.

$$ {}^{Y}\mathbf{R}_{P} = \begin{bmatrix} \cos\theta_{P} & 0 & \sin\theta_{P} \\ 0 & 1 & 0 \\ -\sin\theta_{P} & 0 & \cos\theta_{P} \end{bmatrix} \tag{3.2} $$

Finally the roll joint angle, θ_R, specifies the relative attitude of the Roll CS with respect to the Pitch CS.

$$ {}^{P}\mathbf{R}_{B} = {}^{P}\mathbf{R}_{R} = \begin{bmatrix} 1 & 0 & 0 \\ 0 & \cos\theta_{R} & -\sin\theta_{R} \\ 0 & \sin\theta_{R} & \cos\theta_{R} \end{bmatrix} \tag{3.3} $$

The rotation of the Body CS with respect to the World CS is simply the concatenation of these transformations.

$$ \begin{aligned} {}^{W}\mathbf{R}_{B} &= {}^{W}\mathbf{R}_{Y}\,{}^{Y}\mathbf{R}_{P}\,{}^{P}\mathbf{R}_{B} \\ &= \begin{bmatrix} \mathrm{c}\theta_{Y}\,\mathrm{c}\theta_{P} & \mathrm{c}\theta_{Y}\,\mathrm{s}\theta_{P}\,\mathrm{s}\theta_{R} - \mathrm{s}\theta_{Y}\,\mathrm{c}\theta_{R} & \mathrm{c}\theta_{Y}\,\mathrm{s}\theta_{P}\,\mathrm{c}\theta_{R} + \mathrm{s}\theta_{Y}\,\mathrm{s}\theta_{R} \\ \mathrm{s}\theta_{Y}\,\mathrm{c}\theta_{P} & \mathrm{s}\theta_{Y}\,\mathrm{s}\theta_{P}\,\mathrm{s}\theta_{R} + \mathrm{c}\theta_{Y}\,\mathrm{c}\theta_{R} & \mathrm{s}\theta_{Y}\,\mathrm{s}\theta_{P}\,\mathrm{c}\theta_{R} - \mathrm{c}\theta_{Y}\,\mathrm{s}\theta_{R} \\ -\mathrm{s}\theta_{P} & \mathrm{c}\theta_{P}\,\mathrm{s}\theta_{R} & \mathrm{c}\theta_{P}\,\mathrm{c}\theta_{R} \end{bmatrix} \end{aligned} \tag{3.4} $$

So for the proposed gimbal test stand, the joint angles are equivalent to the x-y-z-Euler angles used to express the attitude of the Body CS as discussed in Section 2.4.

$$\theta_R = \theta_H, \quad \theta_P = \phi_H, \quad \theta_Y = \psi_H \tag{3.5}$$

3.3.2 Differential Kinematics

The helicopter's angular rates and accelerations can be expressed as functions of joint rotation rates and accelerations.

The yaw joint rotates the Yaw CS about its z-axis with angular rate $\dot{\theta}_Y$. Transforming ${}^{Y}\mathbf{z}_Y$ to the Body CS yields the helicopter's rate of rotation as a function of the yaw joint.

$$\begin{aligned} {}^{B}\boldsymbol{\omega}_B\left(\dot{\theta}_Y\right) &= {}^{B}\mathbf{R}_P \; {}^{P}\mathbf{R}_Y \; {}^{Y}\hat{\mathbf{z}}_Y \; \dot{\theta}_Y \\ &= \begin{bmatrix} \mathrm{s}\theta_P \\ -\mathrm{c}\theta_P \mathrm{s}\theta_R \\ \mathrm{c}\theta_P \mathrm{c}\theta_R \end{bmatrix} \dot{\theta}_Y \end{aligned} \tag{3.6}$$

The pitch joint rotates the Pitch CS about its y-axis with angular rate $\dot{\theta}_P$. Transforming ${}^{P}\mathbf{y}_P$ to the Body CS yields the helicopter's rate of rotation as a function of the pitch joint.

$$\begin{aligned} {}^{B}\boldsymbol{\omega}_B\left(\dot{\theta}_P\right) &= {}^{B}\mathbf{R}_P \; {}^{P}\hat{\mathbf{y}}_P \; \dot{\theta}_P \\ &= \begin{bmatrix} 0 \\ \mathrm{c}\theta_R \\ \mathrm{s}\theta_R \end{bmatrix} \dot{\theta}_P \end{aligned} \tag{3.7}$$

Finally the roll joint rotates the Roll CS about its x-axis with angular rate $\dot{\theta}_R$. But the Roll CS and the Body CS are identical, so no transformation is required to express the helicopter's rate of rotation as a function of the roll joint.

$$ {}^{B}\boldsymbol{\omega}_{B}\left(\dot{\theta}_{R}\right)=\begin{bmatrix}1\\0\\0\end{bmatrix}\dot{\theta}_{R} \tag{3.8} $$

The affect of the individual rotations superposes linearly to yield the helicopter rotation rate as a function of the joint rotation rates.

$$ \begin{bmatrix}{}^{B}\omega_{x}\\{}^{B}\omega_{y}\\{}^{B}\omega_{z}\end{bmatrix}=\begin{bmatrix}1 & 0 & \mathrm{s}\theta_{P}\\0 & \mathrm{c}\theta_{R} & -\mathrm{c}\theta_{P}\,\mathrm{s}\theta_{R}\\0 & \mathrm{s}\theta_{R} & \mathrm{c}\theta_{P}\,\mathrm{c}\theta_{R}\end{bmatrix}\begin{bmatrix}\dot{\theta}_{R}\\\dot{\theta}_{P}\\\dot{\theta}_{Y}\end{bmatrix} \tag{3.9} $$

The relationship between joint accelerations and helicopter attitude accelerations is identical to the rate relationship presented in (3.9).

$$ \begin{bmatrix}{}^{B}\dot{\omega}_{x}\\{}^{B}\dot{\omega}_{y}\\{}^{B}\dot{\omega}_{z}\end{bmatrix}=\begin{bmatrix}1 & 0 & \mathrm{s}\theta_{P}\\0 & \mathrm{c}\theta_{R} & -\mathrm{c}\theta_{P}\,\mathrm{s}\theta_{R}\\0 & \mathrm{s}\theta_{R} & \mathrm{c}\theta_{P}\,\mathrm{c}\theta_{R}\end{bmatrix}\begin{bmatrix}\ddot{\theta}_{R}\\\ddot{\theta}_{P}\\\ddot{\theta}_{Y}\end{bmatrix} \tag{3.10} $$

For small joint angles this mapping is well behaved, for example:

$$ \begin{aligned}{}^{B}\omega_{x}&=\dot{\theta}_{R}, & \left|\theta_{R}\right|&\approx 0\\{}^{B}\omega_{y}&=\dot{\theta}_{P}, & \left|\theta_{P}\right|&\approx 0\\{}^{B}\omega_{z}&=\dot{\theta}_{Y}, & \left|\theta_{Y}\right|&\approx 0\end{aligned} \tag{3.11} $$

For large joint angles however problems arise. When $\theta_{P}=90^{\circ}$ the matrix in (3.9) becomes singular. This is the so-called gimbal lock singularity. It occurs when two joints become collinear, making one of the joints redundant, and reducing the degree of freedom of the stand. At joint positions near gimbal lock a related problem occurs. For the helicopter to achieve a given angular velocity, certain joints must rotate at much

higher speed than the helicopter itself. For the helicopter to achieve a desired yaw rate, ${}^{B}\omega_z = \alpha$, at a stand position of $\theta_Y, \theta_R \approx 0, \quad \theta_P \approx 60^\circ$ the joint rates must be as follows:

$$\begin{bmatrix} 0 \\ 0 \\ \alpha \end{bmatrix} = \begin{bmatrix} 1 & 0 & 0.5 \\ 0 & 1 & 0 \\ 0 & 0 & 0.5 \end{bmatrix} \begin{bmatrix} \ddot{\theta}_R \\ \ddot{\theta}_P \\ \ddot{\theta}_Y \end{bmatrix} \tag{3.12}$$

$$\begin{aligned} \dot{\theta}_R &= -\alpha \\ \dot{\theta}_P &= \ 0 \\ \dot{\theta}_Y &= 2\alpha \end{aligned} \tag{3.13}$$

The gimbal lock singularity will always be present when three separate 1 DOF joints are used in the design. However, by designing the stand so that all joint axes are perpendicular to one another in the stand's zero position, gimbal lock can be avoided.

3.3.3 Balance

The problem caused by an imbalance can be seen in the simplified 1 DOF stand depicted in Figure 11.

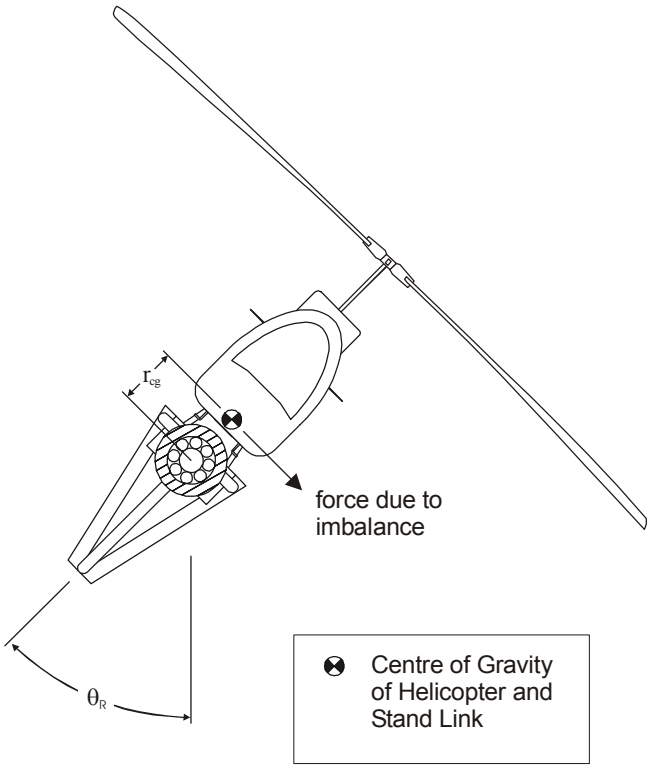

Figure 11: Imbalance example

The imbalance depicted will cause a torque about the helicopter's roll axis.

$$\tau_b = Mgr_{cg} \sin\theta \tag{3.14}$$

where

τ_b is the torque due to imbalance,
r_{cg} is the distance from the axis of rotation to the centre of gravity,
θ is the joint angle.

To ensure the system is balanced each joint axis must coincide with the centre of mass of the components moving relative to that joint. The generalized torque due to an imbalance in the test system, assuming the axes have a common intersection, is:

$$ {}^{B}\boldsymbol{\tau}_{b} = {}^{B}\mathbf{r}_{cg} \times {}^{B}\mathbf{g} \tag{3.15} $$

where

${}^{B}\boldsymbol{\tau}_{b}$	is the 3 dimensional torque due to imbalance expressed in the Body CS,
${}^{B}\mathbf{r}_{cg}$	is the 3 dimensional offset between the centre of mass and the intersection of the stand axes expressed in the Body CS,
${}^{B}\mathbf{g}$	is the force of gravity expressed in the Body CS.

Ensuring that the system can be balanced will be a critical aspect of the stand design. For the proposed gimbal test stand discussed in Section 3.2, the conditions required to maintain balance are: the centre of mass of the helicopter plus roll link, and the centre of mass of the pitch link must both coincide with the intersection point of the three axes, and the centre of mass of the yaw link must lie along the yaw joint axis.

3.3.4 Moment of Inertia

The moment of inertia of the test stand plus helicopter will be larger than the helicopter's free flight inertia. Three mechanisms will contribute to the difference; the inertia of moving parts of the stand, the separation between the axes of rotation of the stand and the principal axes of the helicopter, and the differential kinematics relating joint rates to helicopter attitude rates.

To understand the change in inertia when the helicopter and stand are combined, consider the simplified 1 DOF system depicted in Figure 12.

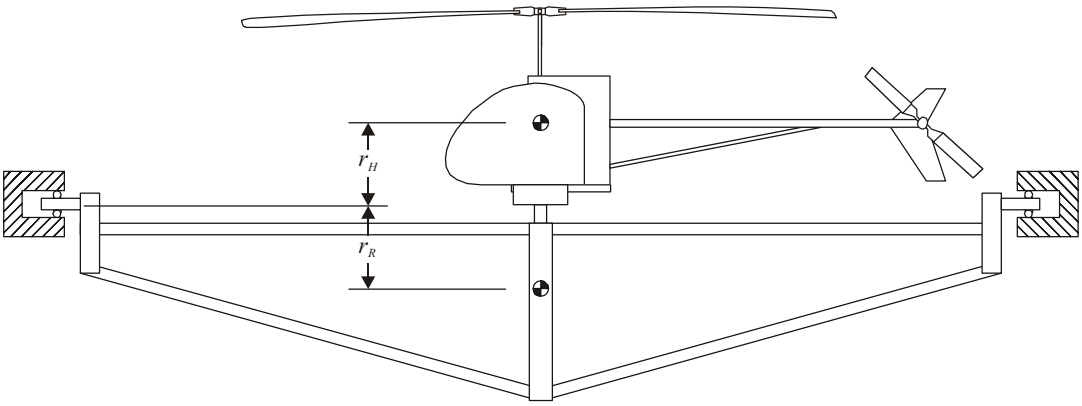

Figure 12: Combining Moment of Inertia

The helicopter will be rotating about an axis that has been offset from the helicopter's centre of mass by r_H. Also, the roll link will be rotating about an axis offset from its centre of mass by r_R. Using the parallel axis theorem, the total moment of inertia of the system about its axis of rotation can be expressed as follows:

$$I_{xx}^{Tot} = I_{xx}^{H} + I_{xx}^{R} + r_H^2 m_H + r_R^2 m_R \tag{3.16}$$

where

I_{xx}^{Tot} is the total moment of inertia about the joint axis,
I_{xx}^{H} is the moment of inertia about the helicopter's roll axis,
I_{xx}^{R} is the moment of inertia about the stand link's roll axis,
m_H is the mass of the helicopter,
m_R is the mass of the stand link.

From (3.16) it is clear that r_H and r_R must be kept as small as possible.

Assuming that the sum $r_{Tot} = r_H + r_R$ has been fixed during the design, but that the ratio $\frac{r_H}{r_R}$ is still a free parameter, it is then possible to find the optimal relative location for the axis of rotation.

$$\frac{d}{dr_H}\left(I_{xx}^H + I_{xx}^R + r_H^2 m_H + (r_{Tot} - r_H)^2 m_R\right) = 0$$
$$2r_H m_H = 2(r_{Tot} - r_H)m_R \tag{3.17}$$

Thus the total inertia is minimized when the axis of rotation coincides with the centre of mass of the moving parts. This result is in accordance with the balance requirement detailed in Section 3.3.3.

It is possible to find the combined inertial effects of the 3 DOF stand plus helicopter by, for example, applying Lagrangian dynamics. Such a derivation is beyond the scope of this work. However, it is possible to make some observations about the effect of the stands inertia based on Lagrangian ideas. In particular, it is clear that the generalized inertia of the stand plus helicopter as seen from the Body CS will be a 3x3 matrix. The entries of the matrix will be trigonometric functions of the joint angles.

For small joint angles the entries of the generalized inertia matrix will simply be the superposition of relevant inertia components of the stand links and of the helicopter:

$$\hat{\hat{I}}^{Tot} = \begin{bmatrix} I_{xx}^H + I_{xx}^R + r_H^2 m_H + r_R^2 m_R & 0 & I_{xz}^H \\ 0 & I_{yy}^H + I_{yy}^R + I_{yy}^P & 0 \\ I_{zx}^H & 0 & I_{zz}^H + I_{zz}^R + I_{zz}^P + I_{zz}^Y \end{bmatrix} \tag{3.18}$$

The terms I_{yx}^H and I_{zy}^H are zero due to the helicopters symmetry in the x-z plane of the Body CS. All of the cross terms for the stand links are zero due to symmetry. From (3.18) it can be seen that only some of the link inertia components are relevant to the total system inertia; for example, only one of the yaw link inertia components appears.

For the joint angle case discussed at the end of Section 3.3.2 a yaw rate caused significantly increased motion in the joints. The generalized inertia matrix for that scenario, in the neighbourhood of $\theta_Y, \theta_R \approx 0, \quad \theta_P \approx 60^\circ$, can be solved heuristically by considering the link motion, (3.13).

$$\hat{\hat{I}}^{Tot}_{\theta_P=60^\circ} = \begin{bmatrix} I^H_{xx} + I^R_{xx} + r_H^2 m_H + r_R^2 m_R & 0 & I^H_{xz} \\ 0 & I^H_{yy} + I^R_{yy} + I^P_{yy} & 0 \\ I^H_{zx} & 0 & I^H_{zz} + I^R_{zz} + I^P_{xx} + I^P_{zz} + 2I^Y_{zz} \end{bmatrix} \quad (3.19)$$

Clearly the helicopter's effective yaw inertia in this scenario is very high.

Minimizing the total system inertia will allow the stand to more closely represent helicopter free flight.

3.3.5 Rotor hub offset

The problem of rotor hub offset can be seen in the simplified 1 DOF stand depicted in Figure 13.

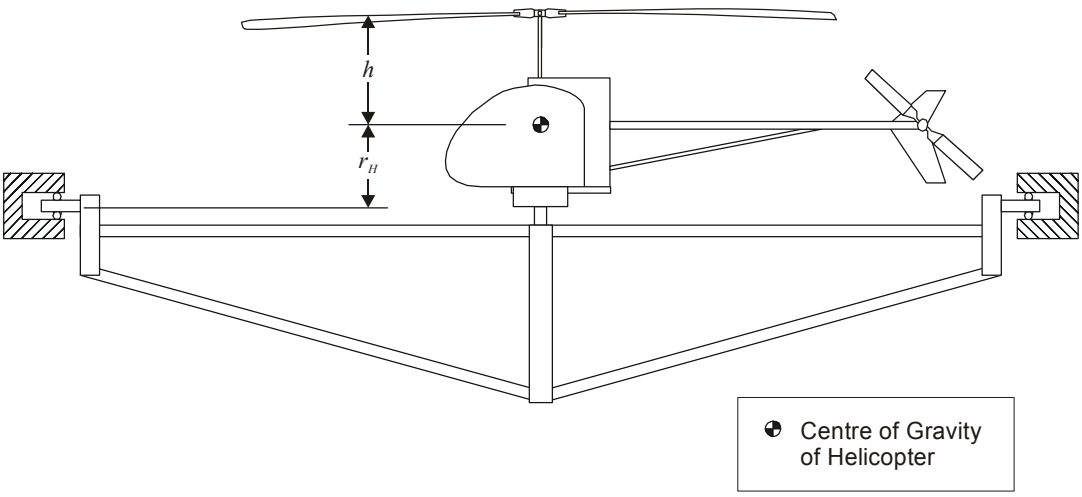

Figure 13: Distance from shaft to centre of gravity

In the helicopter equations of motion (2.13) & (2.14), it was assumed that the distance between the hub and the helicopter's centre of gravity was h. However, with the offset depicted in Figure 13 h must be replaced by $h' = h + r_H$. Thus the offset changes the pitch and roll moments developed due to main rotor thrust tilt. This would have a substantial effect on the attitude control moments of an articulated rotor helicopter, but it will have only a small effect on the hingeless rotor of an RC helicopter. The offset also changes the local airspeed of the rotor blades as a result of helicopter pitch and roll motion. The local airspeed variation can have a significant effect on blade and flybar flapping.

Hub offset is the most subtle of the effects discussed here. It is important to note that fuel use and payload variation can cause significant shifts in the centre of gravity of a free flying helicopter. In any case, addressing the balance and inertia considerations will help to minimize hub offset as well. If the stand's contribution to hub offset can be kept small compared the helicopter's inherent offset, the effect will be similar to that of a heavy payload.

3.4 Practical Considerations

The usefulness of the stand as a test apparatus will hinge on how it addresses the three remaining requirements. Position sensing is easily provided, by adding optical encoders to the joint bearings. Structural considerations, which ensure safe operation, and accuracy of position sensing, are discussed in Section 3.4.1. The electrical requirements will be discussed in Section 3.4.2.

3.4.1 Structure

In order to meet the safe operation requirement, the stand must be robust enough to transfer the helicopter's load to the ground with minimal compliance. In addition, any flexure in the links, or play in the joints, will reduce the precision of the attitude measurements. Compliance in the stand could even introduce small but significant translational motion. This would make the constrained dynamics unpredictable.

In Section 5.1.1 the helicopter specifications are listed. The helicopter's dead load under gravity is about 40N; the maximum thrust of the main rotor is about 60N. To allow some safety margin, a maximum load of 100N is assumed. To ensure minimal compliance, link structures will be designed with deflection of less than 1 cm under the expected maximum load. To ensure structural integrity, the joint bearings will be tightly fitted, with load handling capability several times higher than the expected maximum.

The proposed design has a critical problem. The Yaw bearing has to support the mass of the system in an unstable configuration under the translational loads developed by the helicopter. It was determined that yaw bearing design for this stand configuration would be very difficult.

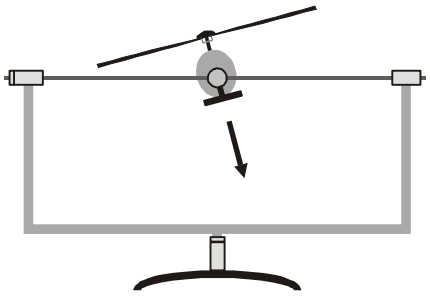

Figure 14: Balance problem due to thrust loading

Several options were considered to address this problem. Inverting the design, allowing the system to hang below the Yaw bearing, was considered; a hanging configuration reduces the dynamic load on the yaw bearing. Such a configuration would require either a very large supporting structure or a suitable beam in the ceiling of the lab to hang from. After briefly investigating the use of such a structural element, this idea was dropped. A Revised Gimbal Test Stand concept that does not exhibit the Yaw bearing problem was eventually adopted. This revised concept is presented in Section 3.5.

3.4.2 Electrical Connection

The stand must provide power to the helicopter's main motor. The motor's specifications are listed in Section 5.1.2. At full power the motor can draw 70 Amps at 40 Volts from a remote power supply. In practice the motor current will not exceed 35 Amps. So the stand must provide a two wire electrical hook-up rated to at least 50 Amps, and the wires must cross all three joints without interfering with rotation.

The three optical encoders for attitude sensing each require four wire low-level harnesses. Because the encoders can be located on the stationary side of the associated joint, this implies that one harness does not have to cross any joints, another only crosses one joint, and the final harness must cross two joints.

To allow wiring to cross the joints without interfering with rotation, each joint will be designed to allow the use of sliprings.

3.5 Revised Concept & Detailed Specifications

After considering all of the requirements discussed in this chapter a Revised Gimbal Test Stand concept was developed. In the revised stand, the joints were rearranged, placing the yaw joint closest to the helicopter.

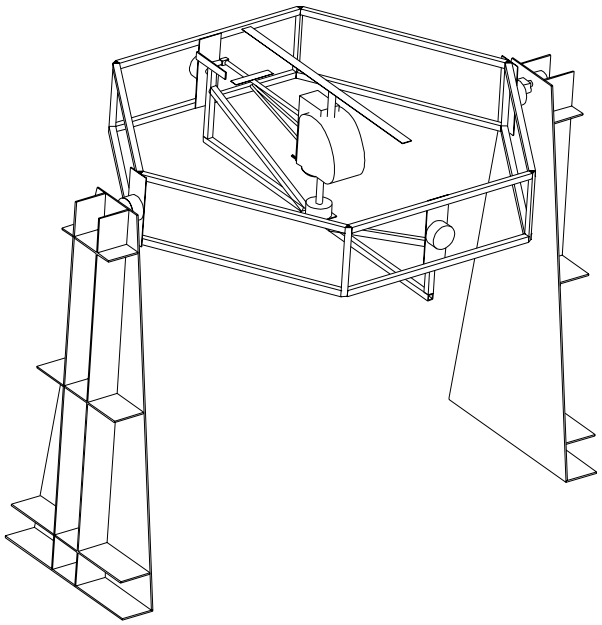

Figure 15: Early version of the Revised Gimbal Test Stand

In this revised design a very small yaw link is fixed to the helicopter. The pitch link is isolated from the helicopter yaw, but rolls and pitches with the helicopter. The roll link is isolated from both yaw and pitch.

This approach has several advantages over the original design. First, it greatly improves the stability of the system by reducing the load on the yaw bearing. Also, by mounting the helicopter directly to the yaw axle, the number of large links is reduced to two, significantly reducing stand inertia. Finally, the support structure can support either the pitch link or the roll link. This allows critical flexibility in the final implementation.

Range of Motion	Unlimited rotation in three attitude degrees of freedom
Size	Must operate without interference in a floor area of 15'x15' and a height of 8.5'.
Balance	
Yaw balance	The yaw axis must be inline with the helicopter's centre of mass. The yaw axis must be parallel to the rotor shaft.
Pitch balance	The pitch axis must be perpendicular to the yaw axis. The pitch axis must be inline with the centre of mass of the helicopter plus moving parts (yaw link, yaw joint, and pitch link).
Roll balance	The roll axis must be perpendicular to both the yaw axis and the pitch axis. The roll axis must intersect the pitch axis at the centre of mass of the roll link.
Inertia	The helicopter's centre of mass must be as close as possible to the combined centre of mass of the yaw link, yaw joint, and pitch link.
Stand Inertia	The stand inertia should be less than the helicopter's inertia about each axis of rotation.
Deflection	Stand links must deflect less than 1 cm under 100N load.
Position Sensing	An optical encoder must be provided on each axis.
Electrical	
Motor Power Supply	2-wire 50A slipring on each joint (yaw, pitch and roll)
Optical Encoders	4-wire low current slipring on pitch joint, and 6-wire low current slipring on roll joint.

Table 1: Test Stand Design Requirements

Chapter 4

Design Review

With the specifications set, the detailed design of the test stand was addressed. The objective was broken into five major components: the Helicopter Mount, the Yaw Bearing, the Pitch Frame, the Stand Supports, and the Roll Frame. This chapter summarizes the most important issues regarding the design and construction of these five components. Detailed documentation is included in the Appendices and is referenced in the pertinent section.

4.1 Overview of Current Configuration

The test stand as constructed to date consists of a fully functional 2 DOF test stand made up of the first four components. The preliminary design of the fifth component, the Roll Frame, is also complete.

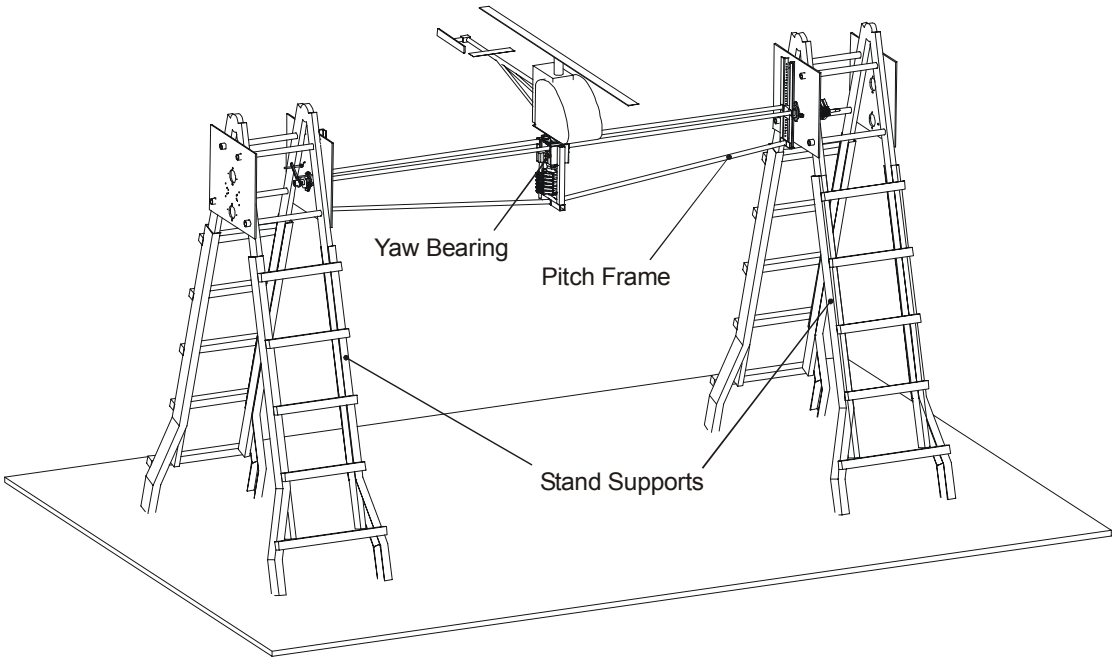

Figure 16: Current test stand configuration

With the exception of the Roll Frame the current stand configuration meets all of the specifications as outlined in Table 1. However, in practice the joints are limited to ± 4-6 revolutions because joint sliprings are not in use. The sliprings add significant mass and friction to the stand, and current experimentation does not require truly unlimited rotation.

A manual for the set-up and operation of the 2 DOF test stand is included in Appendix A, and a complete bill of materials along with as built drawings for the 2 DOF test stand are included in Appendix B. Notes on the design of new parts, and implementation of improvements, as described throughout this chapter are included in Appendix C.

4.2 Helicopter Mount

As detailed in Section 3.3.3 and Section 3.3.4 balancing the system is critical. To this end an x-y-z- position adjustment, located where the helicopter would mount to the yaw shaft, was envisioned. Several designs were considered and rejected over weight and size concerns.

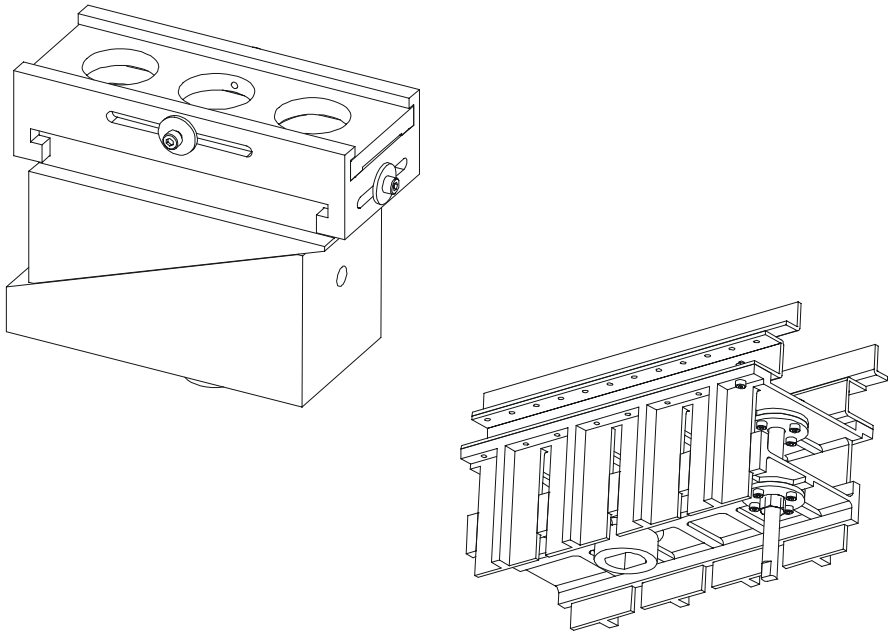

Figure 17: Some rejected x-y-z- adjustment mechanisms

The lightest of the x-y-z- adjustments considered would have been over 1 kg, and would have added at least 10 cm of separation between the helicopter and the yaw bearing.

In fact, the helicopter is inherently balanced laterally, in the y-axis of the Body CS, so lateral balance adjustment is not essential. Also, to improve handling qualities ballast is often added to adjust longitudinal balance[9], so no longitudinal adjustment is required.

[9] Ray's Complete Helicopter Manual, [12], suggests that a slightly nose down balance is best for flying qualities on an RC Helicopter.

Balance adjustment in the z-axis remains critical. However, to minimize inertia, the z-axis separation of the helicopter from the yaw bearing and pitch frame, must be minimized. Instead of adjusting the z-axis height at the helicopter mounting position as envisioned, the height of the pitch shaft is adjusted relative to the pitch frame. This mechanism will be discussed in Section 4.4.

The final helicopter mounting mechanism is a block that replaces the fuel tank support in the lower frame of the helicopter. The block has a threaded hole to accept the yaw shaft.

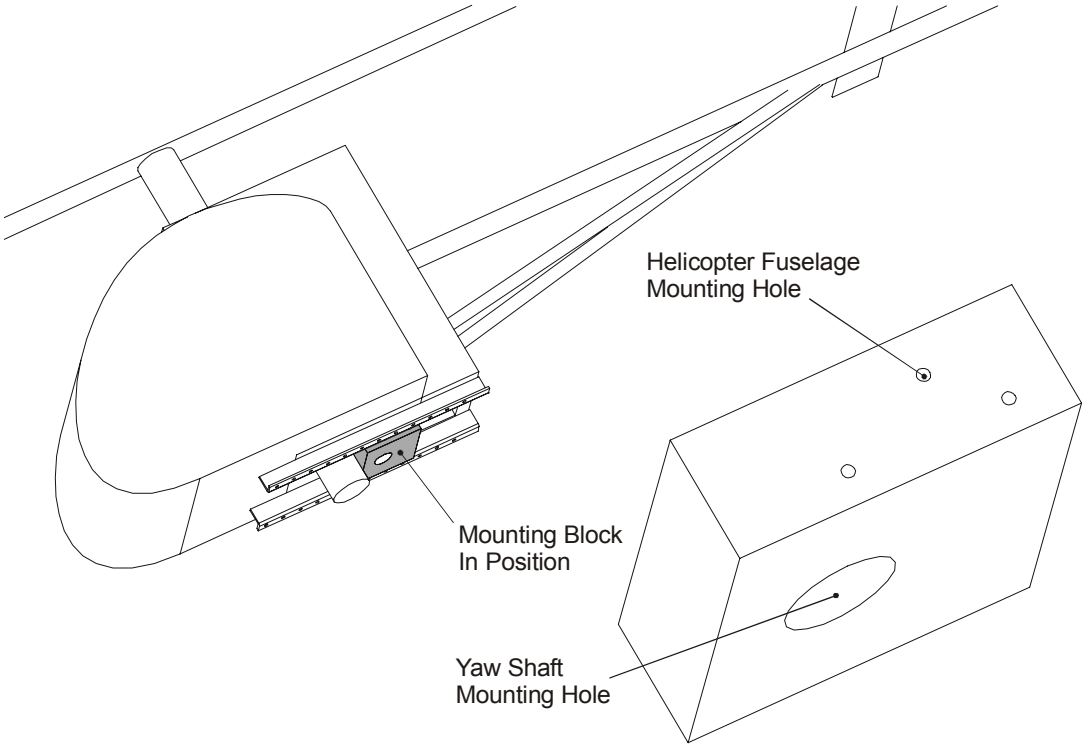

Figure 18: Helicopter Mounting Block

A concept drawing for a mounting block that provides longitudinal balance adjustment is presented in Appendix C.

4.3 Yaw Bearing

The yaw bearing design was shaped by several requirements. The yaw shaft diameter must be close to 1” to accommodate a 1/2” hole for wiring. Standard deep groove bearings designed for 1” diameter shafts can easily stand up to the loads applied by the helicopter so detailed load analysis was not necessary. A standard two bearing arrangement called cross-location was chosen for its simplicity, and its ability to adequately stabilize the shaft [13].

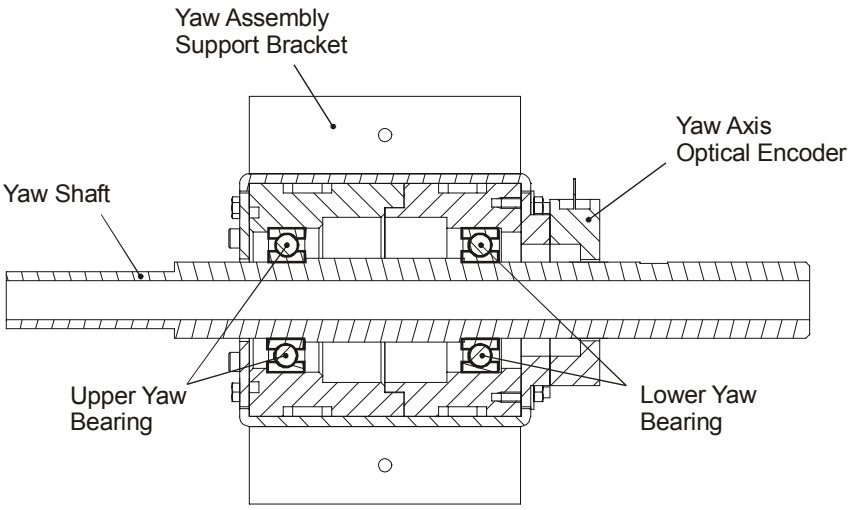

Figure 19: Yaw bearing cross section showing bearing arrangement.

Cross-location involves a shaft with a raised centre section. Two bearings sit against each side of the raised section on the shaft. Bearing blocks close over the outside of the bearings like a clamshell. In this way axial motion of the shaft is not possible.

The yaw subsystem must also provide attachment facilities for a slipring and an optical encoder.

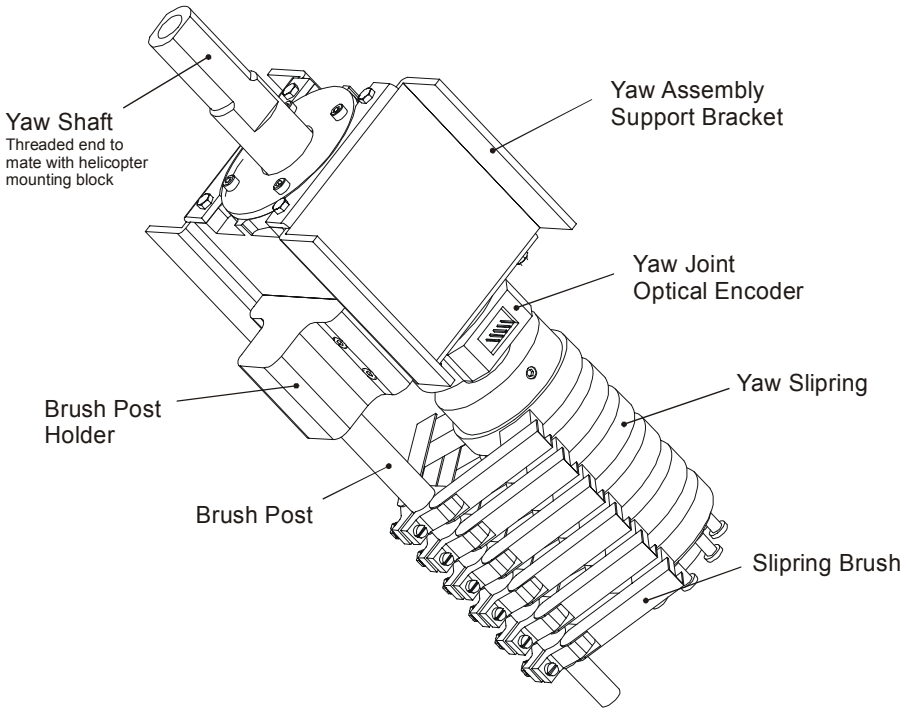

Figure 20: Final Yaw Subsystem

The yaw slipring brush post holder in Figure 20 has not been fabricated and the sliprings are not currently in use. The design for the slipring brush post holder as pictured, and a simplified alternative can be found in Appendix C. An alternative bearing arrangement with lighter bearing blocks has been considered; details are presented in Appendix C. The yaw bearing without sliprings weighs 1.75 kg; the improved arrangement is expected to weigh a little over 1 kg.

4.4 Pitch Frame

The pitch frame should be as simple and light a structure as possible, but stiff enough to support the load of the helicopter and main rotor thrust, as outlined in the stand specifications.

As mentioned in Section 4.3, the pitch frame must also provide z-axis balance adjustment. This was accomplished by allowing the pitch shafts to be raised and lowered relative to the yaw bearing mounting position. Of course the pitch frame also had to provide attachment facilities for a slipring and optical encoder. The final pitch frame is shown below.

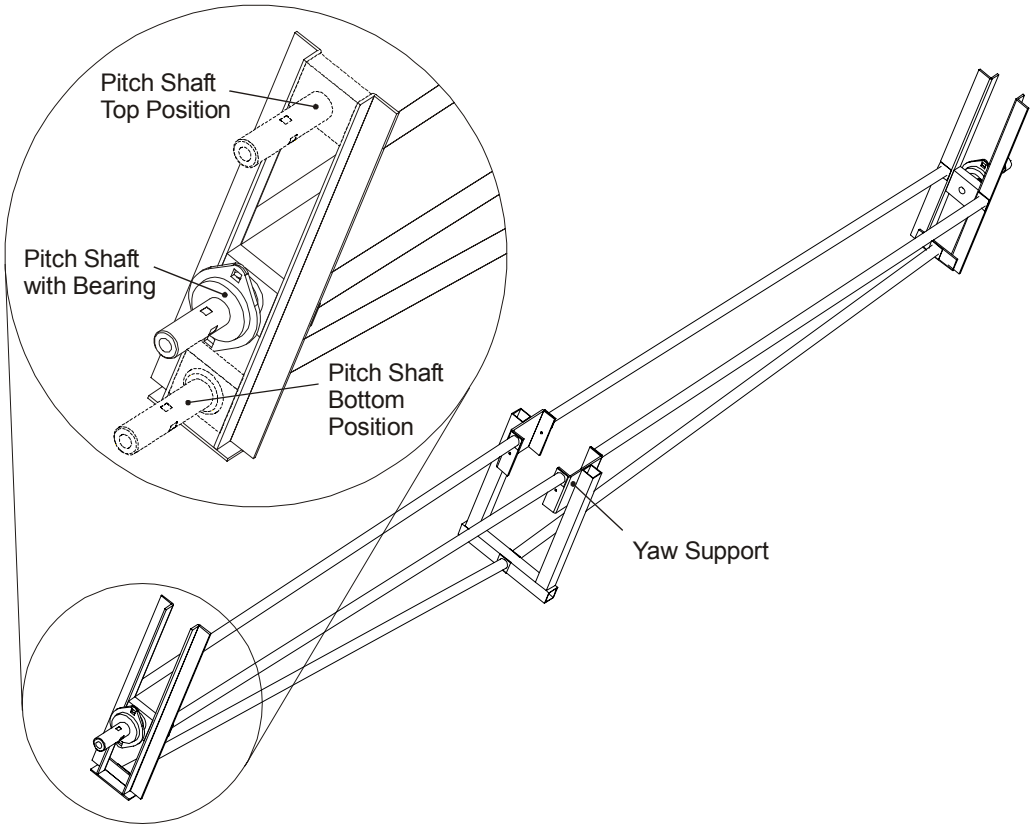

Figure 21: Pitch Frame

The structure of the pitch frame was simulated using static structural simulation software. The static deflection of the completed pitch frame is consistent with the simulations, and meets the specified maximum deflection of 1 cm for a 100 N load. Under dynamic load, however, the structure oscillates. Excited near resonance the deflection can be large. However, the helicopter does not excite the pitch link near its resonance so the

compliance under dynamic load is not considered to be a problem. Nonetheless, ideas for improving the stiffness of the current design are presented in Appendix C. The pitch frame is the heaviest part of the stand, at 3 kg, any measure to stiffen the frame must not add significantly to the mass.

Finally, a helicopter mounting plate that eliminates the yaw bearing has been designed, and is presented in Appendix C. This plate would allow the stand to be reconfigured in several new ways at the cost of losing one degree of freedom.

4.5 Stand Support

The stand support structure must be strong and stable to transfer loads imparted by the helicopter to the ground without shifting. Custom designed supports as initially envisioned would have been expensive and cumbersome. It was found that an ideal off the shelf solution existed. A particular type of adjustable height stepladder with parallel side rails was chosen. The stepladders are lightweight and compact when folded, but they are stable under heavy dynamic loads. Also, the height adjustment mechanism adds considerable flexibility to the test stands configuration space.

Adapter plates were attached to the ladders to allow for bearing, slipring and encoder mounting. The adapter plates also allow for fine-tuning of the support height, and provide ample space for future modifications. The wide separation between the stand supports makes axial alignment of the bearings difficult. To address this problem stamped flange-mount ball bearings, which allow up to 3° of shaft misalignment, are used.

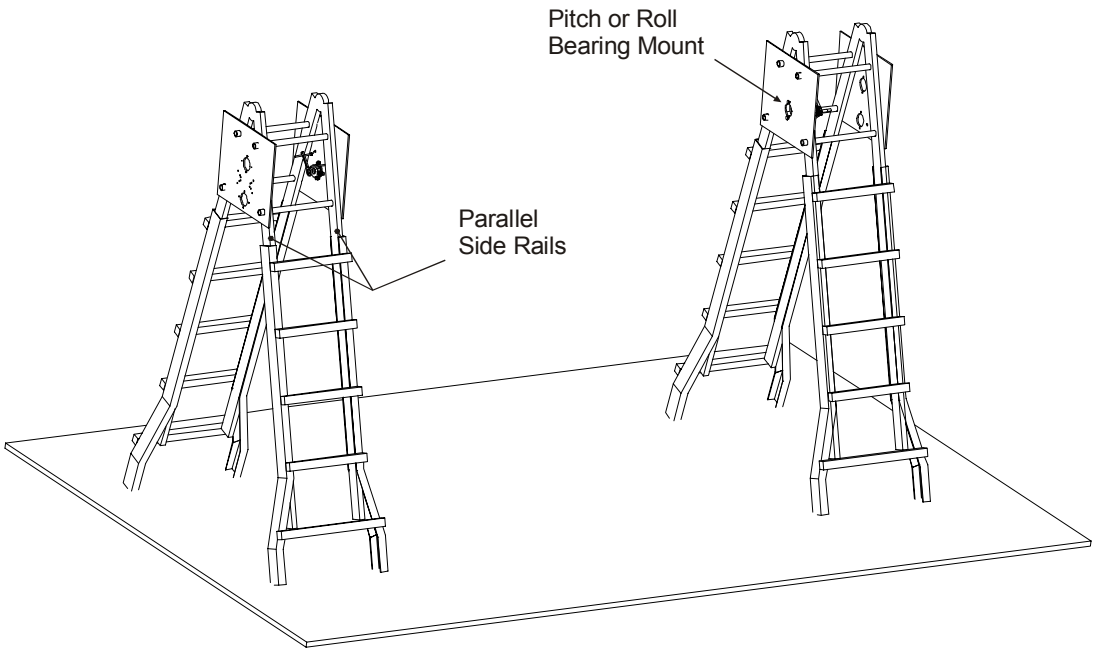

Figure 22: Stand Supports

4.6 Roll Frame

The roll frame has not been completed. Several preliminary sketches of possible structures have been considered. In order to meet the balance requirement the roll axis must intersect the pitch axis at the centre of mass of the roll link. For unlimited rotation the roll link must also provide a wide enough opening for the helicopter to freely pitch and yaw. The design depicted in Figure 23 below meets these basic geometrical requirements.

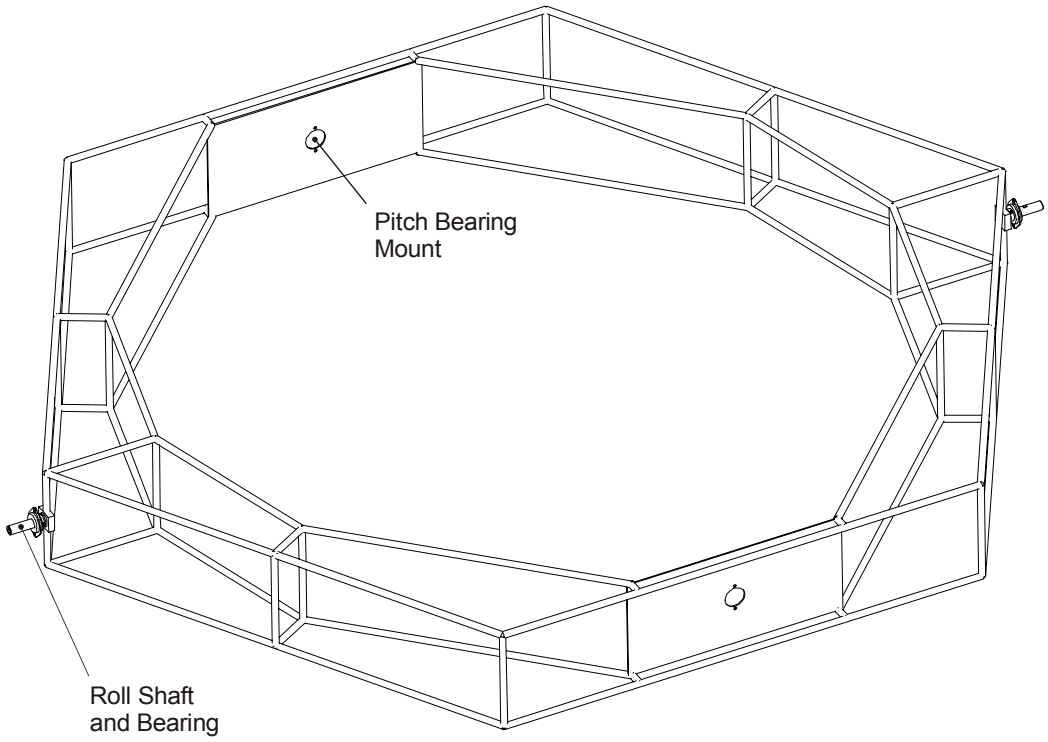

Figure 23: Roll frame concept

This design is expected to meet the specification for deflection under load. However, the structure is expected to weigh 8 kg, considering the geometry this must represent extremely high inertia relative to the helicopter. Also, due to the large diameter of this structure, a folding or disassembly mechanism is needed; this will increase the weight further.

The roll frame uses the same axles, bearings, optical encoders, and sliprings used in the pitch frame. Thus the stand supports can work equally well with either the pitch frame or the roll frame.

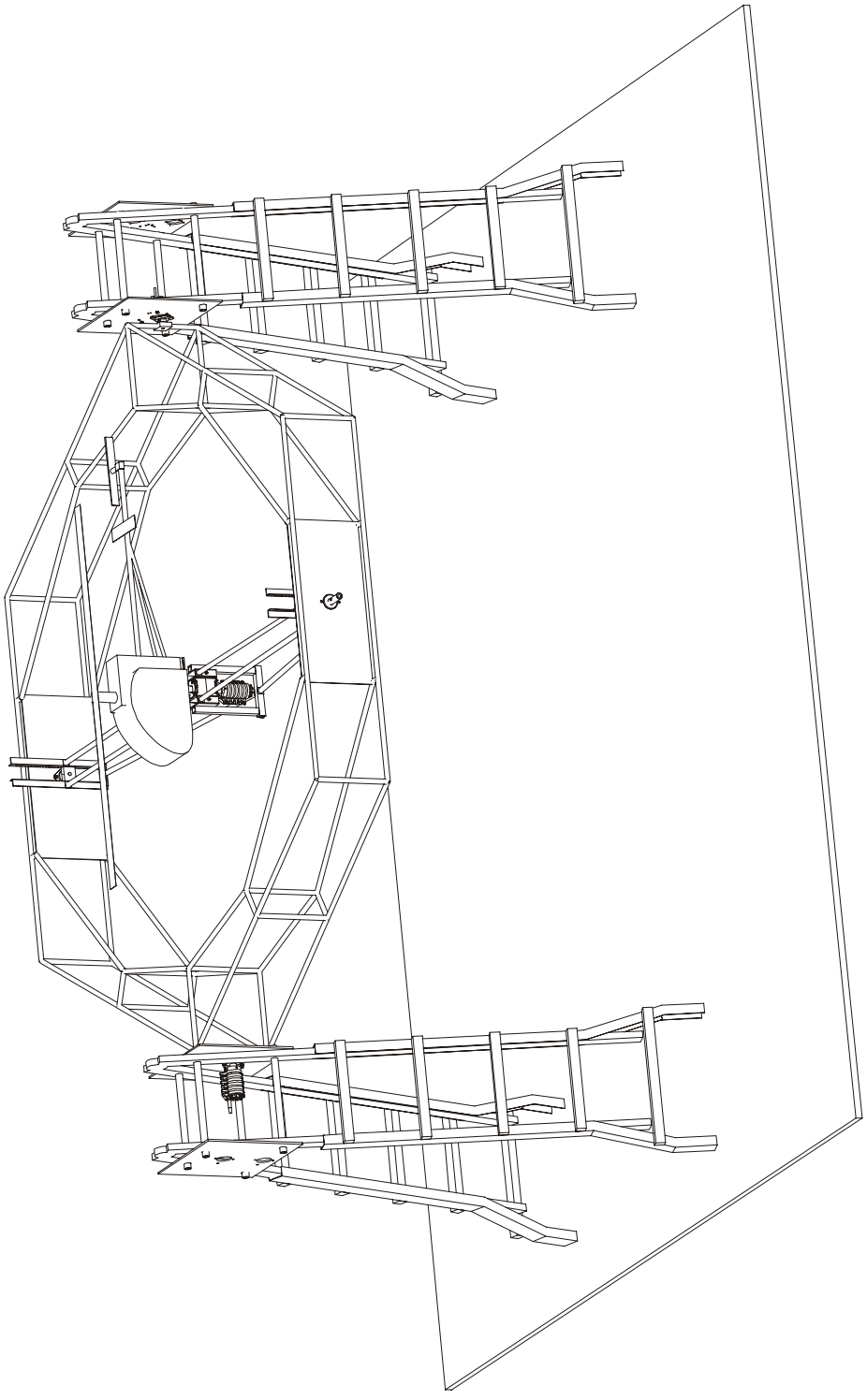

Figure 24: Full 3 DOF Test Stand Design

Chapter 5

Associated Equipment

This chapter contains descriptions and specifications for all of the equipment associated with the helicopter test apparatus. It has been broken into two parts; the first part discusses the RC hobby industry equipment, the helicopter, actuators, and power plant, the second part discusses the data acquisition system and the test stand itself.

For instructions on the use of the test stand and the data acquisition system refer to the manual included in Appendix A. For instructions on the use of the RC hobby industry related equipment, refer to the manual for the specific part, or refer to Ray's helicopter manual [12].

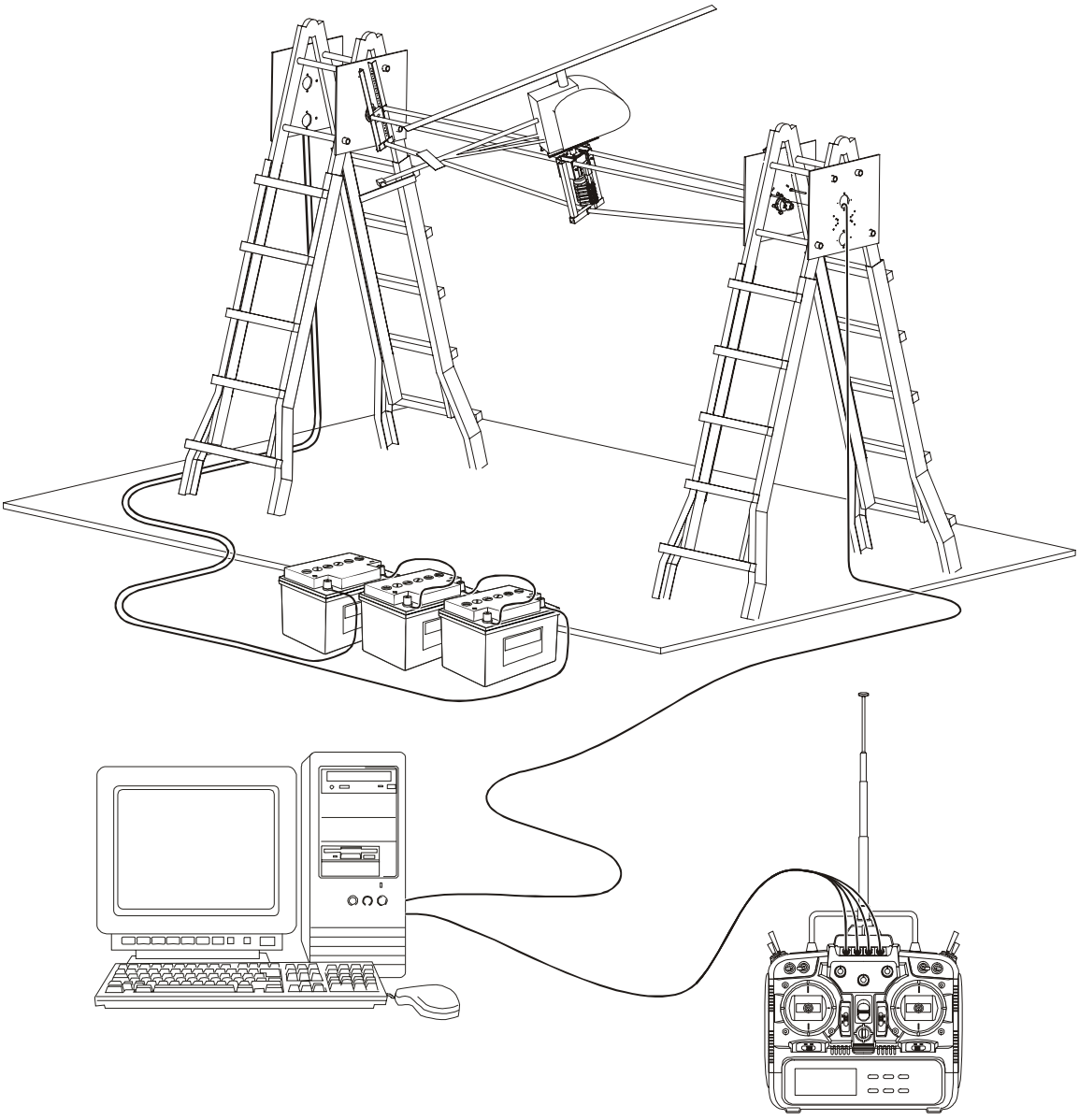

Figure 25: Test System

5.1 RC Hobby Equipment

The required equipment to fly an RC helicopter includes the helicopter itself, the power plant, and the radio control and actuation system.

An RC helicopter is bought as a complete kit, which contains the entire airframe including all mechanical control linkages, and the transmission. The standard power plant is a nitro methane engine built specifically for hobby flying, but gasoline engines and electric motors are sometimes used. The radio control and actuation system is made up of a radio transmitter, which accepts the pilots input, performs some open loop control operations, and broadcasts control signals to the helicopter. The signals are picked up by a radio receiver on the helicopter and sent to actuators. The actuators, called RC servos, are small high torque motors under local closed loop control to provide precise position tracking. The RC transmitter can be seen in Figure 25, and all other RC subsystems are shown in Figure 26.

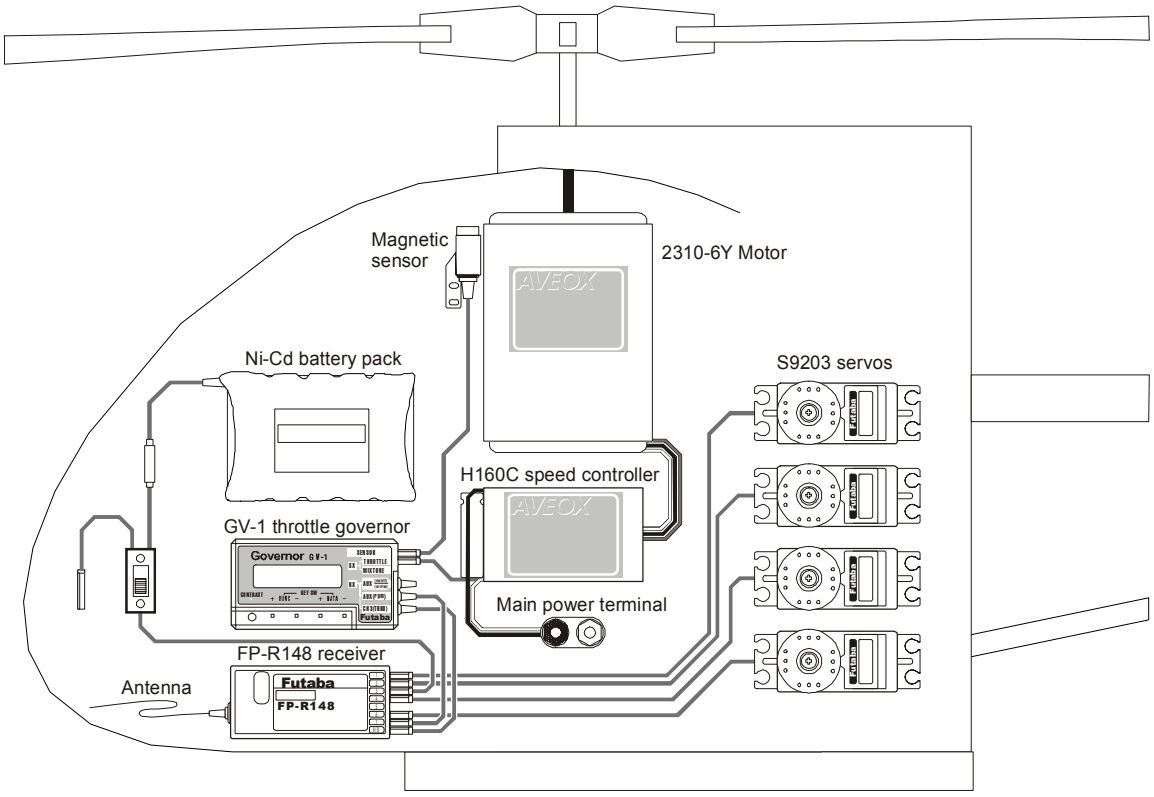

Figure 26: Onboard RC subsystems

5.1.1 Helicopter

The Helicopter model used for this project is a TSK MyStar60. It is currently run in stock configuration, with one exception. The engine mount, fuel tank, and fuel tank support in the original kit have been omitted because the nitro methane engine they were designed for will not be used. The motor mount, which replaces the engine mount, is discussed in Section 5.1.2 and the helicopter mounting block, which replaces the fuel tank support, is discussed in Section 4.2. Table 2 lists some specifications for the MyStar60.

TSK MyStar60 (Helicopter)	
Mass	4-5 kg
Length	1.5 m
Width	15 cm
Height	47 cm
Main Rotor Ø	1.5 m
Tail Rotor Ø	26 cm
Rotor Speed (free flight)	1500-2000 RPM
Gear Ratio	9.55 : 1
Engine Power	1500 W

Table 2: Helicopter Specifications

More information about the helicopter and its operation can be found in the MyStar60 Manual [11], and in Ray's Complete Helicopter Manual [12].

5.1.2 Power Plant

Because of noise and exhaust the standard nitro-methane internal combustion engine is not suitable for indoor use. Instead, an Aveox 2310-6Y brushless DC motor and H160C speed controller were chosen to power the main rotor. Aveox motors and speed controllers are standard RC hobby equipment, but they are not normally used with the MyStar60. A custom motor mount to replace the stock engine mount was needed. A drawing of the motor mount can be found in Appendix B.

Aveox 2310-6Y	
Maximum Power	3200 W
Maximum Speed	10,000 RPM
Speed Constant	360 RPM/Volt
Torque Constant	3.756 InOz /Amp
Input	3-phase power
Output	3-phase hall sensor
Size (L x Ø)	2.75” x 2.25”
Mass	740 g

Table 3: Motor Specifications

Aveox H160C	
Maximum Voltage	50 V
Maximum Current	70 A (<1 minute or well cooled)
Input	Throttle, compatible with RC servo control signals 3-phase hall sensor from motor
Output	3-phase power to motor
Size (L x W x H)	2.4” x 1.25” x 0.60”
Mass	60 g

Table 4: Speed Controller Specifications

The main rotor should spin at 1,750 RPM. With the helicopter’s stock transmission gear ratio of 9.55:1 the motor would then have to spin at 17,000 RPM; however, maximum speed of the 2310-6Y is only 10,000 RPM. This discrepancy will have to be resolved when flight on the stand is meant to very closely mimic free flight.

Three 12 Volt marine lead-acid batteries power the motor and speed controller. At full charge the batteries provide about 14 Volts each, which is ideal for powering the motor to full speed with a little headroom for line and controller losses.

5.1.3 Radio Control and Actuation

The helicopter pilot applies input to the RC radio transmitter. Pilot commands are entered by manipulating two joysticks for the primary flight controls, and a variety of switches and trim pots for auxiliary control. In this project, a Futaba T8UHPS 8-channel transmitter with custom modifications is used. Four 3.5mm stereo miniplugs have been added to the transmitter to interface with the data acquisition system; this modification is discussed briefly in Section 5.2, and a schematic showing the modification is presented in Appendix E. Some important specifications for the Futaba T8UHPS are presented in Table 5.

Futaba T8UHPS	
Input: Pilot Controls	8 RC servo control signals (or channels) 1: Aileron (lateral cyclic pitch), right stick x-axis 2: Elevator (long. cyclic pitch), right stick y-axis 3: Spare* 4: Rudder (tail rotor pitch), left stick x-axis 5: Spare** (opt. gyro control switch) 6: Pitch (collective pitch), left stick y-axis 7: Throttle Governor control switch 8: Throttle*, channel 8 trim pot
Input: Additional***	Left stick override, 3.5mm stereo miniplug Right stick override, 3.5mm stereo miniplug
Output: Transmitted	RF modulated pilot controls
Output: Additional***	Left stick monitor, 3.5mm stereo miniplug Right stick monitor, 3.5mm stereo miniplug

* Channel 3 is normally throttle control, the signal is permanently connected to the left stick y-axis, and thus coupled to the collective pitch. Channel 8 allows throttle adjustment with a dedicated trim pot

** Channel 5 is normally used to control a yaw axis gyro, not implemented for this project

*** Additional inputs and outputs are custom modifications for interfacing with the data acquisition system

Table 5: Transmitter Specifications

Four Futaba S9203 servos actuate Collective Pitch, Aileron, Elevator, and Rudder on the MyStar60. These servos are in the upper range of performance for RC hobby use. The specifications are listed in Table 6.

Futaba S9303	
Control Signal	PWM (angle proportional to pulse width)
Signalling Frequency	50 Hz
Size (L x W x H)	1.59" x 0.79” x 1.56”
Mass	65 g
Speed	250 °/s @4.8V
Torque	79.9 oz-in (0.58 N·m) @4.8V

Table 6: Servo Specifications

A Futaba GV-1 throttle governor controls the helicopter’s throttle. Normally the speed of the power plant described in Section 5.1.2 is very well regulated and does not require additional control. The governor has been added for convenience; it allows the operator to reliably “set and forget” the rotor speed. Important specifications for the Futaba GV-1 are listed in Table 7.

Futaba GV-1	
Sensor	Magnetic revolution counter
Input	3-pos. Switch, Speed 1 - Pilot pass-through - Speed 2 Pilots throttle control
Output	Throttle control
Regulation	1%

Table 7: Throttle Governor Specifications

All of the onboard electronics receive control signals through a Futaba R148DP Receiver.

Futaba R148DP	
Input	RF signal from Transmitter (T8UHPS)
Output	8 individual RC servo control channels

Table 8: Receiver Specifications

Finally, all of the onboard electrical systems, except the motor, are powered by a 4.6V rechargeable nickel cadmium battery pack.

5.2 Data Acquisition System

The core of the data acquisition system is a Sensoray 626 Multifunction I/O PCI Board. The board is installed in a standard Pentium II class PC running the QNX operating system. The Sensoray 626 is connected to the stand's optical encoders to sense position, and to the RC transmitter to control the helicopter. Customized software on the PC can sense and store the stand position and the radio's joystick positions, read and apply signals from a data file, and implement arbitrary closed loop controllers.

Some specifications for the Sensoray 626 are listed in Table 9.

Sensoray 626	
Input	16 16-bit analogue to digital converters 6 counters, preconfigured for use with standard quadrature optical encoders
Output	4 13-bit digital to analogue converters
Other I/O	48 Digital I/O lines, 20 with interrupt capability
Conversion time	A/D conversion 20μs/channel D/A conversion 200μs/channel
Interface	PCI 2.1
Drivers	QNX, Linux, Windows NT/98/ME/2000

Table 9: Data Acquisition Card Specifications

The interface between the Sensoray 626 and the optical encoders will be discussed in Section 5.2.1. The interface between the RC transmitter and the Sensoray 626 will be discussed in Section 5.2.2.

5.2.1 Data Acquisition Card & Optical Encoders

The Sensoray 626 has six counters, which are preconfigured for compatibility with various types of optical encoder. The encoder of choice for the test stand was the U.S.

Digital E3 series quadrature encoder with 2048 cycles per revolution. The resolution of a quadrature encoder is 4x the cycles per revolution, in this case 8192 steps, or 0.044° per step.

To achieve this resolution in practice is very difficult. Any small misalignment will skew the data. The encoders are unlikely to accurately resolve 8192 steps when mounted to the stand. However, when attached to the stand with care, it can be observed that the optical encoders are accurate beyond the operator's resolution, without using exotic mechanical aids.

For a drawing of the electrical connection, see Appendix D. For details regarding the use of the encoders, see the U.S. Digital E3 series datasheet [14], and the Test Stand Manual in Appendix A.

5.2.2 Data Acquisition Card & RC Transmitter

The Sensoray 626 has 4 D/A channels and 16 A/D channels. The RC transmitter interface requires all 4 D/A channels to monitor the 4 pilot controls, and 4 A/D channels to drive the 4 actuators.

The D/A channels have 13-bit resolution and output voltage in the range of ±10V, or 0.0012V per step. The RC radio requires a voltage in the range of 1-3V for full swing of the RC servos, which is equivalent to 1600 steps. This is comparable to the 9-bit, or 1024 step, resolution of the RC transmitter. The A/D channels have a 16-bit resolution. Over the 1-3 volt operating range of the RC radio this represents 13,000 levels, far more resolution than is necessary to accurately represent the signal.

D/A conversion takes 200 μs/channel, and A/D conversion takes 20 μs/channel, the encoders and software operate very quickly compared to these figures, so overall cycle time is less than 1 ms. The RC servo control signal has a cycle time of 20 ms, and it is asynchronous to the data acquisition card. The synchronization of the Sensoray 626 and the RC transmitter can interfere with some types of experiments, but in general synchronization can be ignored as long as the cards sample rate is kept high, over 500 Hz.

5.3 Motor Power Supply

Finally the helicopters motor receives power from a bank of three 12V marine use lead acid batteries. The batteries are controlled and charged via a custom built switch box. For information on the switch box see Appendix D.

Chapter 6

Validation

To demonstrate the stand's functionality and data gathering capabilities, a system identification experiment was performed. The results confirm that the test system is accurate and reliable.

The test system is a powerful tool for a variety of potential investigations. However, the scope of the identification experiment performed is limited, the model extracted is not intended to represent helicopter dynamics.

A simple experiment investigating the Single Input Single Output (SISO) behaviour of the helicopter's longitudinal dynamics is described in 6.1. Analysis of the data using standard linear SISO identification tools is discussed in 6.2.

6.1 Experiment

The experiment was designed to operate the helicopter and associated systems under realistic conditions. The helicopter and associated equipment was set up as described in Appendix A, the Test Stand Manual, with the following additional conditions.

1. Using ballast, the helicopter was trimmed to balance on the stand in the x- and y- axes. The helicopter's centre of gravity was set just below the pitch axis.

2. The collective pitch control was held constant such that the main rotor would produce a moderate positive lift. The lateral cyclic pitch was held constant at the zero input value.

3. The experiment software was configured with a 20 second start up period to allow the main rotor time to reach 7,000 RPM. During this time, tail rotor pitch was controlled manually.

4. After the initial period, a 70 second experiment was begun. During the experiment, the helicopter's yaw was stabilized by constant gain feedback to the tail rotor pitch.

5. The yaw axis was set such that the helicopter was free to pitch but constrained in roll. The pitch limiter was in place at the ±45° position to prevent extreme motion.

The experiment configuration is similar to Figure 25 and the experiment signal flow block diagram is presented in Figure 27.

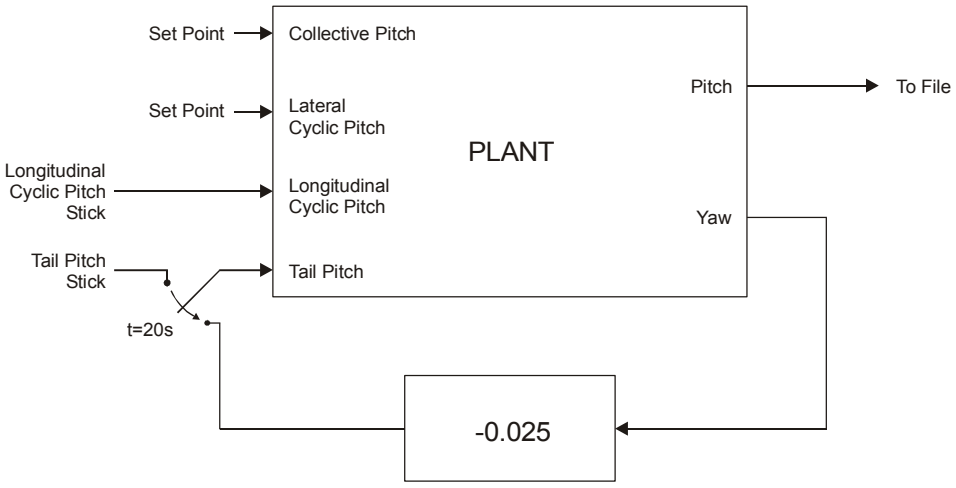

Figure 27: Experiment Block Diagram

At the end of the 20 second preliminary period the system is SISO. Longitudinal Cyclic Pitch input data and Pitch output data for several iterations of the experiment were stored for analysis.

6.2 Analysis

SISO data from the experiments was brought into MATLAB for analysis; a sample dataset is presented in Figure 28.

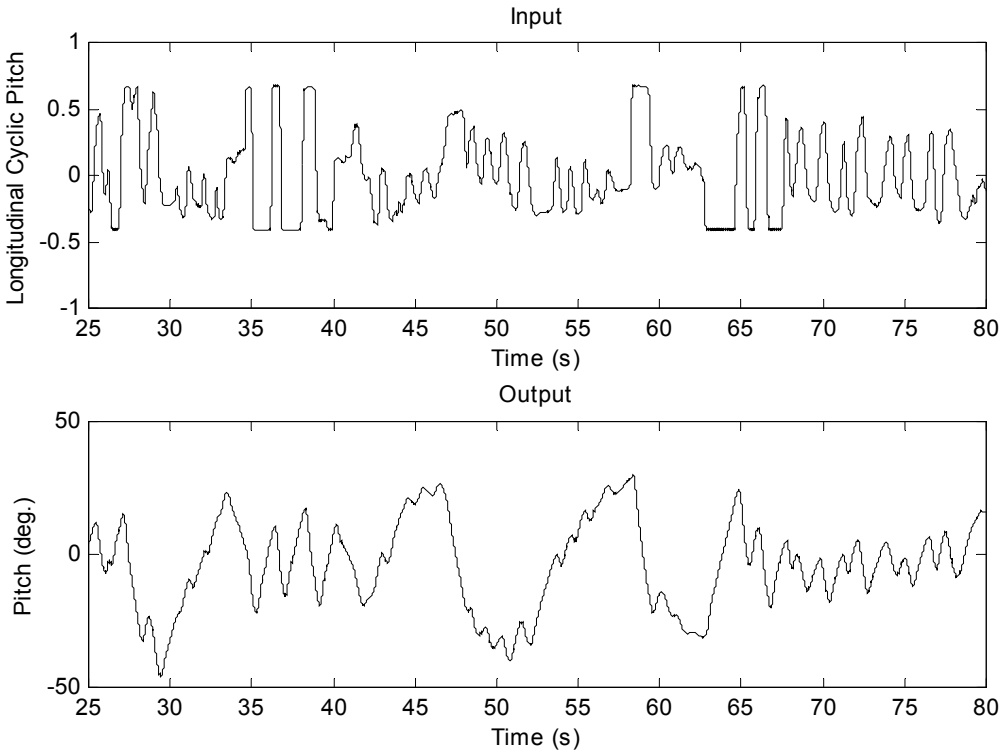

Figure 28: Data used for System Identification

Using the System Identification Toolbox several standard linear black box identification methods were investigated. It was found that a 2nd order state space model generated with the prediction error method closely matched the response of the system. This method was

used to extract a model from the sample dataset in Figure 28[10]. The continuous time equivalent to the identified model is shown in (6.1), followed by the pole zero map, Figure 29.

$$H(s) = \frac{371(s-14)}{(s+0.1)(s+78)} \tag{6.1}$$

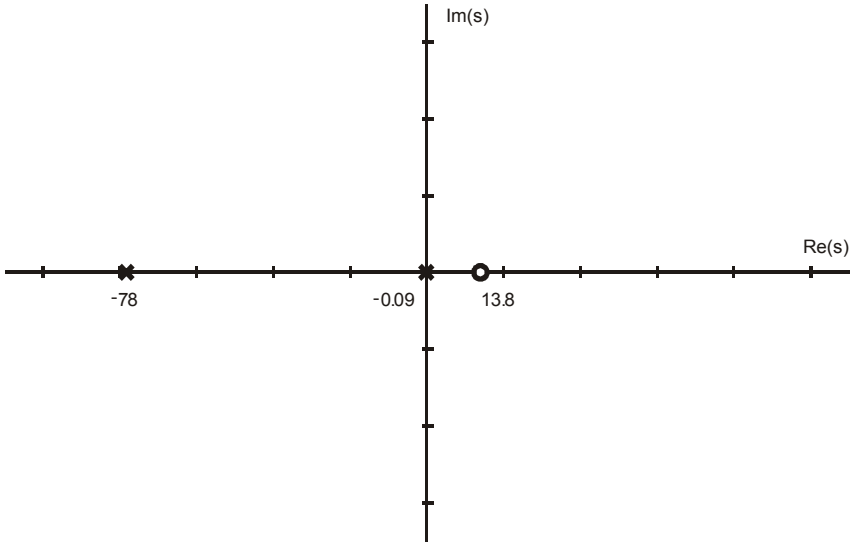

Figure 29: Pole Zero Map

[10] The prediction error method was invoked using the CANSTART and then PEM commands in version 4.0.5 of the System Identification Toolbox and MATLAB 5.3.

The identified model was simulated using a unique dataset. The simulated output is compared to the actual system output in Figure 30.

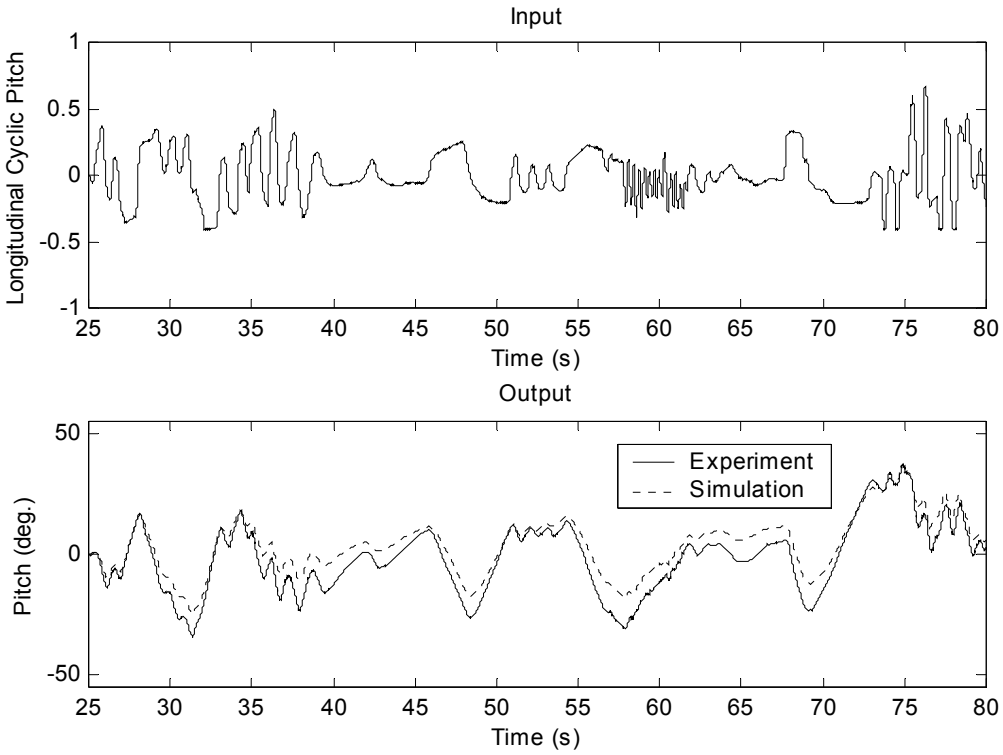

Figure 30: Verification of Identified Model

A further investigation into the repeatability was made. The data from three iterations of the experiment was partitioned to form 11 datasets of 15 second duration. A model was extracted from each dataset. Results for three of the 11 datasets were inconsistent; the remaining 8 agreed well with the system in Figure 29. The gain, and pole/zero locations for the 11 models are listed in Table 10 along with Bode plots for the 8 models in Figure 31.

	Pole #1	Pole #2	Zero	Gain
Model 1	-107	-0.041	4.5	683
Model 2	-102	-0.139	14.5	491
Model 3*	-75	-0.042	-16.8	211
Model 4	-86	-0.140	13.3	545
Model 5*	-43	-0.290	-6.9	351
Model 6*	-109	0.001	2.6	31
Model 7	-102	-0.042	7.0	525
Model 8	-86	-0.120	8.8	632
Model 9	-112	-0.147	9.9	870
Model 10	-69	-0.040	8.5	365
Model 11	-96	-0.275	8.4	869

∗ Models 3, 5 and 6 not included in Bode plots. Models 3 and 5 have minimum phase zeros which cause large discrepancy in their time response. Model 6 has an unstable pole.

Table 10: Model Consistency

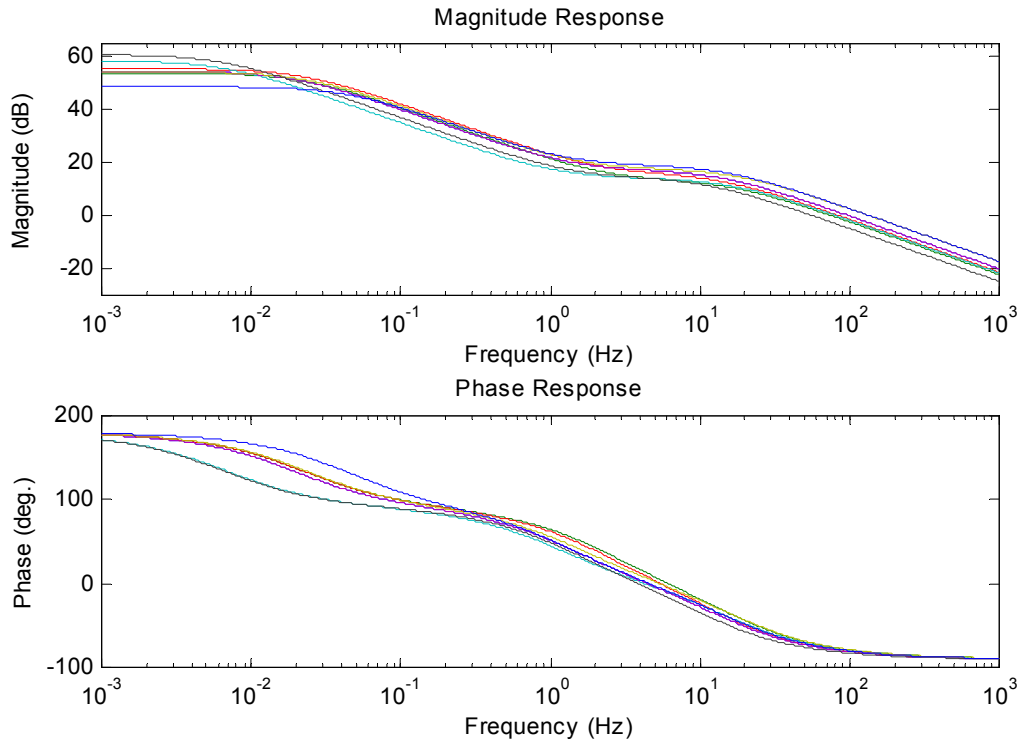

Figure 31: 8 Model comparison in Bode plot

Chapter 7

Conclusions and Future Work

A detailed discussion of the design, construction and verification of a robust apparatus for the flight testing of a model helicopter has been presented. This apparatus was required to mimic free flight while facilitating safe indoor operation and motion tracking through a computer interface. To achieve this goal, the gimbal test stand was designed and built. Simple system identification experiments were performed to validate the stand's performance. The results of the validation experiments confirm that the data acquisition system provides accurate, reliable and repeatable measurements. In addition, the apparatus constrains the helicopter with minimal compliance during operation. While several additions and improvements can be made to enhance the stand's functionality and performance, the work presented in this thesis represents the completion in principal of the model helicopter flight testing apparatus.

Several additions to the gimbal test stand are anticipated. Currently, the stand is limited to two degrees of freedom. However, a design for the third degree of freedom is complete as discussed in Section 4.6. The apparatus is also limited to approximately 5 revolutions in one direction about any axis. Completely unlimited rotation can be implemented readily

by fabricating a Brush Post Holder as discussed in Section 4.3. Finally, to add flexibility to the stand's configuration space the yaw eliminator has been designed, as discussed in Section 4.3.

Improvements to the helicopter, the test stand and the data acquisition system have been considered. The Aveox 2310-6Y electric motor does not turn as fast as the nitro-methane engine normally used in a model helicopter. The transmission gear ratio can be adjusted to better match the helicopter's intended rotor speed, as discussed in Section 5.1.2. Measures to lighten, strengthen and add trim adjustments to the test stand have been suggested throughout Chapter 4 and 5. Currently, the data clocks in the Futaba RC Transmitter and the Data Acquisition PC are not synchronous. Synchronous operation is not required, but it would increase the maximum sample rate of the data acquisition system, as mentioned in Section 5.2.2. These and other improvements are discussed throughout the thesis. However, given the effectiveness of the apparatus as demonstrated by the validation experiments, none of these measures are considered to be critical.

The gimbal test stand will be a powerful tool to aid in the development of an autonomous robot helicopter at the Systems Control Group at the University of Toronto. A wide variety of experiments can now be carried out with minimal preparation time; many such experiments would be impossible without the gimbal test stand. The primary applications envisioned for the gimbal test stand are system identification and control system development. The gimbal test stand will also be invaluable in the development of onboard position sensors. Finally, the gimbal test stand will provide reliably performance estimates in real world conditions for all the systems on the robot helicopter.

Appendix A

Gimbal Test Stand Manual

CONTENTS

Section

1

YAW ASSEMBLY

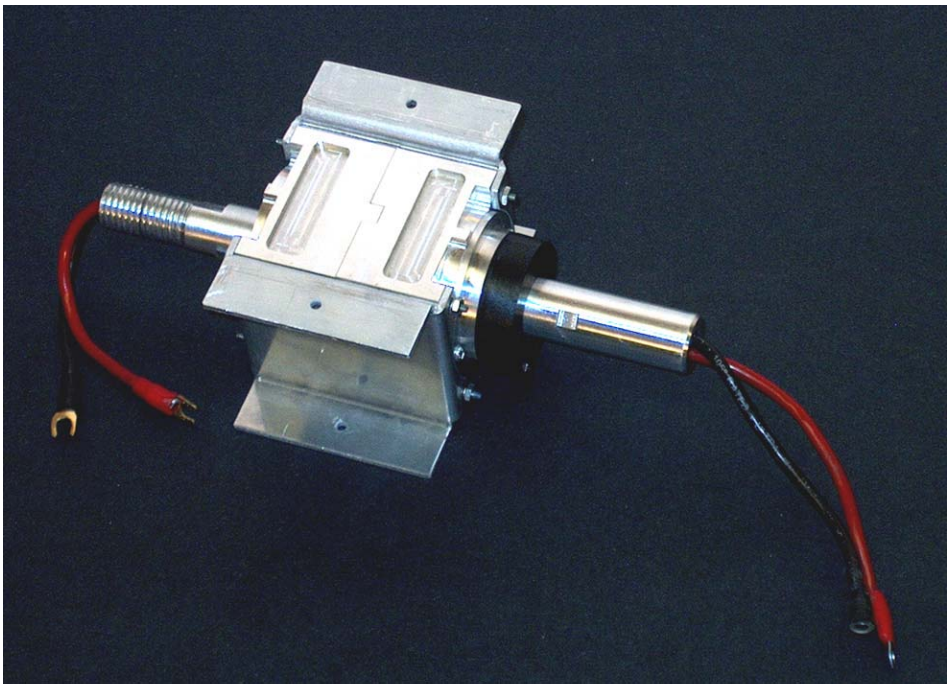

Figure 1: Completed Yaw Assembly

1.1 Before You Begin

Before attempting to assemble the Yaw Degree of Freedom Assembly, check the following:

- Confirm that all parts shown in Figure 2, and described in Table 1 are available.
- Confirm that all parts are clean and free of dust and debris. If necessary, wipe parts with a tack cloth.
- Confirm that bearings inside the Upper and Lower Bearing Housings (Figure 2: Y-1 and Y-2) are seated properly and rotate easily.

  Note: The bearings are a tight fit in the housings, not a press fit. They should not require special lubrication or service. If removal is necessary, force must be applied evenly to prevent binding. This may require a special jig.

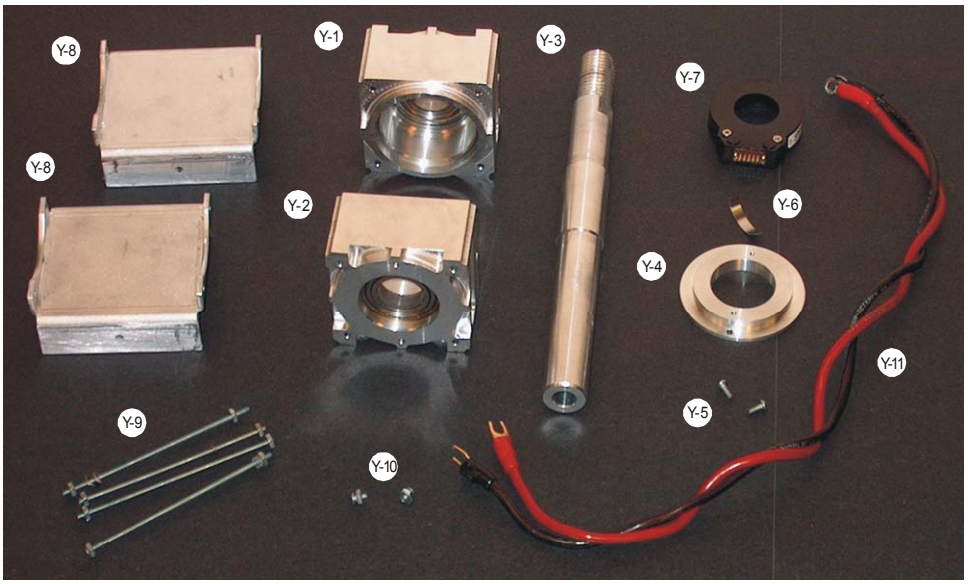

Figure 2: Yaw DOF Components

Ref.	Description
Y-1	Upper Bearing Housing (Dwg. YAW-1) Bearing (SKF 6005-2Z)
Y-2	Lower Bearing Block (Dwg. YAW-2) Bearing (SKF 6005-2Z)
Y-3	Yaw Shaft (Dwg. YAW-3)
Y-4	Yaw Encoder Support (Dwg. YAW-4)
Y-5	2x 1/2" 4-40 Machine Screws
Y-6	1.2" x .3" x .008" Shim Stock
Y-7	Yaw Encoder (US Digital E3-2048-1000-H)
Y-8	2x Yaw Assembly Support Bracket (YAW-5)
Y-9	4x 4" 6-32 Threaded-Rods 8x Lock Washers 8x 6-32 Nuts
Y-10	2x 1/4" 6-32 Machine Screws 2x 6-32 Nuts
Y-11	2x 12" 4-Guage Hook-Up Wire with Terminals

Table 1: Yaw DOF Components

1.2 Bearings

1. Fit the threaded-end of the Yaw Shaft (Figure 2: Y-3) in the Upper Bearing Housing (Figure 2: Y-1) as shown in Figure 3.

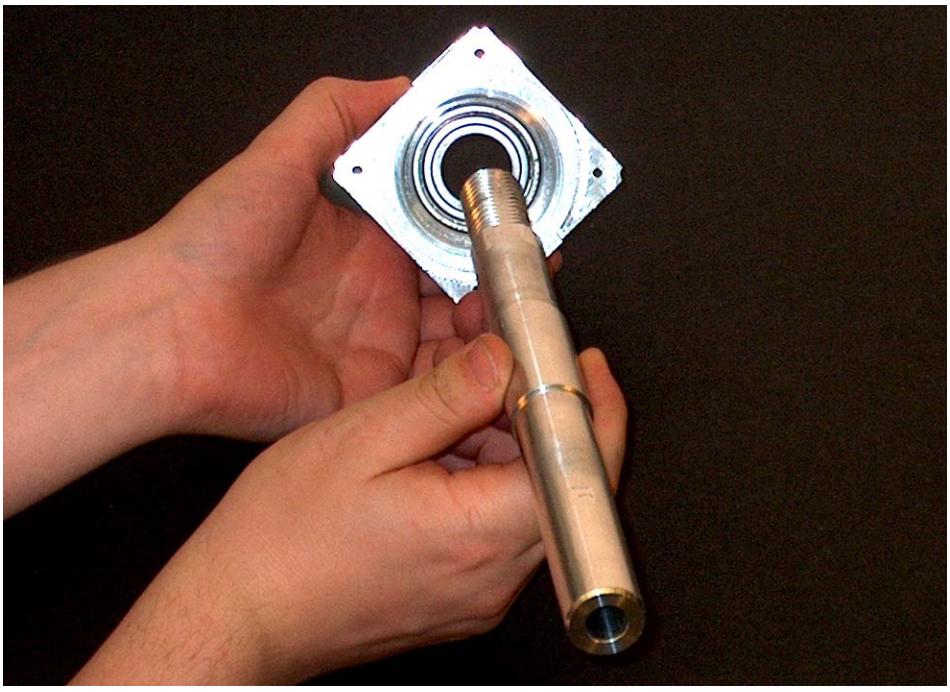

Figure 3: Insert Yaw Shaft in Upper Bearing Housing

2. Fit the non-threaded end of the Yaw Shaft in the Lower Bearing Housing (Figure 2: Y-2) as shown in Figure 4.

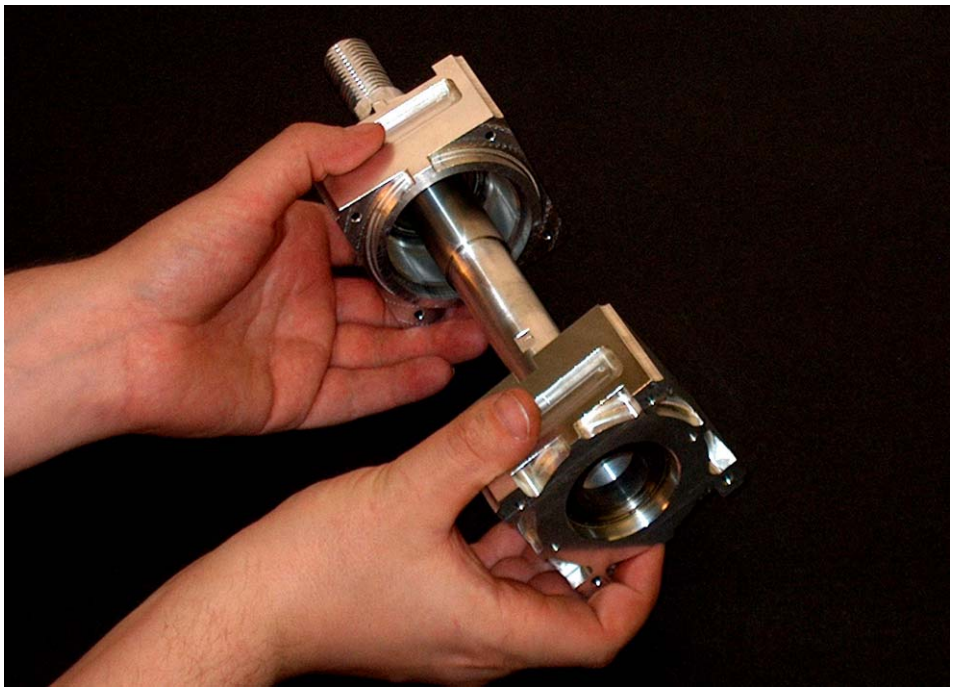

Figure 4: Slide Lower Bearing Housing into place

3. Align and push the Upper and Lower Bearing Housings together.

   Note: Keying is provided on the housings to assist alignment. Confirm that that the four through-holes parallel to the shaft are aligned. If not aligned, separate the housings and rotate the bottom housing 180º. Then, repeat step 3.

4. Attach the Yaw Assembly Support Brackets (Figure 2: Y-8) to the assembled bearing housings as shown in Figure 5. Four through holes in the bearing housings should align with holes in the support brackets.

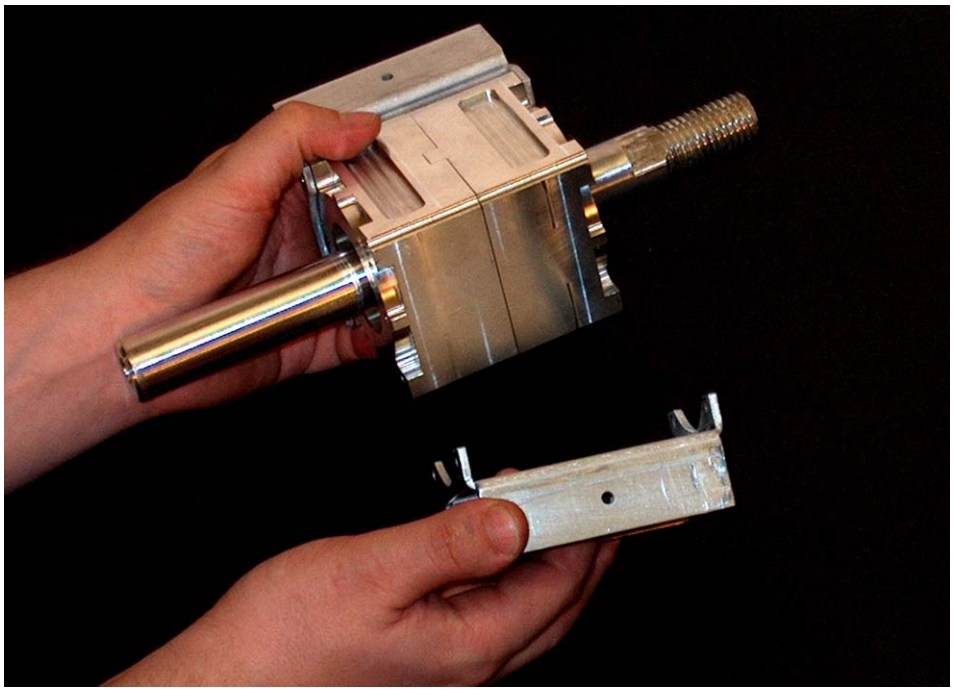

Figure 5: Fit Yaw Assembly Support Brackets[1]

5. Insert the four Threaded-Rods (Figure 2: Y-9) and tighten them evenly to secure the support brackets to the bearing housings.

[1]Slipring brush post holder mounting holes on bearing housings do not exist at time of writing. 90° rotation of bearing housings relative to support brackets may be required to expose brush post holder mounting holes.

1.3 Yaw Axis Optical Encoder

The Yaw Axis Optical Encoder (Figure 2: Y-7) is to be mounted on the Yaw Shaft. The Yaw Axis Optical Encoder is designed for a 1.000" diameter shaft but the Yaw Shaft is 0.984" in diameter. A 0.008" Sheet Metal Shim (Figure 2: Y-6) is to be used to correct this mismatch.

Become familiar with the US Digital E3 series Optical Encoder datasheet & assembly instructions before proceeding.

1. Slide the Yaw Encoder Support (Figure 2: Y-4) into position as shown in Figure 6 and secure it loosely with mounting screws (Figure 2: Y-5).

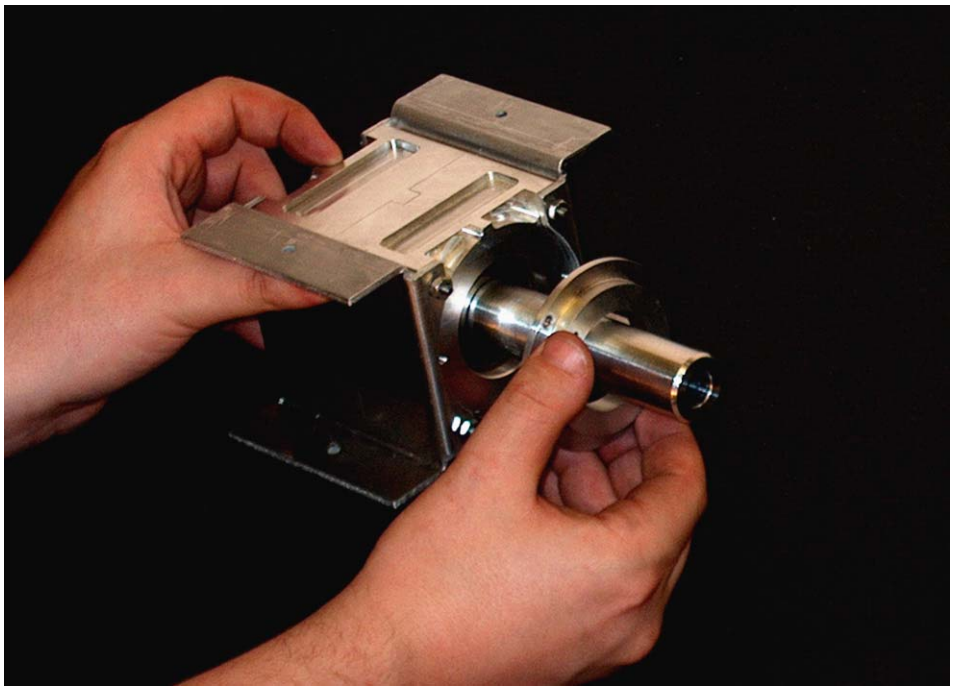

Figure 6: Position Yaw Encoder Support

2. Slide the optical encoder base over the shaft.

3. Slip the centring tool over the shaft and into the centre hole of the encoder base.

4. Place the shim in the small gap between the shaft and centring tool as shown in Figure 7.

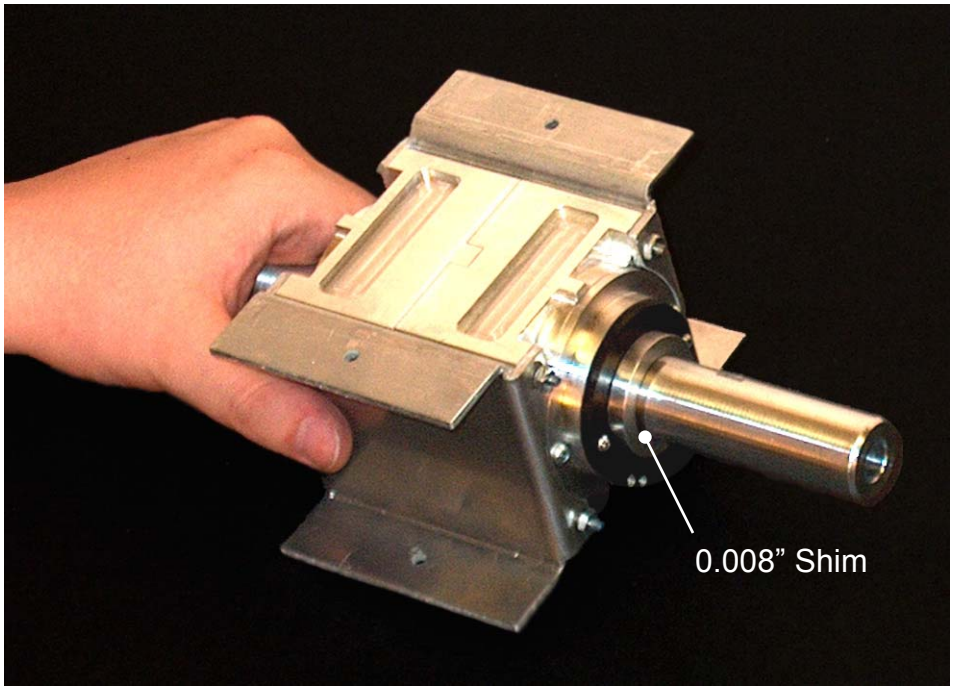

Figure 7: Mount Encoder Base with Shim and Centring Tool

5. Apply pressure to tightly sandwich the shim between yaw shaft and centring tool. While pressure is applied tighten the encoder base mounting screws, and the yaw encoder support mounting screws. This ensures alignment of the encoder base and the shaft.

6. Remove the centering tool and retrieve the shim for later use.

7. Snap spacer tool onto the lower part of the hub/disk assembly with the hub set screws facing away from the spacer tool.

8. Slide the hub/disk assembly with the spacer tool over the shaft until the spacer tool is resting flush on the encoder base. The spacer tool should be clear of encoder base mounting screws.

9. Place the shim in the small gap between the shaft and hub/disk assembly in the quadrant opposite the setscrews.

10. Tighten both encoder hub setscrews with a hex wrench while pressing the hub toward the encoder base as shown in Figure 8.

11. Note: The encoder hub setscrews must contact the yaw shaft directly to ensure correct spacing. The shim must not interfere with setscrews.

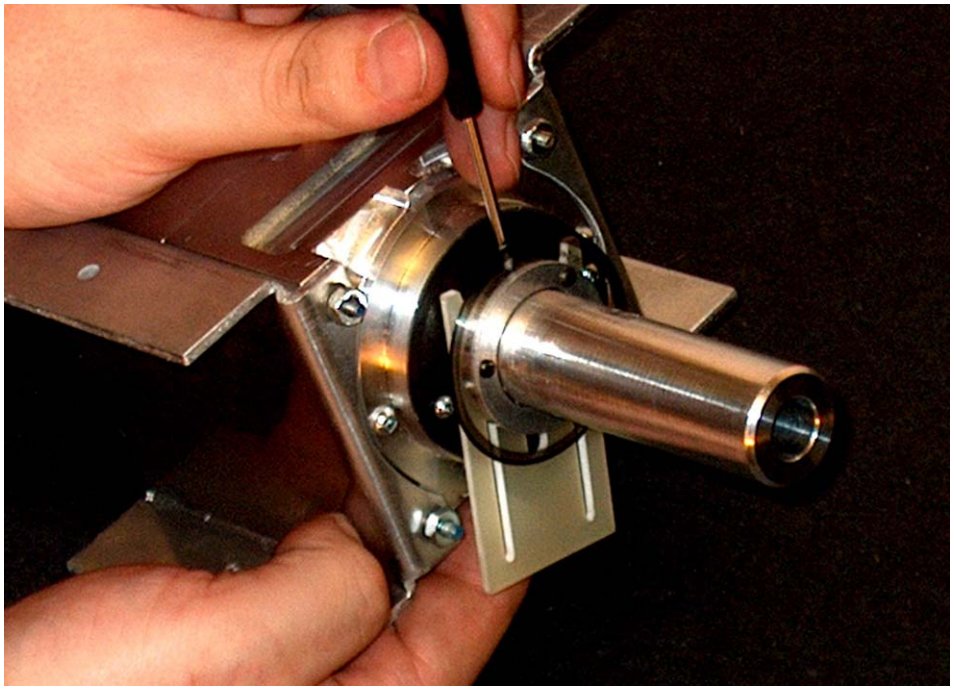

Figure 8: Attach Encoder Hub/Disk Assembly

12. Remove the spacer tool.

13. Mount the optical encoder module with two 4-40 1/2" pan head screws.

14. Place the cover over the assembly and secure with the two 4-40 5/8" flat head screws.

1.4 Power Cable

1. Thread the 4-Guage Hook-Up Wire (Figure 2: Y-11) through the centre hole in the yaw shaft, with spade connectors toward threaded-end of shaft as shown in Figure 1.

Section

2

PITCH ASSEMBLY

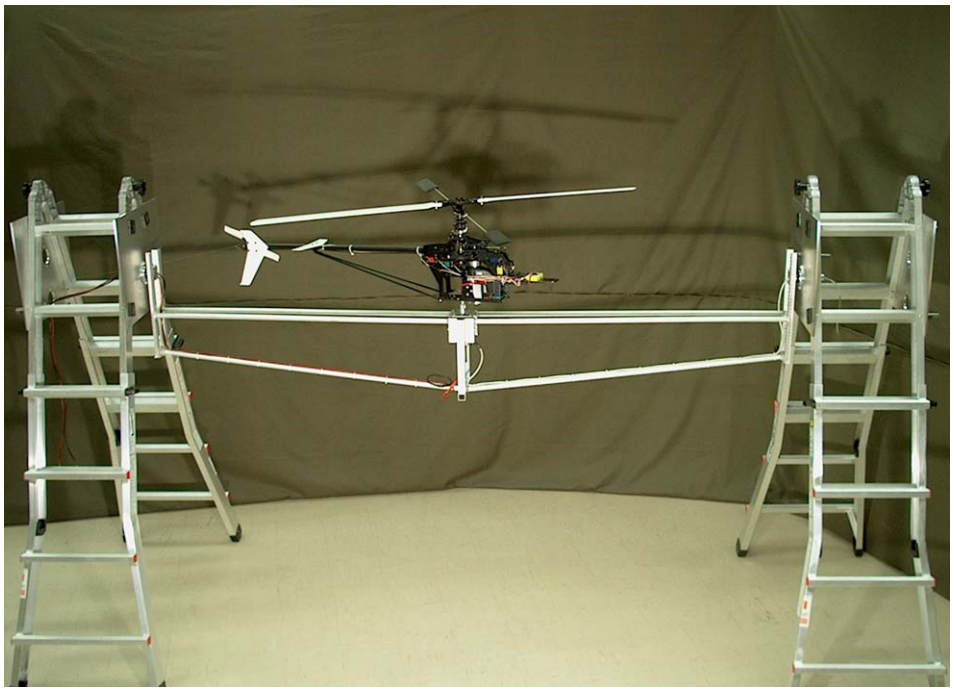

Figure 9: Complete Stand

2.1 Before You Begin

Before attempting to assemble the Pitch Degree of Freedom Assembly, check the following:

- Confirm that all of the parts in Figure 10 & Figure 11, and described in Table 2 are available.
- Confirm that the area to be used for the stand is level, and at least 12’ x 8’.
- Choose the operational height of the pitch bearings from Table 3.

  Note: The Pitch Support Ladders are adjustable in 1’ increments from 4’-7’ tall. The pitch support plates can be configured at three different heights for fine adjustment.

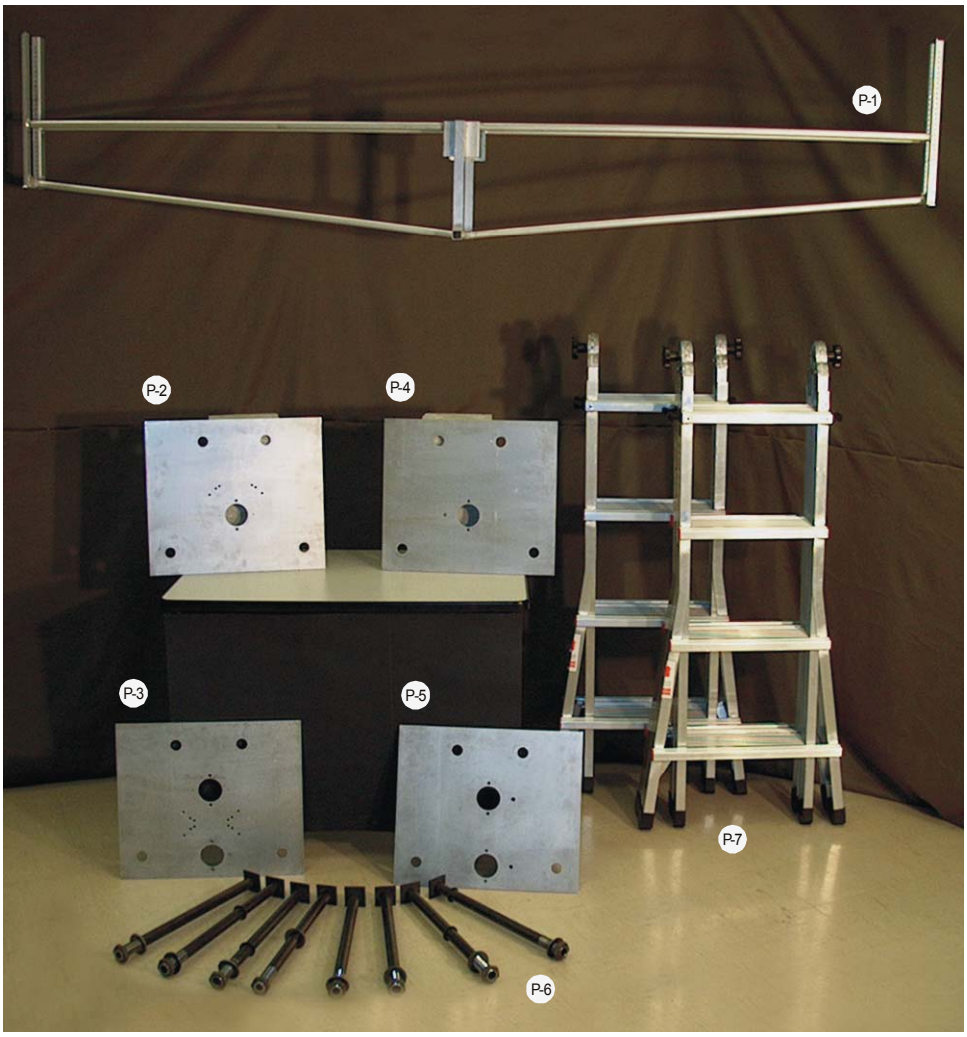

Figure 10: Pitch DOF Components

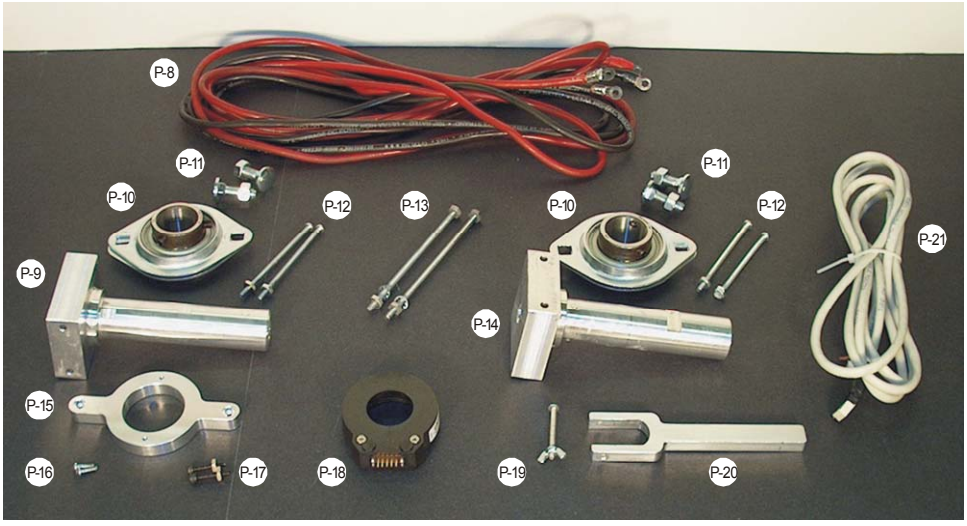

Figure 11: Pitch DOF Components

Ref.	Description
P-1	Pitch Frame (PITCH-04)
P-2	Encoder Side Pitch Support A (PITCH-05)
P-3	Encoder Side Pitch Support B (PITCH-06)
P-4	Slipring Side Pitch Support A (PITCH-07)
P-5	Slipring Side Pitch Support B (PITCH-08)
P-6	8x ¾” Pipe with welded end stop 8x 1" Serrated Belleville Washer 8x ¾” Pipe Nut
P-7	2x Pitch Support Ladder (Featherlight Industries JLT-18)
P-8	2x 12' 4-Guage Hook-Up Wire with Terminals
P-9	Slipring Side Pitch Shaft (PITCH-01)
P-10	Pitch Bearing (FYH SBPFL-205-16KG5)
P-11	4x ¾" Carriage Bolts (5/8-20 thread) 4x 5/8-20 Nuts
P-12	4x 4" 4-40 Machine Screws 4x 4-40 Nuts
P-13	2x 5" 6-32 Machine Screws 4x Lock Washers 4x 6-32 Nuts
P-14	Encoder Side Pitch Shaft (PITCH-02)
P-15	Pitch Encoder Support (PITCH-03)
P-16	2x ½" 4-40 Machine Screws
P-17	2x ½" 4-40 Socket Head Cap Screws 2x 4-40 Nuts
P-18	Pitch Encoder (US Digital E3-2048-1000-H)
P-19	2" 6-32 Machine Screw 6-32 Wing Nut
P-20	Pitch Limiter (PITCH-12)
P-21	Yaw Encoder Harness
P-22*	2x 6” 5/8-20 threaded rod 4x 5/8-20 Nuts

* Not Pictured

Table 2: Pitch DOF Components

2.2 Pitch Supports and Bearings

1. Based on the pitch bearing height selected set the Pitch Support Ladders (Figure 10: P-7) to the position indicated in Table 3.

Pitch Bearing Height	Pitch Support Ladder Height	Pitch Support Style and Bearing Position
6’	7’	Pitch Support B, Upper Position
5’9”	7’	Pitch Support A
5’6”	7’	Pitch Support B, Lower Position
5’	6’	Pitch Support B, Upper Position
4’9”	6’	Pitch Support A
4’6”	6’	Pitch Support B, Lower Position
4’	5’	Pitch Support B, Upper Position
3’9”	5’	Pitch Support A
3’6”	5’	Pitch Support B, Lower Position

Table 3: Pitch Bearing Height Selection

2. Align the ladder faces about 9’ apart. See Figure 9 for the correct orientation.

3. Based on the pitch bearing height selected, and referring to Table 3, attach either Encoder Side Pitch Support A (Figure 10: P-2) or Encoder Side Pitch Support B (Figure 10: P-3) to the inside face of one of the ladders using four Attachment Pipes (Figure 10: P-6) as shown in Figure 12.

   Note: Use serrated bevelled washers between the ladder and the mounting plate on the four Attachment Pipes to help align and lock the plate in position.

Figure 12: Attach Mounting Plate

4. Place the remaining Encoder Side Pitch Support (A or B) on the opposite face of the ladder and fasten with pipe nuts.

5. Based on the pitch bearing height selected, and referring to Table 3, Attach a Pitch Bearing (Figure 11: P-10) to the Encoder Side Pitch Support using Carriage Bolts (Figure 11: P-11). Do not tighten.

   Note: The Carriage Bolts must be loose to allow bearing axis alignment later in the assembly process.

6. Insert the Encoder Side Pitch Shaft (Figure 11: P-14) into the Pitch Bearing, align the shaft with the bearing setscrews as shown in Figure 13. Fully tighten the setscrews.

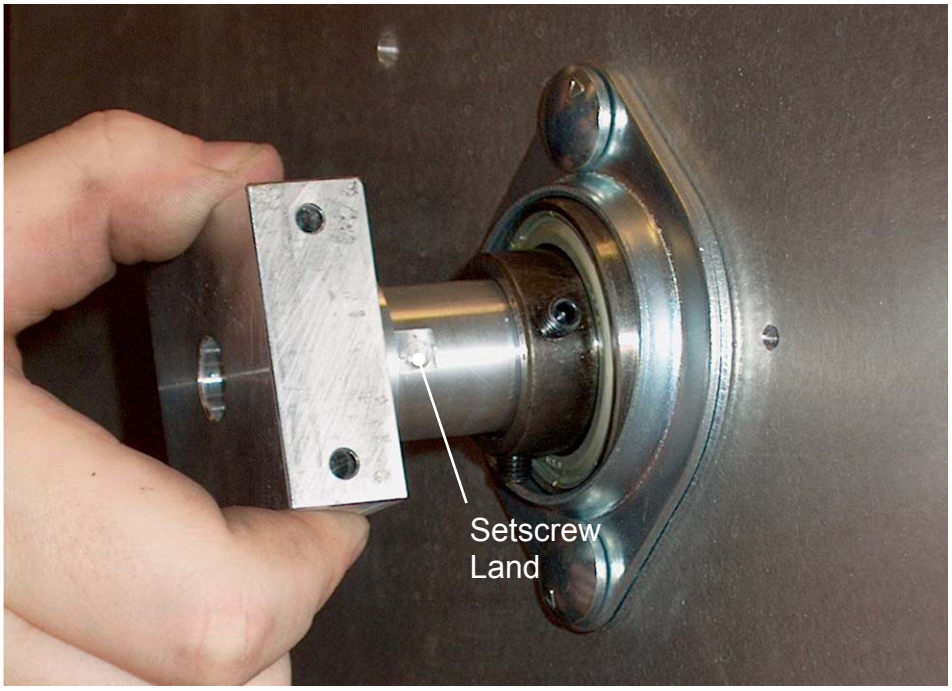

Figure 13: Insert Pitch Shaft and Align Setscrews with Setscrew Lands

7. Repeat steps 3 – 6 for the slipring side bearing.

2.3 Pitch Axis Optical Encoder

Become familiar with U.S. Digital E3 series Optical Encoder datasheet & assembly instructions before proceeding.

1. Position the Pitch Encoder Support (Figure 11: P-15) and secure loosely with socket head cap screws (Figure 11: P-17).

2. Position the optical encoder base. Fasten loosely with machine screws.

3. Slip the centring tool over the shaft and into the centre hole of the encoder base.

4. With the encoder alignment tool in place, fully tighten the Pitch Encoder Support, the encoder base plate and the encoder side Pitch Bearing as shown in Figure 14.

Figure 14: Encoder Side Pitch Shaft Alignment

2.4 Attach Pitch Frame and Yaw Assembly

The height of the pitch axis relative to the helicopter mount position is adjustable in 0.5” increments from –7.5” to 6”. The pitch axis should be aligned with the centre of mass of the helicopter plus pitch frame. Use the same mounting height on both the encoder side and the slipring side.

1. Raise the Pitch Frame (Figure 10: P-1) into place on the Slipring Side Pitch Shaft. Attach the Pitch Frame to the shaft with two machine screws (Figure 11: P-12). Fasten loosely

2. Raise the Pitch Frame into place on the Encoder Side Pitch Shaft and attach it with machine screws. Fasten loosely

Figure 15: Attach Pitch Frame

3. Swing the Pitch Frame; confirm that it freely rotates about the pitch axis. If not, adjust the position of the support ladders and the alignment of the Slipring Side Pitch Bearing until motion is satisfactory.

4. Tighten the Slipring Side Pitch Bearing, and the four Pitch Frame to Pitch Shaft Fasteners.

5. Raise the yaw assembly into position above the centre of the Pitch Frame.

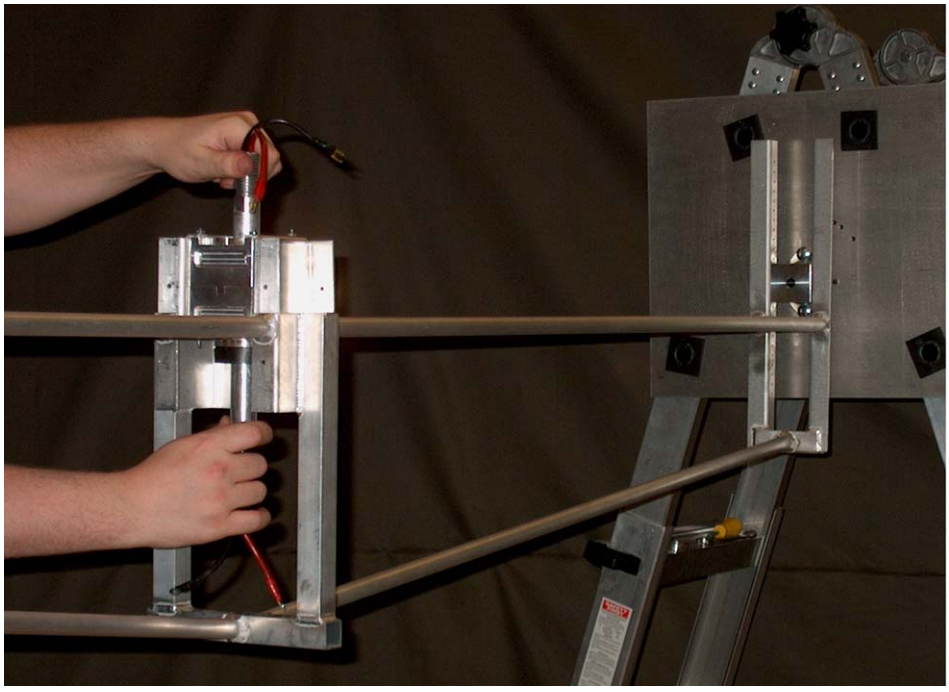

Figure 16: Slide Yaw Assembly into Position

6. Attach the yaw assembly with two pieces of threaded-rod (Figure 11: P-13).

7. Connect the pitch assembly power wires (Figure 11: P-8) to the yaw assembly power wires with machine screws (Figure 2: Y-10) and insulate the exposed conductors with electrical tape or heat shrink tubing.

8. Run the pitch assembly power wire along the Pitch Frame and thread it through the Slipring Side Pitch Shaft.

9. Connect the yaw encoder harness (Figure 11: P-21) to the yaw encoder and run the wire along the Pitch Frame and through the Encoder Side Pitch Shaft.

10. Tie all wires to the Pitch Frame to prevent interference with moving parts.

2.5 Pitch Limiter

The pitch axis is capable of virtually unlimited rotation (the only obstruction is twisting wires). Facility for limiting the rotation of the pitch axis has been integrated into the stand.

1. Select the desired range of motion from Figure 17, which shows the hole positions on the Encoder Side Pitch Support.

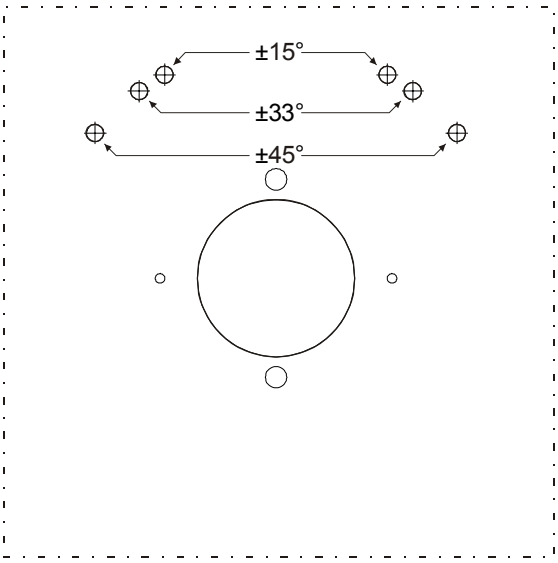

Figure 17: Pitch limiter hole positions

2. Attach the pitch limiter (Figure 11: P-20) to the encoder side pitch shaft with a machine screw and wing nut (Figure 11: P-19).

3. Attach two pieces of 6" 5/8-20 Threaded Rod (P-22) to the Encoder Side Pitch Support using 4 5/8-20 nuts. Ensure that the threaded rod does not interfere with the Pitch Frame.

Section

3

DATA ACQUISITION

3.1 Before You Begin

Before attempting to assemble the data acquisition system check the following

- Find or configure a PC with the QNX operating system and ensure that there is a free PCI slot.
- Confirm that all parts in Figure 18 described in Table 4 are available.
- Copy the helicopter test stand software in /expermnt directory on the Helicopter Test Stand CD to the PC.
- Set up an RC receiver with servos for testing (see Futaba 8UHPS manual).

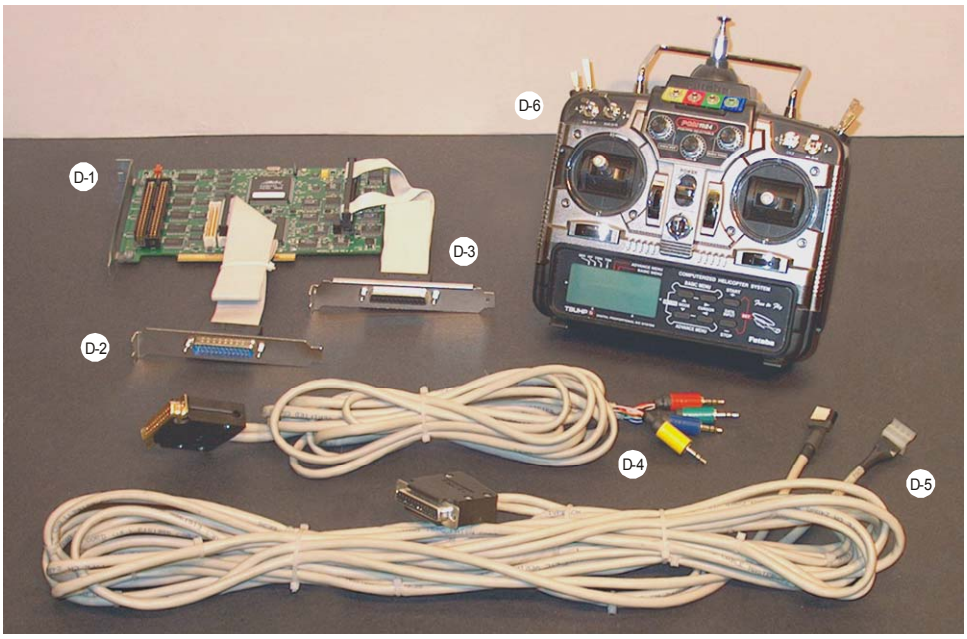

Figure 18: Data Acquisition Components

Ref.	Description
D-1	Data Acquisition Card (Sensoray 626)
D-2	Encoder Riser (IDE-26F to DB-25M Cable)
D-3	Transmitter Riser (IDE-50F to DB25F Cable)
D-4	Transmitter Cable (DB-25M to 4x 3.5mm Stereo Mini)
D-5	Encoder Cable (DB-25F to 2x Encoder Connector)
D-6	RC Transmitter (Futaba 8UHPS)

Table 4: Data Acquisition Components

3.2 Electrical Connection

Note: To complete steps 1-4 below, refer to Figure 19: Encoder Connection Schematic.

1. Attach the Encoder Riser (Figure 18: D-2) and the Transmitter Riser (Figure 18: D-3) to the Sensoray 626 (Figure 18: D-1), and insert them into the preconfigured PC.

2. Connect the yaw connector on the Encoder Cable (Figure 18: D-5) to the Yaw Encoder Harness on the test stand.

3. Connect the pitch connector on the Encoder Cable directly to the Pitch Encoder.

4. Connect the Encoder Cable to the Encoder Riser.

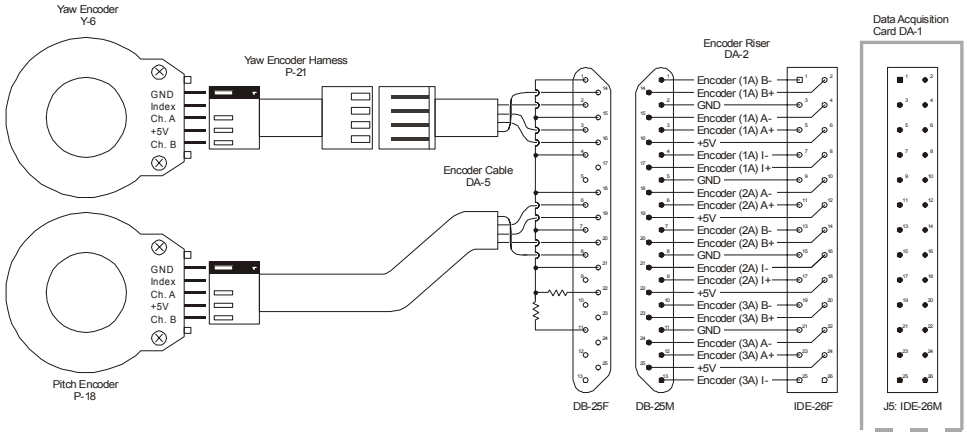

Figure 19: Encoder Connection Schematic

Note: To complete steps 5-6 below, refer to Figure 20: Transmitter Schematic.

5. Connect the colour-coded miniplugs on the Transmitter Cable (Figure 18: D-4) to their corresponding colour coded miniplug jacks on the RC Transmitter (Figure 18: D-6), yellow-red-green-blue from left to right.

6. Connect the Transmitter Cable to the Transmitter Riser on the back of the PC.

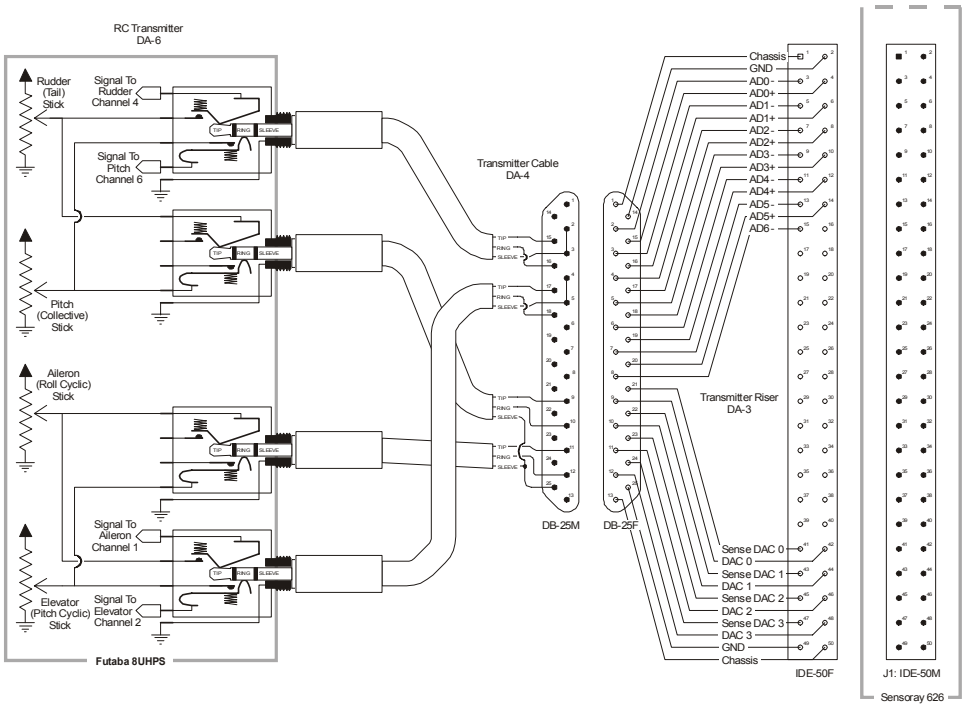

Figure 20: Transmitter Schematic

3.3 Test the data acquisition system.

1. Turn on the RC Transmitter and the corresponding RC Receiver.

2. Run the helicopter test stand software by typing ./belt Enter in the directory the software was copied to. This will bring up the first screen, Figure 21.

```
# ./belt

GEN_CTRL: Hit any key to interrupt the experiment...

SEG: 0015, OFFSET: 0013e000, SIZE: 4096
SEG: 001d, OFFSET: 0013f000, SIZE: 4096
SEG: 0025, OFFSET: 00140000, SIZE: 4096

EXP_FromFileHandler: Please specify the data source fileEXP_FromFileHandler: (Hi
t enter for default: data)
```

Figure 21: Software Start-Up Screen Shot

3. Press Enter when asked for a source data file, this brings up the internal data display, Figure 22. Move the yaw and pitch axes of the stand and confirm that the display accurately reflects the motion.

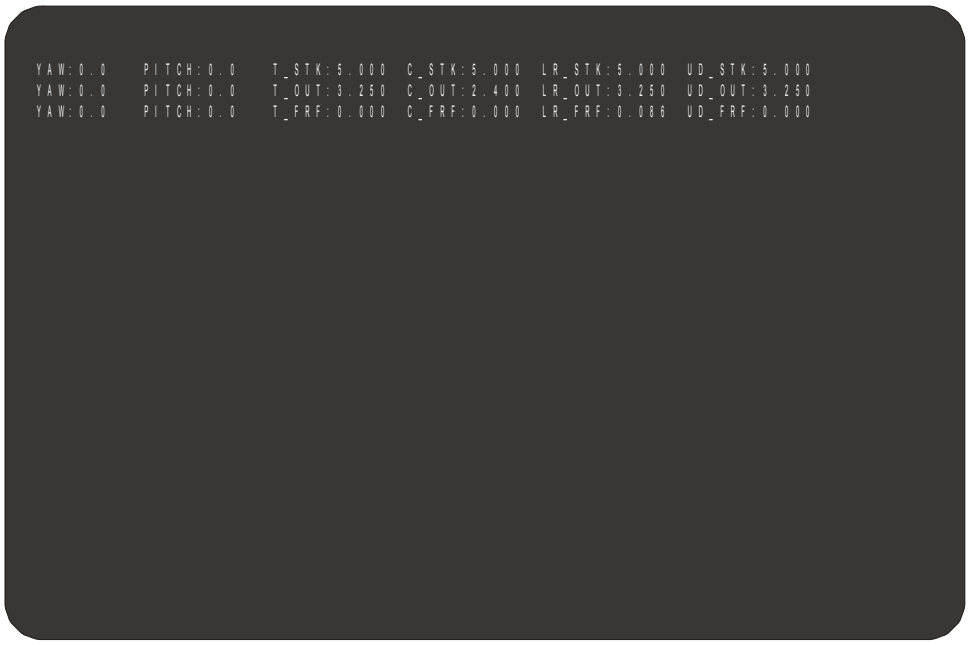

Figure 22: Internal Data Display Screen Shot

4. Move the transmitter joysticks and confirm that the servos attached to the receiver move appropriately, and that the display changes appropriately.

5. Press Enter to stop the data acquisition. A filename for storage of the output data will be requested, Figure 23. Press Enter again to accept the default filename and quit the program.

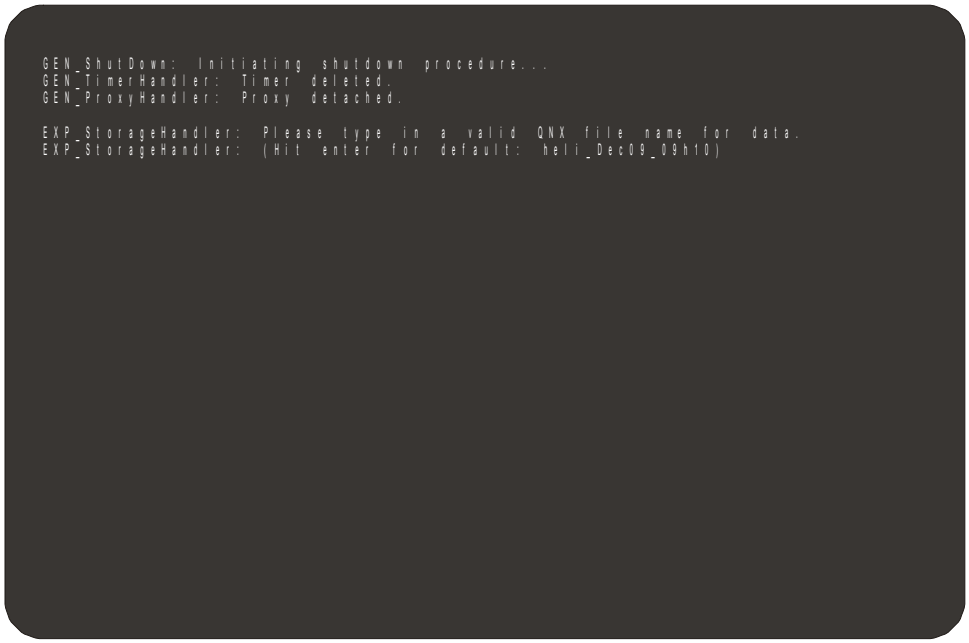

Figure 23: Output File Screen Shot

3.4 Operation

The helicopter test stand software and source code consists of 15 files. Modifications to the experiment can be performed by editing the following three files: *expermnt.h*, *control.c*, and *control.h*.

1. Specify basic properties of the experiment (e.g. sample rate and run time) by editing *expermnt.h*. Follow the comments carefully.

2. Implement computations for the experiment in *control.c* and *control.h*.

   Note: All available input and output data is accessed through a 15 element array, *(*ps_internal_data).f_value*. Specific variables are accessed using the enumerated indices in Table X.

Index	Description
TIME	Current sample time
YAW	Yaw bearing angle in decrees relative to start position
PITCH	Pitch bearing angle in decrees relative to start position
Q3	Extra optical encoder channel
TAIL_OUT	Tail rotor pitch, or rudder, servo control signal
COLL_OUT	Collective pitch servo control signal
LRCY_OUT	Lateral cyclic pitch, or aileron, servo control signal
UDCY_OUT	Longitudinal cyclic pitch, or elevator, servo control signal
TAIL_STK	Left stick x-axis position

COLL_STK	Left stick y-axis position
LRCY_STK	Right stick x-axis position
UDCY_STK	Right stick y-axis position
TAIL_FRF	Input data from file, column 1
COLL_FRF	Input data from file, column 2
LRCY_FRF	Input data from file, column 3
UDCY_FRF	Input data from file, column 4

Table 5: Indices to access input and output data

For example, the current state of the right stick's x-axis is stored in *(*ps_internal_data).f_value[LRCY_STK]*.

Only the current samples are available. Previous samples, such as integration lags, must be stored in variables local to *control.c*.

3. If external data is required prepare an input data file. A model of the input data file is included along with the experiment source code. The file must consist of four columns, and it must have at least as many rows as the experiment will have samples.

Section

4

POWER SUPPLY

4.1 Before You Begin

Before attempting to assemble the Power Supply, check the following:

- Before connecting the Power Supply, make sure all of the parts in Figure 24 described in Table 6 are available.
- Become familiar with Figure 25: Switch Box Controls and Terminals and Figure 26: Power Supply Schematic.

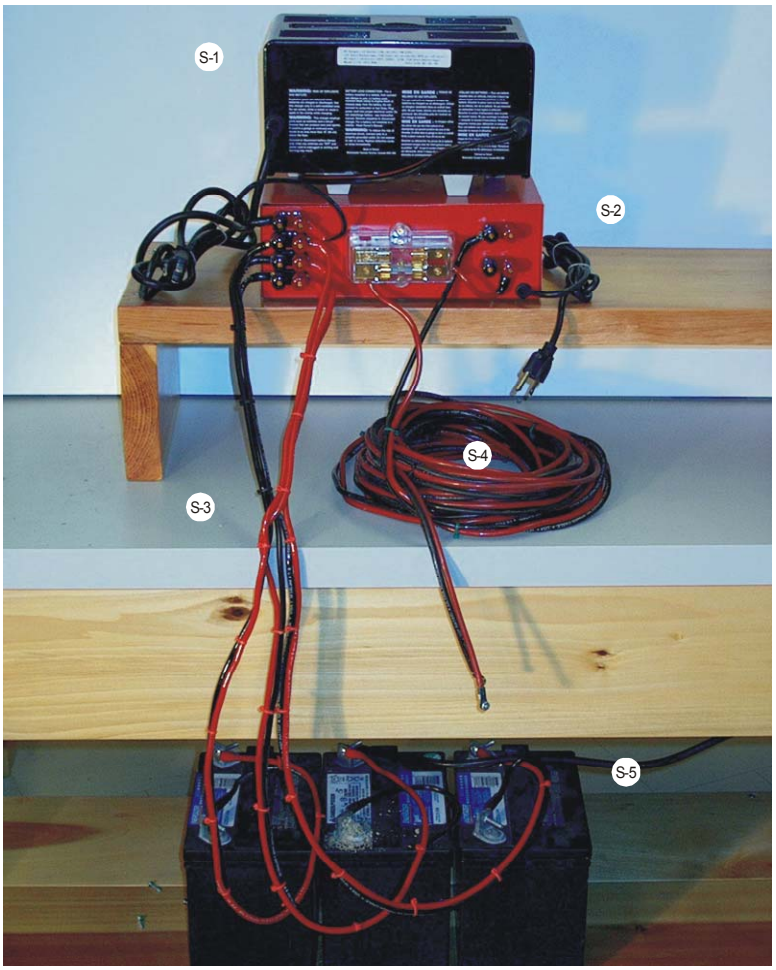

Figure 24: Power Supply Components

Ref.	Description
S-1	Mastercraft 11-1569-6 Battery Charger
S-2	Switch Box (SCHEM-1)
S-3	2x 12" 4-Guage Hook-Up Wire with Terminals
S-4	2x 12" 4-Guage Hook-Up Wire with Terminals Screws
S-5	3x 12V Marine Gel Cell

Table 6: Power Supply Components

4.2 Electrical Connection

1. Connect the three Marine Gel Cell Batteries (Figure 24: S-5) to the Switch Box (Figure 24: S-2) with the Battery Hook-Up Wires (Figure 24: S-3); one battery to each of the three battery terminals on the switch box. See Figure 25.

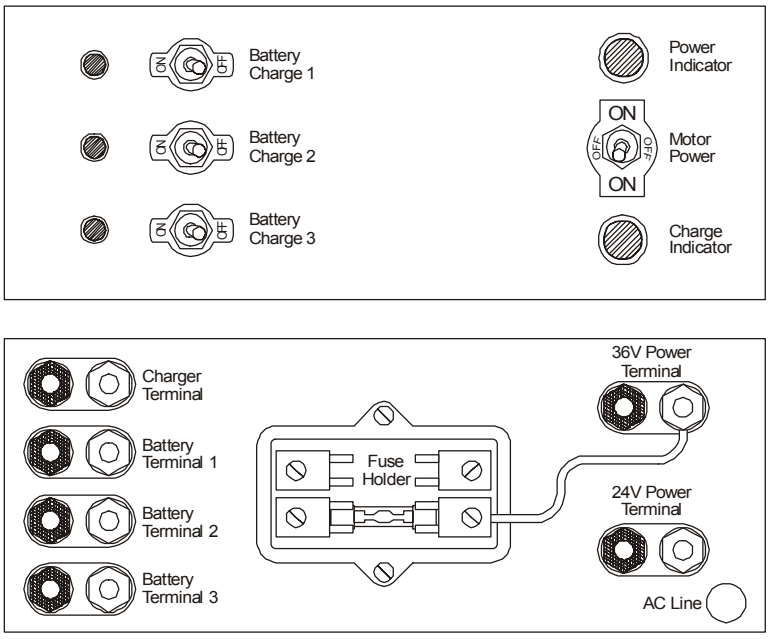

Figure 25: Switch Box Controls and Terminals

2. Connect the Battery Charger (Figure 24: S-1) to the battery charger terminals on the switch box. Do not plug the battery charger into the AC line at this time.

3. Connect the Motor Power Hook-Up Wires (Figure 24: S-4) to the Switch Box: red wire to fuse; black wire to either negative power supply terminal.

4. Connect the Voltage Select Jumper from the fuse to either the 24V or 36V terminal on the switch box as required.

5. Double-check the polarity of all connections. Connect the switchbox to the AC line and turn the Control Switch to the Motor Power position. Check the

voltage on the 24V and 36V terminals and the voltage on the Motor Power Hook-Up Wires. When connections are correct turn the Control Switch on the Switch Box to the off position and unplug the switch box.

6. Connect the Motor Power Hook-Up Wires to the Pitch DOF Hook-Up Wire with ¼" 6-32 machine screws and nuts (similar to Figure 2: Y-10). Cover the connections with electrical tape or heat shrink tubing to prevent accidental short circuits.

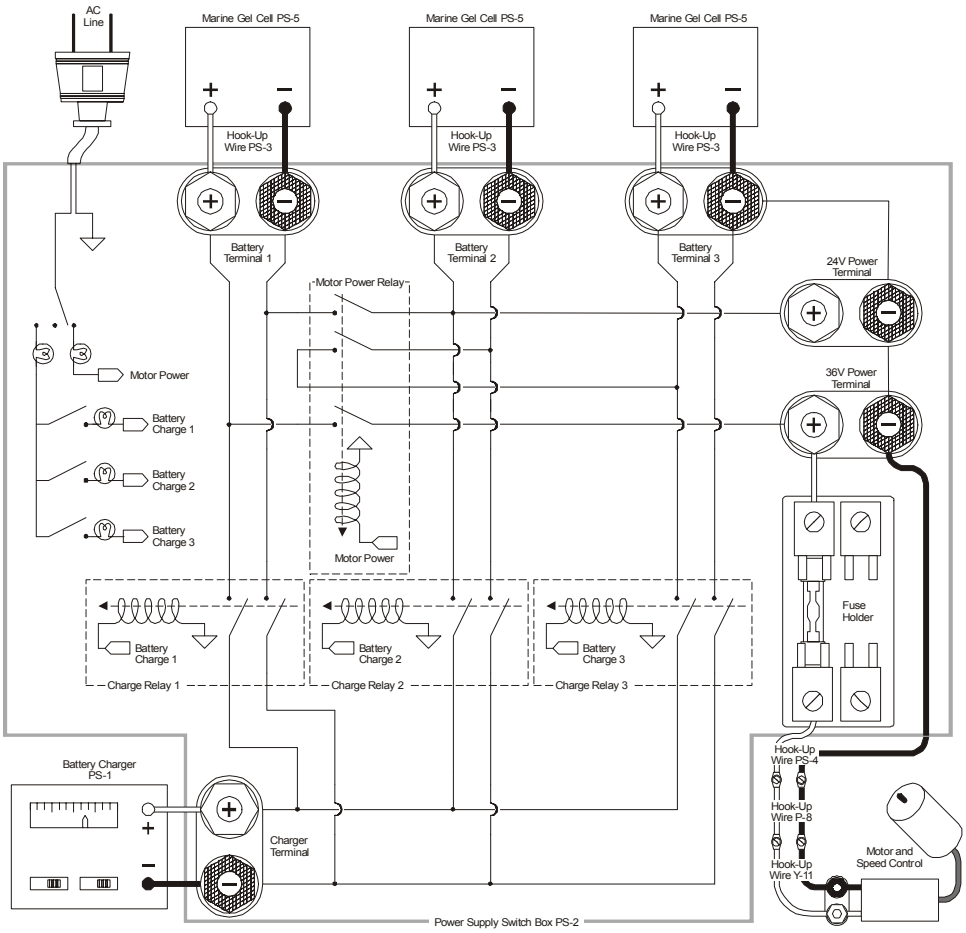

Figure 26: Power Supply Schematic

Appendix B

Bill of Materials and As Built Drawings

Yaw Assembly Parts

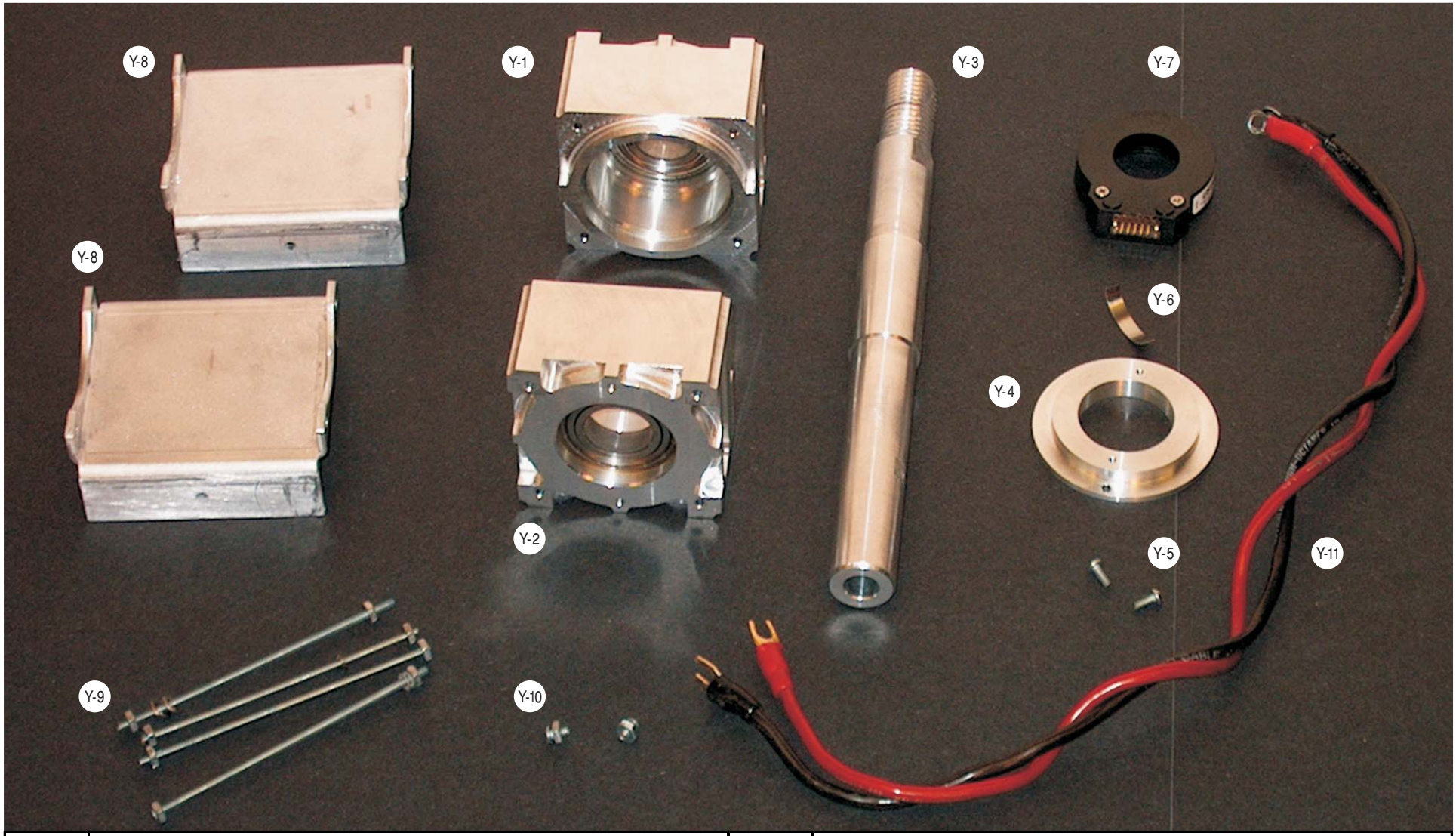

Ref.	Description	Ref.	Description
Y-1	Upper Bearing Housing (dwg. YAW-01) Bearing (SKF 6005-2Z)	Y-7	Yaw Encoder (US Digital E3-2048-1000-H)
Y-2	Lower Bearing Housing (dwg. YAW-02) Bearing (SKF 6005-2Z)	Y-8	2x Yaw Assembly Support Bracket (YAW-05)
Y-3	Yaw Shaft (dwg. YAW-03)	Y-9	4x 4" 6-32 Threaded Rods 8x Lock Washers 8x 6-32 Nuts
Y-4	Yaw Encoder Support (dwg. YAW-04)	Y-10	2x 1/4" 6-32 Machine Screws 2x 6-32 Nuts
Y-5	2x 1/2" 4-40 Machine Screws	Y-11	2x 12" 4-Guage Hook-Up Wire with Terminals
Y-6	1.2" x .3" x .008" Shim Stock		

Pitch Assembly Parts (page 1 of 2)

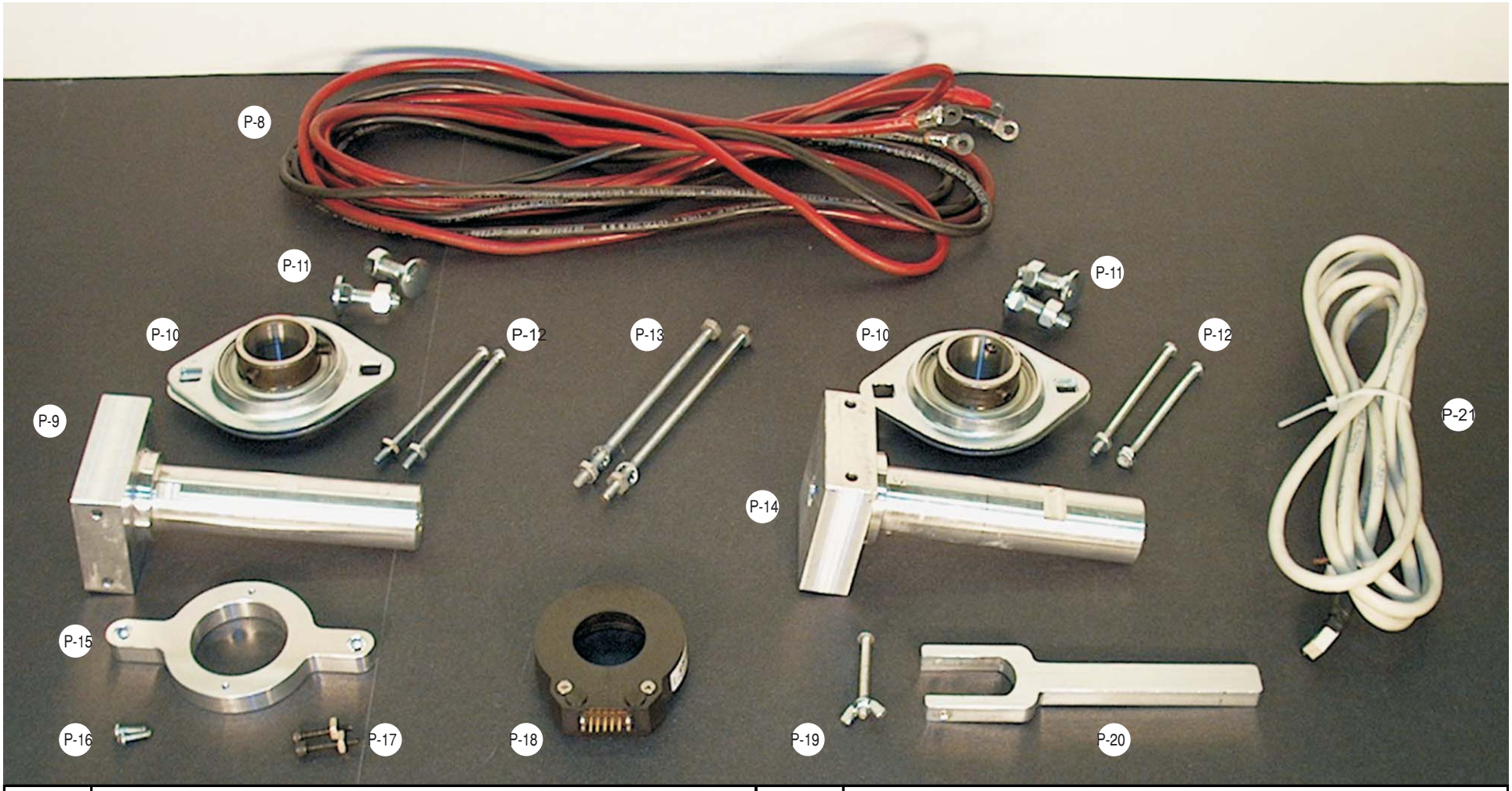

Ref.	Description	Ref.	Description
P-8	2x 12' 4-Guage Hook-Up Wire with Terminals	P-14	Encoder side Pitch Shaft (PITCH-02)
P-9	Slipring Side Pitch Shaft (PITCH-01)	P-15	Pitch Encoder Support (PITCH-03)
P-10	Pitch Bearing (FYH SBPFL-205-16KG5)	P-16	2x 1/2" 4-40 Machine Screws
P-11	4x 3/4" 5/8-20 Carriage Bolts 4x 5/8-20 Nuts	P-17	2x 1/2" 4-40 Socket Head Cap Screws 2x 4-40 Nuts
P-12	4x 4" 4-40 Machine Screws 4x 4-40 Nuts	P-18	Pitch Encoder (US Digital E3-2048-1000-H)
P-13	2x 5" 6-32 Machine Screws 4x Lock Washers 4x 6-32 Nuts	P-19	2" 6-32 Machine Screw 6-32 Wing Nut
		P-20	Pitch Limiter (PITCH-04)
		P-21	Yaw Encoder Harness

Not Pictured: P-22, 2x 6” 5/8-20 Threaded Rod, 4x 5/8-20 Nuts

Pitch Assembly Parts (page 2 of 2)

Ref.	Description
P-1	Pitch Bar (PITCH-04)
P-2	Encoder side Pitch Support A (PITCH-05)
P-3	Encoder side Pitch Support B (PITCH-06)
P-4	Slipring side Pitch Support A (PITCH-07)
P-5	Slipring side Pitch Support B (PITCH-08)
P-6	8x 3/4” Pipe (with welded end stops) 8x 1” Serrated Belleville Washer 8x 3/4” Pipe Nut
P-7	2x Pitch Support Ladder (Featherlight Industries JLT-18)

Data Acquisition Parts

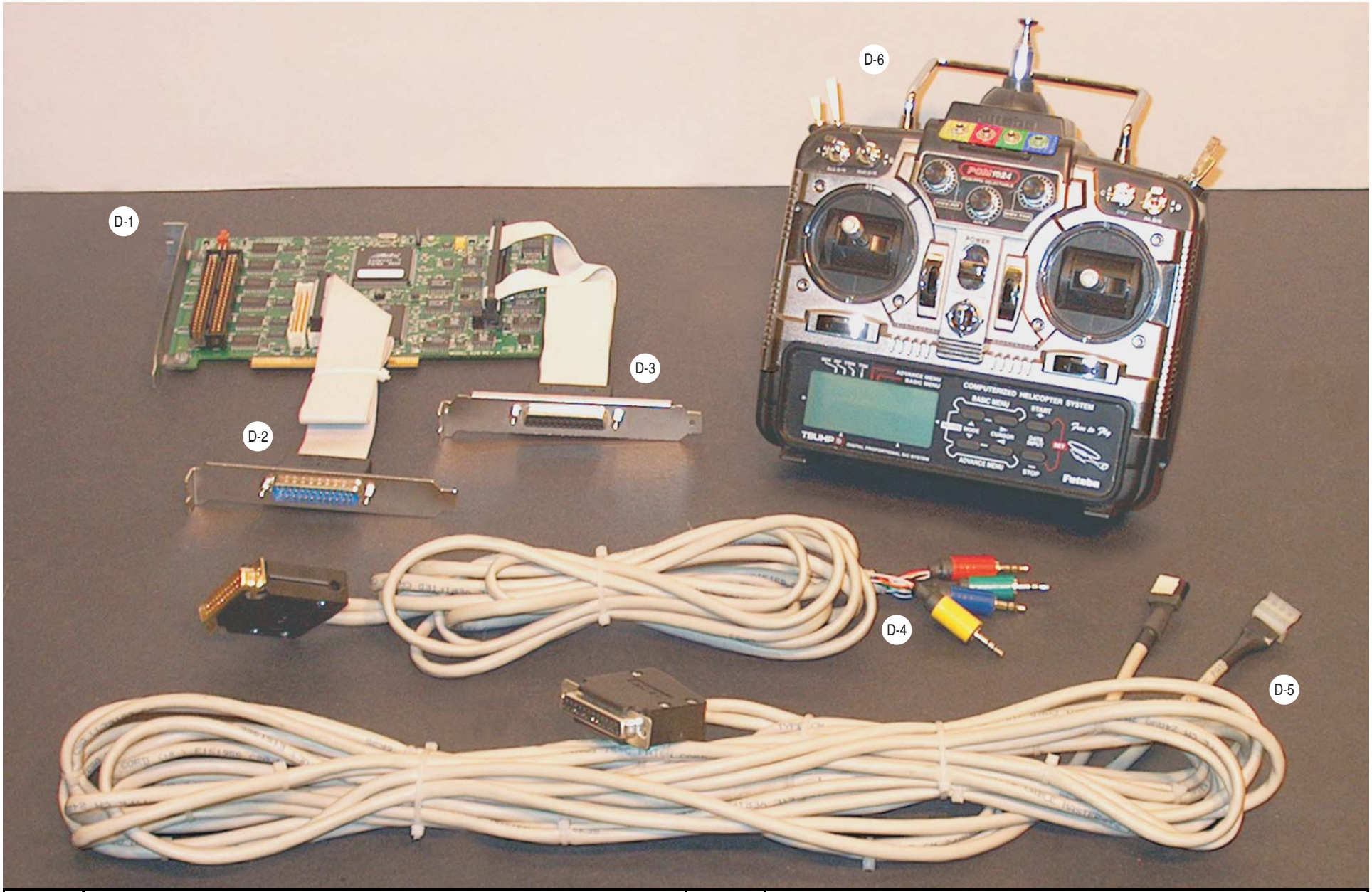

Ref.	Description	Ref.	Description
D-1	Data Acquisition Card (Sensoray 626)	D-4	Transmitter Cable (DB-25M to 4x 3.5mm Stereo Miniplugs)
D-2	Encoder Riser (IDE-26F to DB-25M Cable)	D-5	Encoder Cable (DB-25F to 2x Encoder Connector)
D-3	Transmitter Riser (IDE-50F to DB25F Cable)	D-6	RC Transmitter (Futaba 8UHPS)

Power Supply Parts

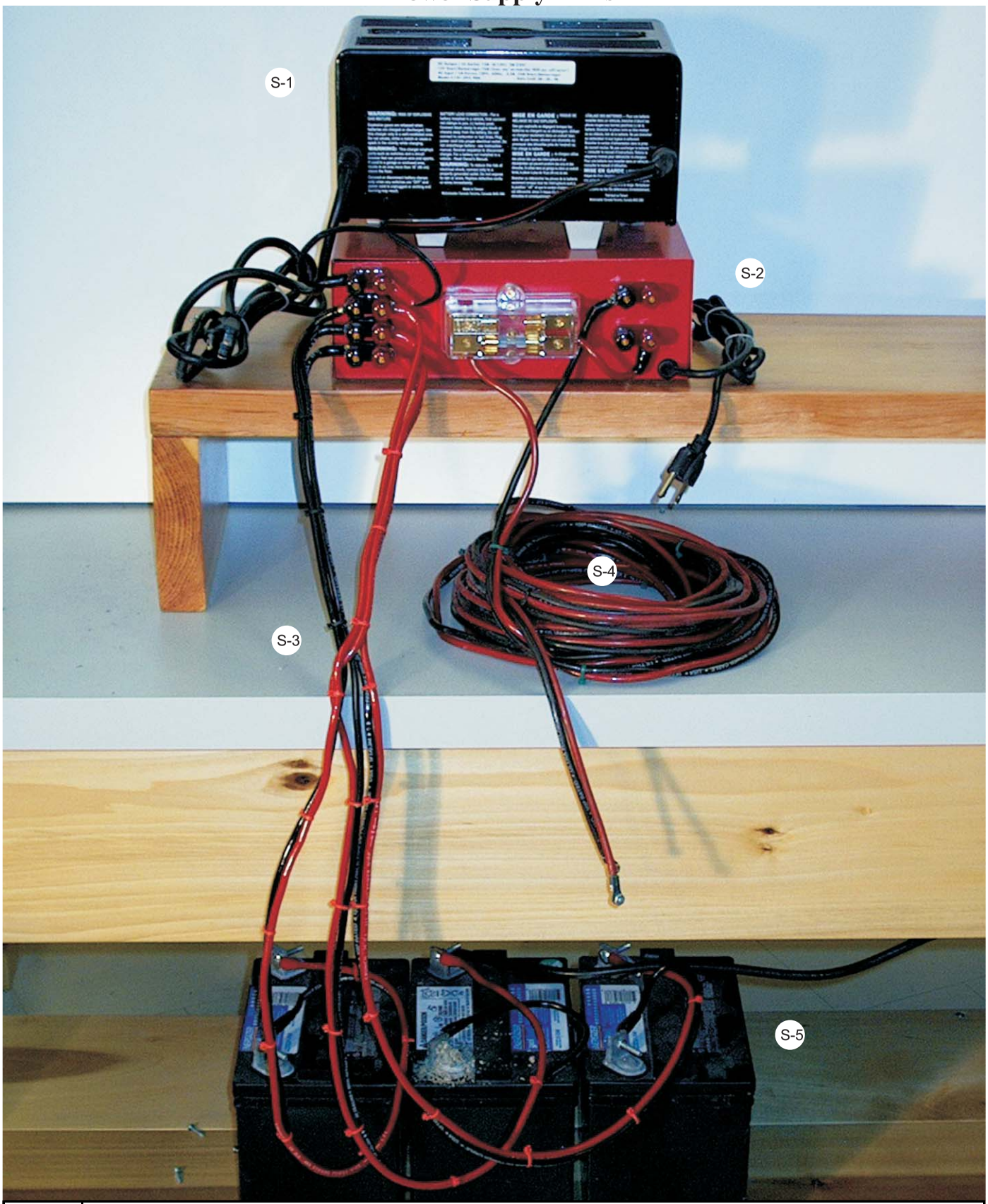

Ref.	Description
S-1	Mastercraft 11-1569-6 Battery Charger
S-2	Switch Box (SCHEM-1)
S-3	2x 12" 4-Guage Hook-Up Wire with Terminals
S-4	2x 12" 4-Guage Hook-Up Wire with Terminals Screws
S-5	3x 12V Marine Gel Cell

REVISION HISTORY			
REV	DESCRIPTION	DATE	APPROVED
A	INITIAL DWG.	NOV.13/01	
B	ADDED BOLT HOLE DIMENSIONS	NOV. 19/01	

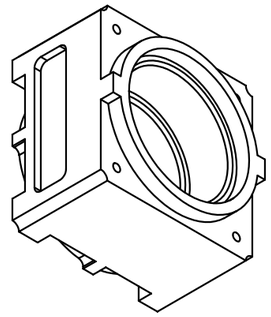

NOTE:
THIS DRAWING GIVES FINISHED DIMENSIONS FOR A MODIFIED PART BASED ON THE EXISTING UPPER BEARING HOUSING DRAWING, WHICH SHOULD BE REFERRED TO AS A GUIDE IN DETERMINING ALL MACHINING OPERATIONS. THIS DRAWING IS NOT TO BE USED TO PRODUCE A NEW PART FROM BLANK STOCK, BUT ONLY FOR THE PURPOSE OF MODIFYING AN EXISTING PART.

		REV	REV STATUS
		SH	

NEXT ASSY	USED ON
APPLICATION	

MATERIAL:
ALUMINUM ALLOY
7075-T6
FINISH: NONE
REMOVE BURRS AND SHARP EDGES

TOLERANCE +/-0.005

UNITS IN INCHES

CAMERON KERR
46 NOVELLA ROAD, CONCORD, ONTARIO
L4K 5J9

TITLE
HELICOPTER IDP
REVISED UPPER BEARING HOUSING

SIZE	CAGE CODE	DWG NO	REV
B		YAW-01	B

SCALE 1:1 | THIRD ANGLE PROJECTION | SHEET 1 OF 1

REVISION HISTORY			
REV	DESCRIPTION	DATE	APPROVED
A	INITIAL DRAWING	JAN.14/01	
B	REDESIGNED	FEB.4/01	
C	DELETED CBORE ON .257 THRU HOLES	FEB.12/01	
D	ADDED LIGHTENING HOLES	MAR.18/01	

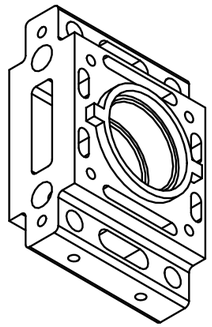

DRAWING NOT TO SCALE

NOTE:
THIS DRAWING GIVES ORIGINAL DIMENSIONS FOR A PART THAT WAS LATER MODIFIED

						REV	REV STATUS
						SH	

		UNLESS OTHERWISE SPECIFIED DIM ARE IN INCHES TOL ON ANGLE ± .25° 2 PL ± .04 3 PL ± .004 INTERPRET DIM AND TOL PER ASME Y14.5M - 1994	MATERIAL: ALUMINUM ALLOY 7075-T6 REMOVE ALL BURRS AND SHARP EDGES
		THIRD ANGLE PROJECTION	
NEXT ASSY	USED ON		
APPLICATION			

CAMERON KERR
179 CHISHOLM AVENUE, TORONTO ONTARIO
M4C 4V9

TITLE
UPPER BEARING HOUSING
TEST CELL YAW ASS'Y

SIZE	CAGE CODE	DWG NO	REV
C		UPPERBEARINGHOUSING.ICD	D

SCALE 1:1 SHEET 1 OF 1

REVISION HISTORY			
REV	DESCRIPTION	DATE	APPROVED
A	INITIAL DWG.	NOV.13/01	
B	ADDED BOLT HOLE DIMENSIONS	NOV. 19/01	

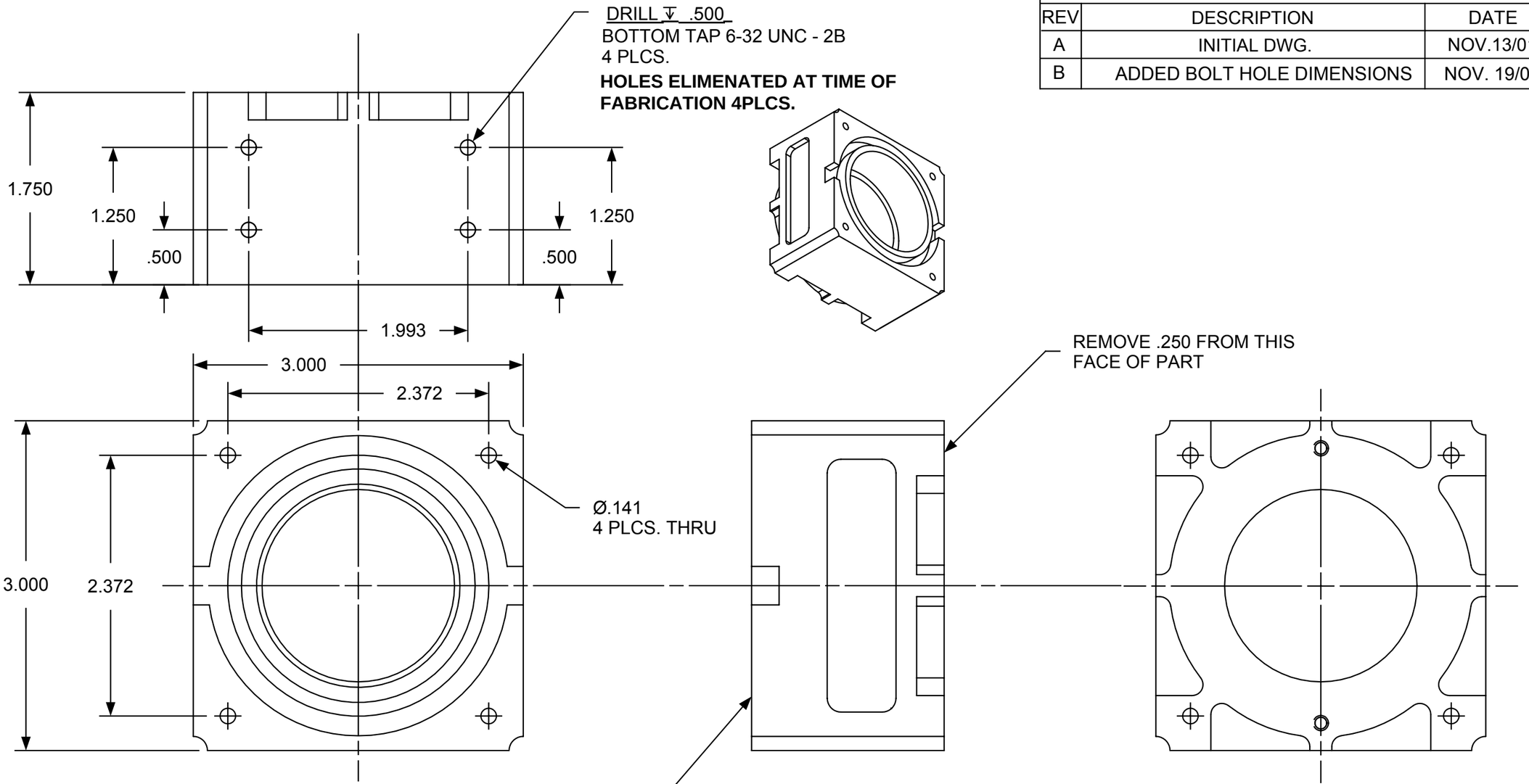

NOTE:
THIS DRAWING GIVES FINISHED DIMENSIONS FOR A MODIFIED PART BASED ON THE EXISTING LOWER BEARING HOUSING DRAWING, WHICH SHOULD BE REFERRED TO AS A GUIDE IN DETERMINING ALL MACHINING OPERATIONS. THIS DRAWING IS NOT TO BE USED TO PRODUCE A NEW PART FROM BLANK STOCK, BUT ONLY FOR THE PURPOSE OF MODIFYING AN EXISTING PART.

	REV	REV STATUS
	SH	

NEXT ASSY	USED ON
APPLICATION	

MATERIAL:
ALUMINUM ALLOY
7075-T6
FINISH: NONE
REMOVE BURRS AND SHARP EDGES

TOLERANCE +/-0.005

UNITS IN INCHES

CAMERON KERR
46 NOVELLA ROAD, CONCORD, ONTARIO
L4K 5J9

TITLE
HELICOPTER IDP
REVISED LOWER BEARING HOUSING

SIZE	CAGE CODE	DWG NO	REV
B		YAW-02	B

SCALE 1:1 | THIRD ANGLE PROJECTION | SHEET 1 OF 1

REVISION HISTORY			
REV	DESCRIPTION	DATE	APPROVED
A	INITIAL DRAWING	JAN.14/01	
B	REDESIGNED	FEB.4/01	
C	DELETED CBORE ON .257 THRU HOLES	FEB.12/01	
D	ADDED LIGHTENING HOLES	MAR.18/01	

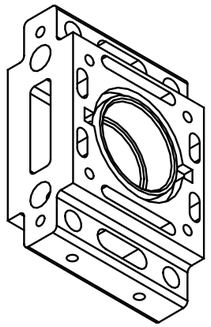

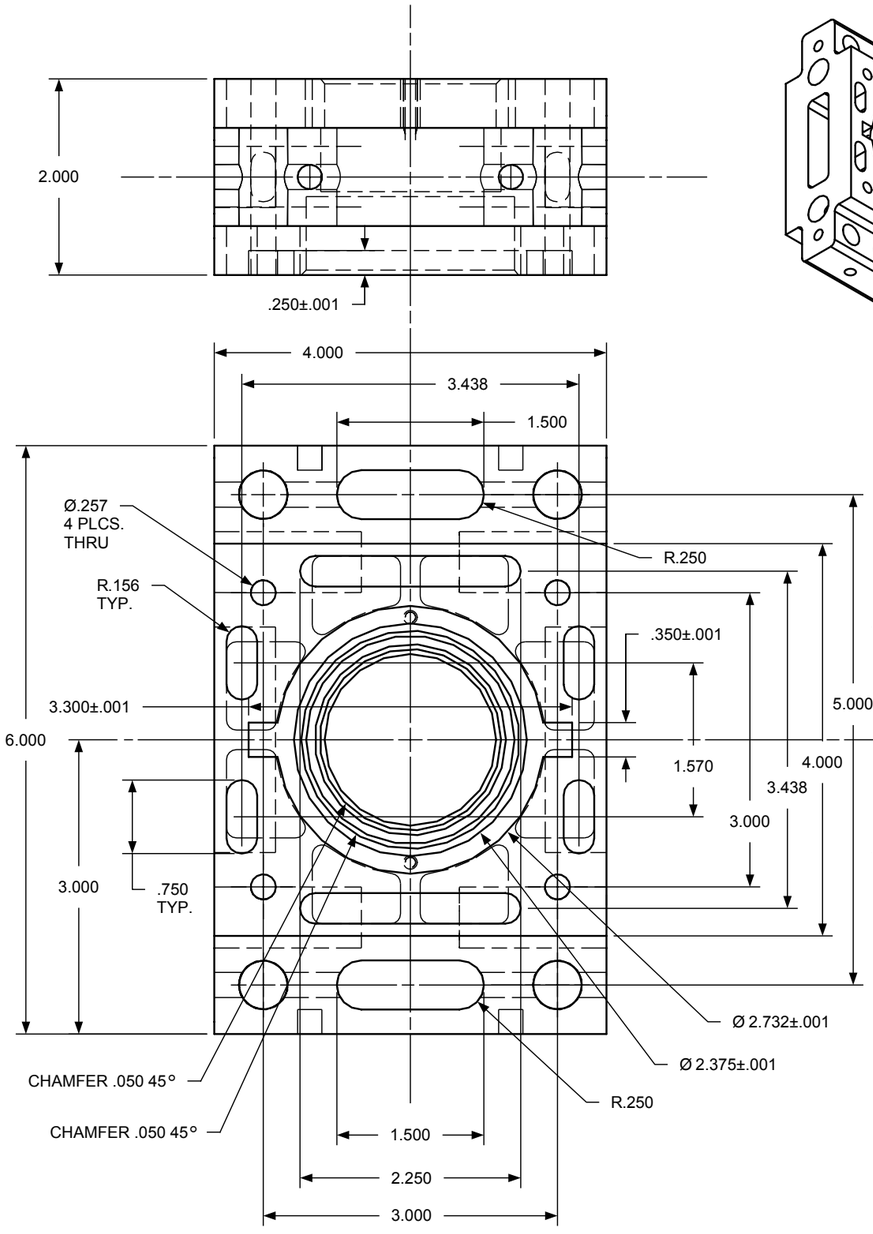

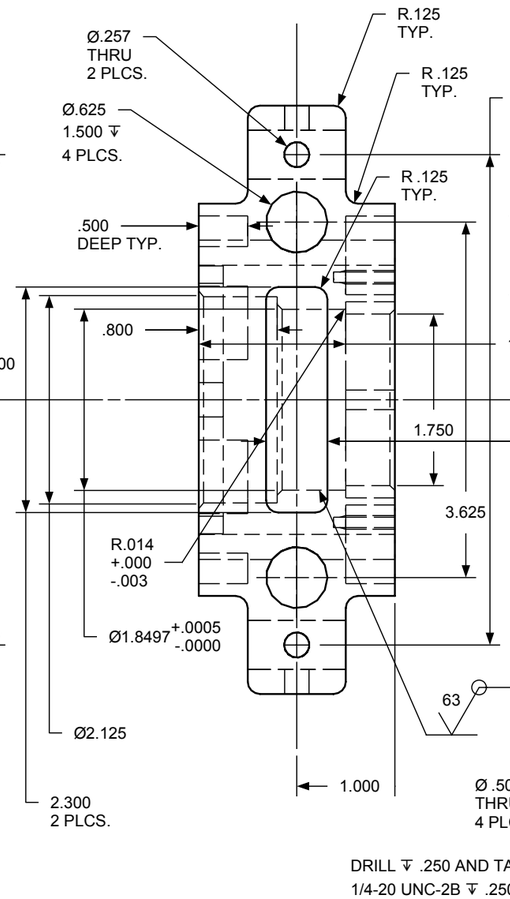

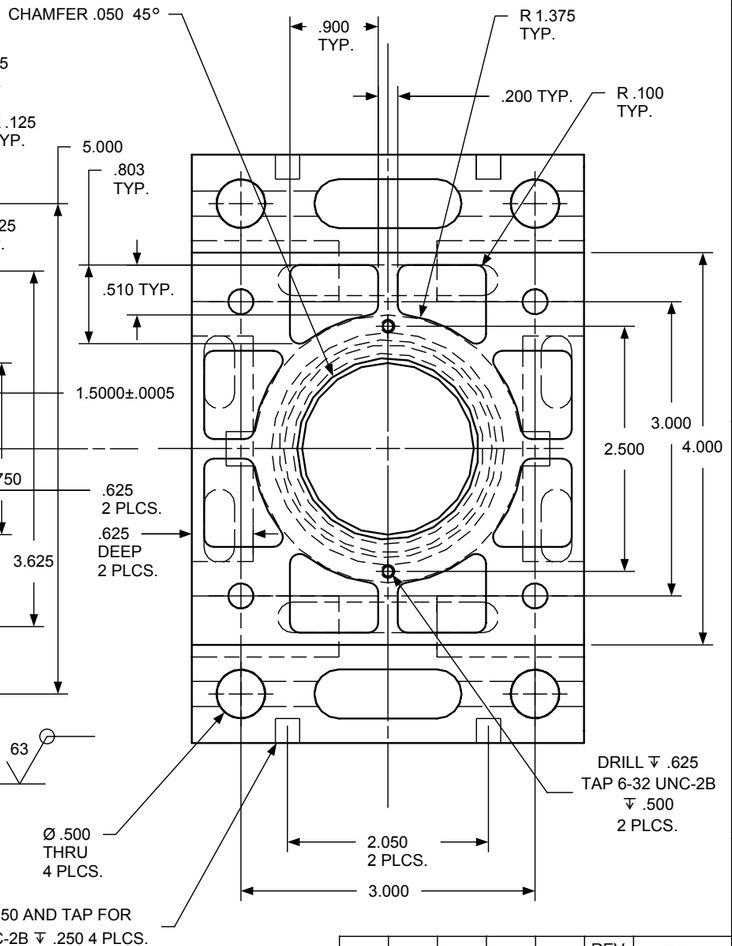

DRAWING NOT TO SCALE

NOTE:
THIS DRAWING GIVES ORIGINAL DIMENSIONS FOR A PART THAT WAS LATER MODIFIED

REV	REV STATUS
SH	

NEXT ASSY	USED ON
APPLICATION	

UNLESS OTHERWISE SPECIFIED
DIM ARE IN INCHES
TOL ON ANGLE ± .25°
2 PL ± .04 3 PL .004
INTERPRET DIM AND TOL PER
ASME Y14.5M - 1994

THIRD ANGLE PROJECTION

MATERIAL:

ALUMINUM ALLOY
7075-T6
REMOVE ALL BURRS
AND SHARP EDGES

CAMERON KERR
179 CHISHOLM AVENUE, TORONTO, ONTARO
M4C 4V9

TITLE
LOWER BEARING HOUSING
TEST CELL YAW ASS'Y

SIZE	CAGE CODE	DWG NO	REV
C		LOWERBEARINGHOUSING.ICD	D

SCALE 1:1 SHEET 1 OF 1

REVISION HISTORY			
REV	DESCRIPTION	DATE	APPROVED
A	INITIAL DRAWING	JAN.12/01	
B	REVISED DIMENSIONS	FEB.4/01	

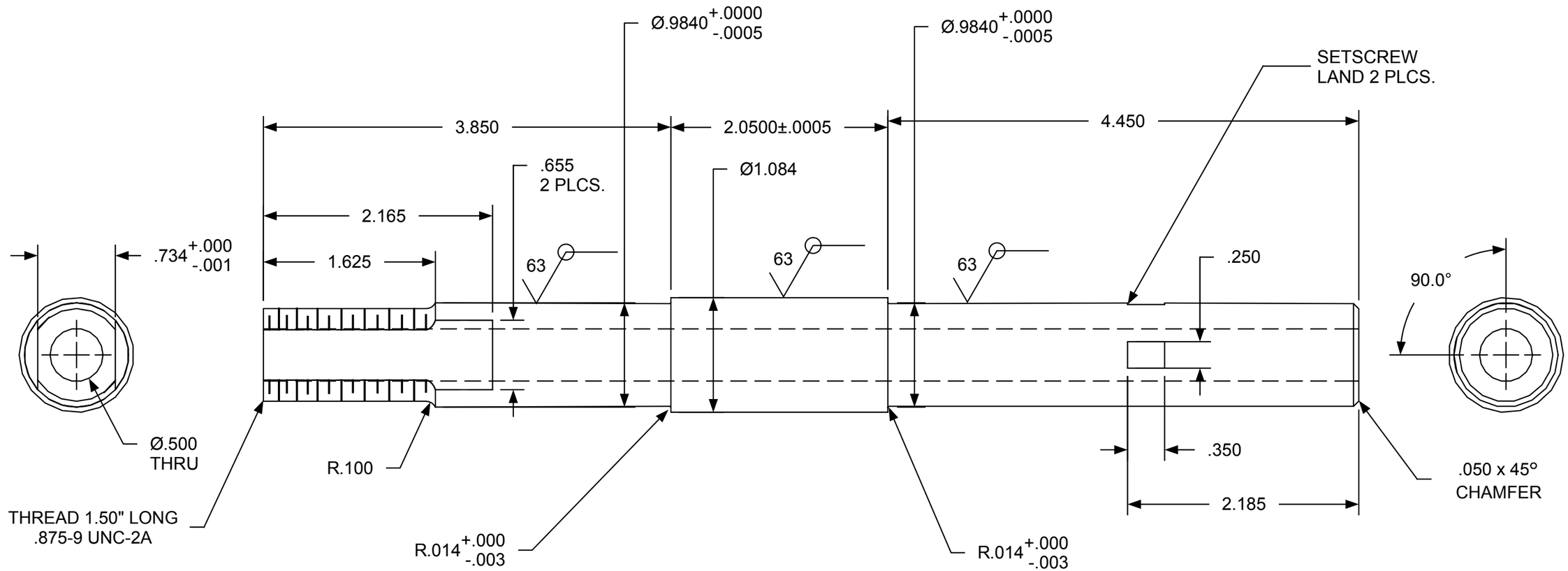

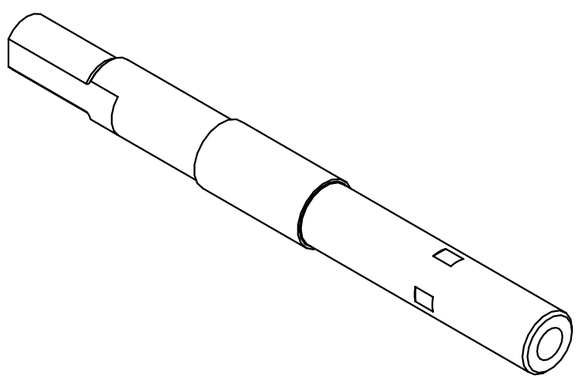

		MATERIAL: 7075-T6 ALUMINUM REMOVE ALL BURRS AND SHARP EDGES	CAMERON KERR 179 CHISHOLM AVENUE, TORONTO ONTARIO M4C 4V9
			TITLE: YAW BEARING SHAFT TEST CELL YAW ASS'Y
		TOLERANCE +/-0.004 UNLESS OTHERWISE NOTED	SIZE B | DWG NO YAW-03 | REV B
NEXT ASSY	USED ON		
APPLICATION		UNITS IN INCHES	SCALE 1:1 | THIRD ANGLE PROJECTION | SHEET 1 OF 1

REVISION HISTORY			
REV	DESCRIPTION	DATE	APPROVED
A	INITIAL DWG.	OCT. 07/01	
B	MODIFIED BENDS	NOV. 06/01	

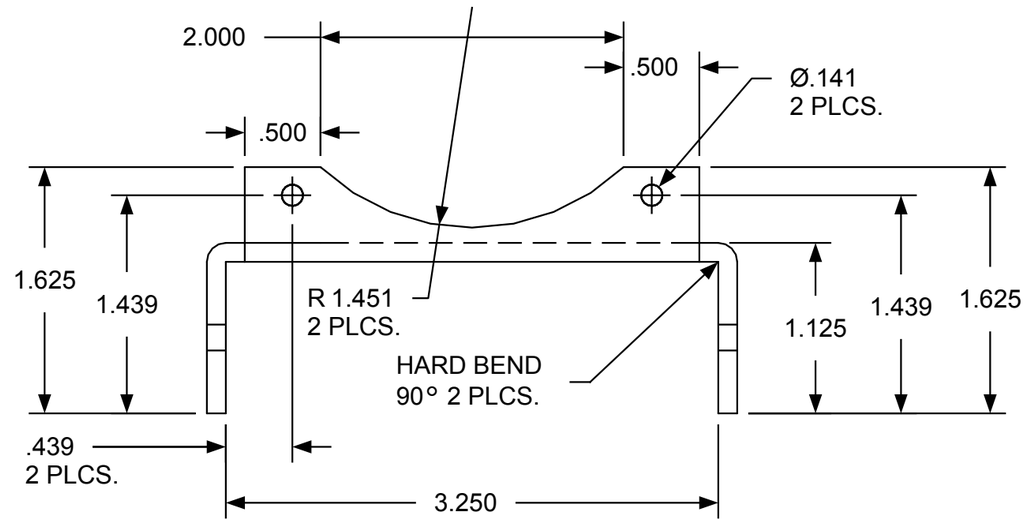

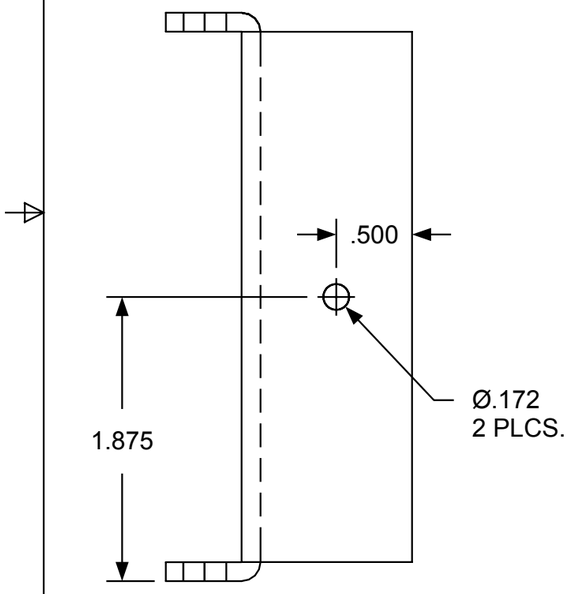

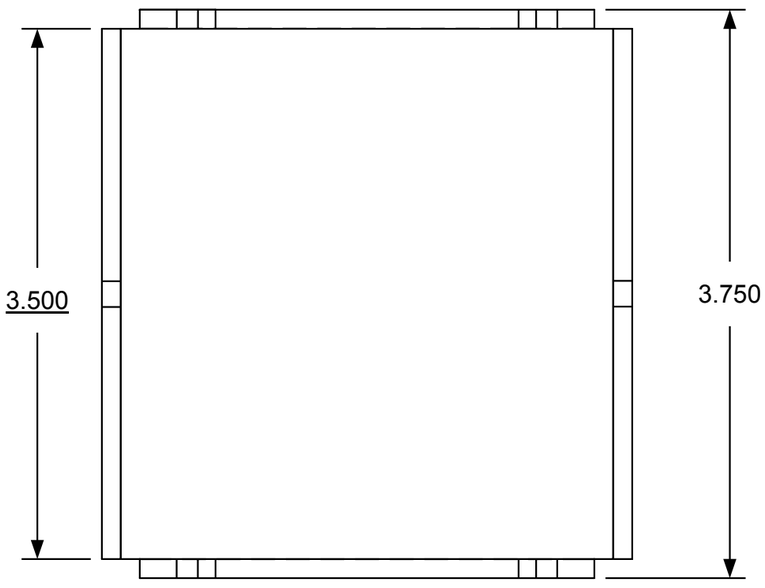

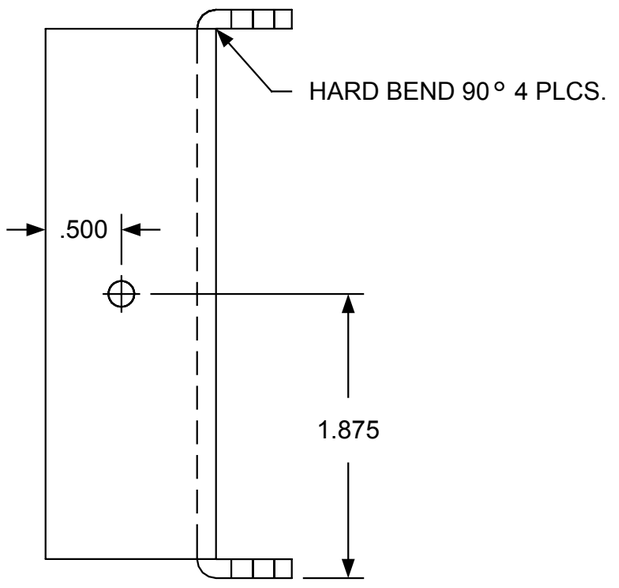

	REV
	SH

REV STATUS

NEXT ASSY	USED ON
APPLICATION	

MATERIAL:
0.125 ALUMINUM
5052 H32
FINISH: NONE

REMOVE BURRS AND
SHARP EDGES

TOLERANCE +/-0.005

UNITS IN INCHES

CAMERON KERR
179 CHISHOLM AVENUE, TORONTO ONTARIO
M4C 4V9

TITLE

HELICOPTER IDP
SUPPORT BRACKET, YAW ASSY

SIZE	CAGE CODE	DWG NO	REV
B		YAW-05	B

SCALE 1:2 | THIRD ANGLE PROJECTION | SHEET 1 OF 1

REVISION HISTORY			
REV	DESCRIPTION	DATE	APPROVED
A	INITIAL DWG.	OCT.17/01	
B	FYH BEARING MODS	NOV.24/01	

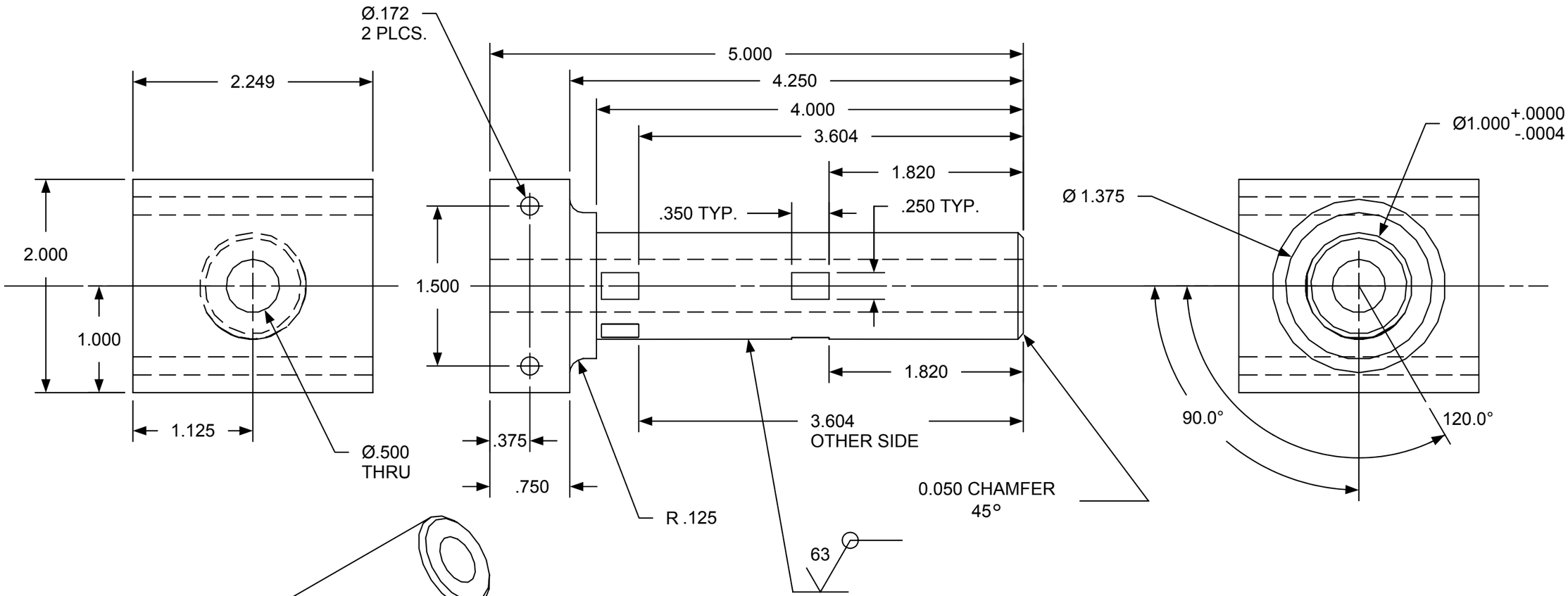

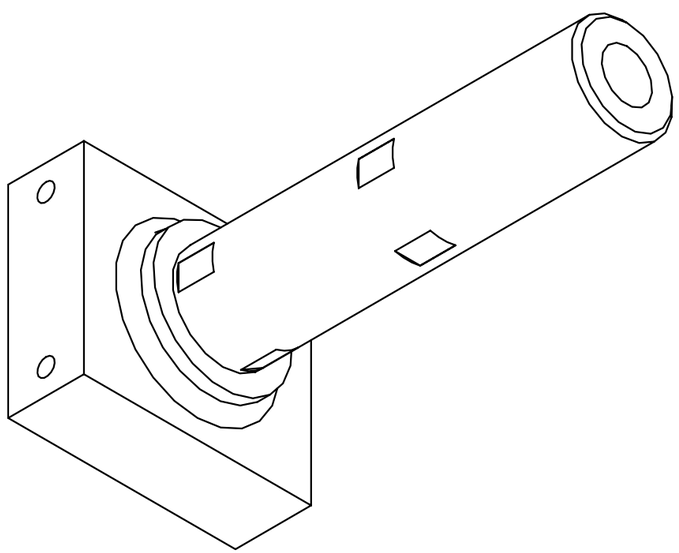

	REV	REV STATUS
	SH	

		MATERIAL: 7075 T6 ALUMINUM FINISH: NONE REMOVE BURRS AND SHARP EDGES	CAMERON KERR 179 CHISHOLM AVENUE, TORONTO ONTARIO M4C 4V9
NEXT ASSY	USED ON	TOLERANCE +/-0.005	TITLE: HELICOPTER IDP PITCH BEARING SHAFT, SLIPRING SIDE
APPLICATION		UNITS IN INCHES	SIZE B · CAGE CODE · DWG NO PITCH-01 · REV B SCALE 1:1 · THIRD ANGLE PROJECTION · SHEET 1 OF 1

REVISION HISTORY			
REV	DESCRIPTION	DATE	APPROVED
A	INITIAL DWG.	OCT.17/01	
B	FYH BEARING MODS	NOV.24/01	
C	ROTATION LIMITER ADDED	DEC.09/01	
D	ROTATION LIMITER CHANGED	OCT.14/02	

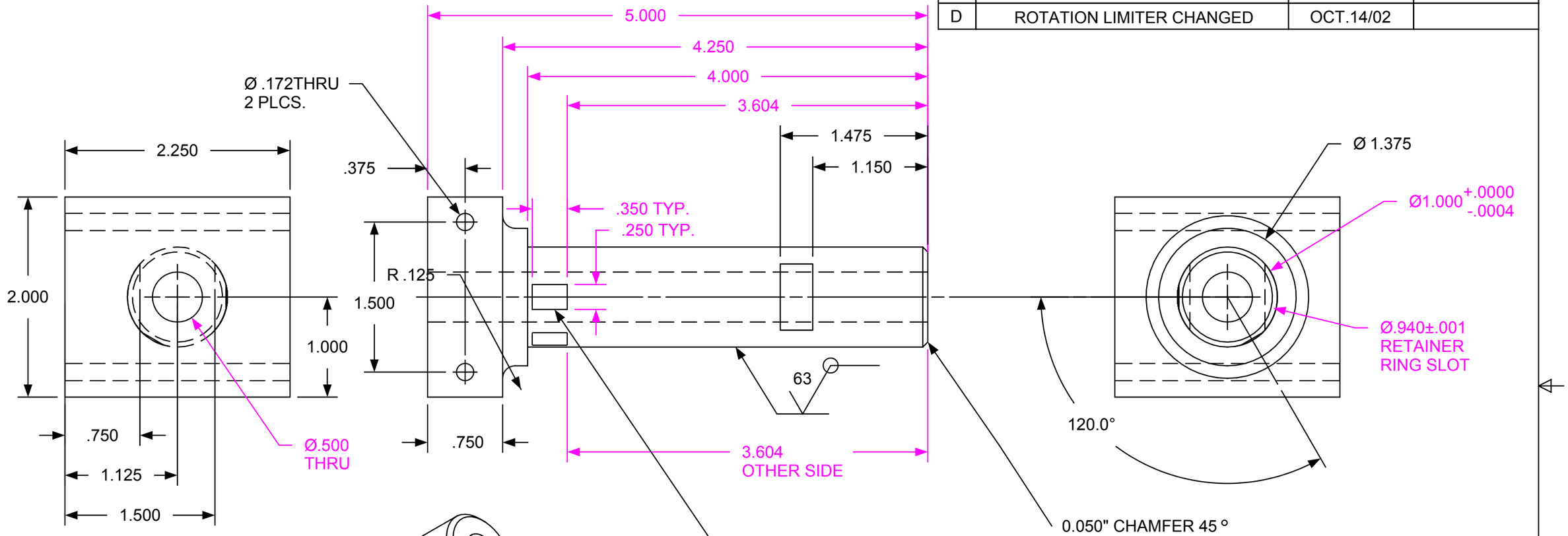

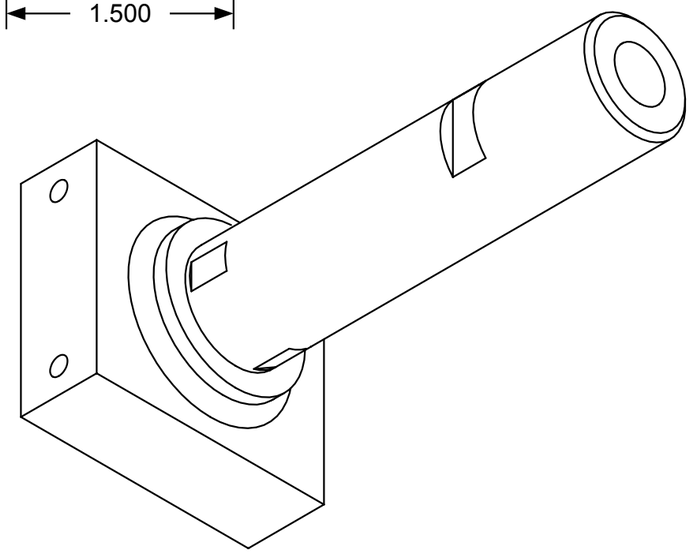

		REV	REV STATUS
		SH	

		MATERIAL: 7075 T6 ALUMINUM FINISH: NONE REMOVE BURRS AND SHARP EDGES	CAMERON KERR 46 NOVELLA ROAD, CONCORD, ONTARIO L4K 5J9
NEXT ASSY	USED ON	TOLERANCE +/-0.005 UNLESS OTHERWISE NOTED	TITLE: HELICOPTER IDP PITCH BEARING SHAFT, DIGITAL ENCODER SIDE
APPLICATION		UNITS IN INCHES	SIZE B · CAGE CODE · DWG NO PITCH-02 · REV C SCALE 1:1 · THIRD ANGLE PROJECTION · SHEET 1 OF 1

REVISION HISTORY			
REV	DESCRIPTION	DATE	APPROVED
A	INITIAL DWG.	OCT.17/01	

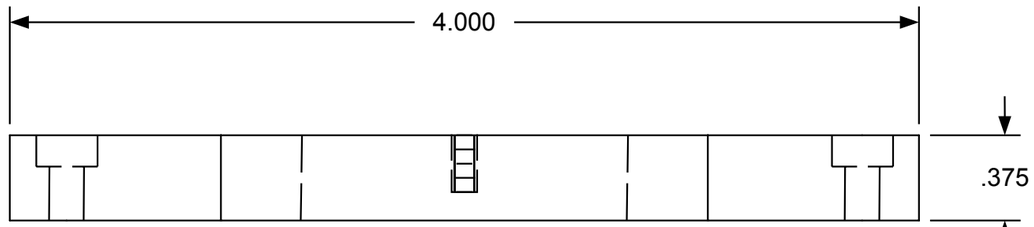

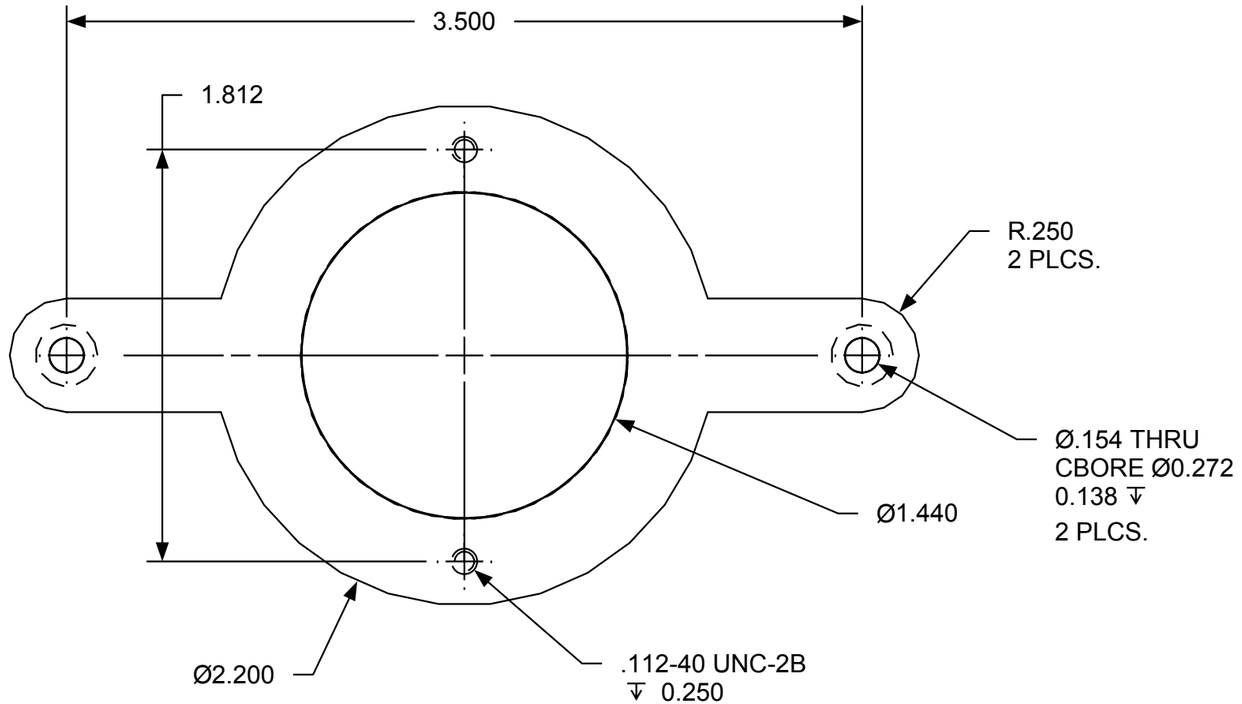

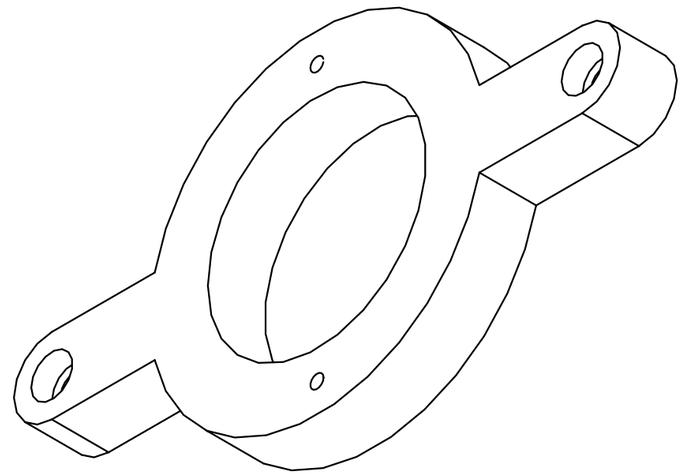

						REV	REV STATUS
						SH	

		MATERIAL: 7075 T6 ALUMINUM FINISH: NONE REMOVE BURRS AND SHARP EDGES	CAMERON KERR 179 CHISHOLM AVENUE, TORONTO ONTARIO M4C 4V9
NEXT ASSY	USED ON	TOLERANCE +/-0.005	TITLE: HELICOPTER IDP PITCH ENCODER SUPPORT
APPLICATION		UNITS IN INCHES	SIZE B · CAGE CODE · DWG NO PITCH-03 · REV A SCALE 1.5:1 · THIRD ANGLE PROJECTION · SHEET 1 OF 1

REV STATUS		REVISION HISTORY			
REV	SH	REV	DESCRIPTION	DATE	APPROVED
		A	INITIAL DRAWING	JAN 27/02	

NOTE: WELDS FROM TUBING ENDS TO OTHER PARTS ARE FIRST CAPPED BY 1" X 1" 0.050" THICK 6061-T6 SHEET AS SHOWN TO PREVENT BLOW THROUGH OF WELDS

MEASURES TO PREVENT BLOW THROUGH NOT REQUIRED

DETAIL A ELIMENATED 12 PLCS.

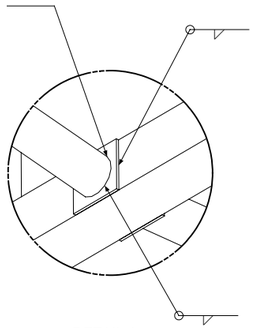

DETAIL A
12 PLCS.

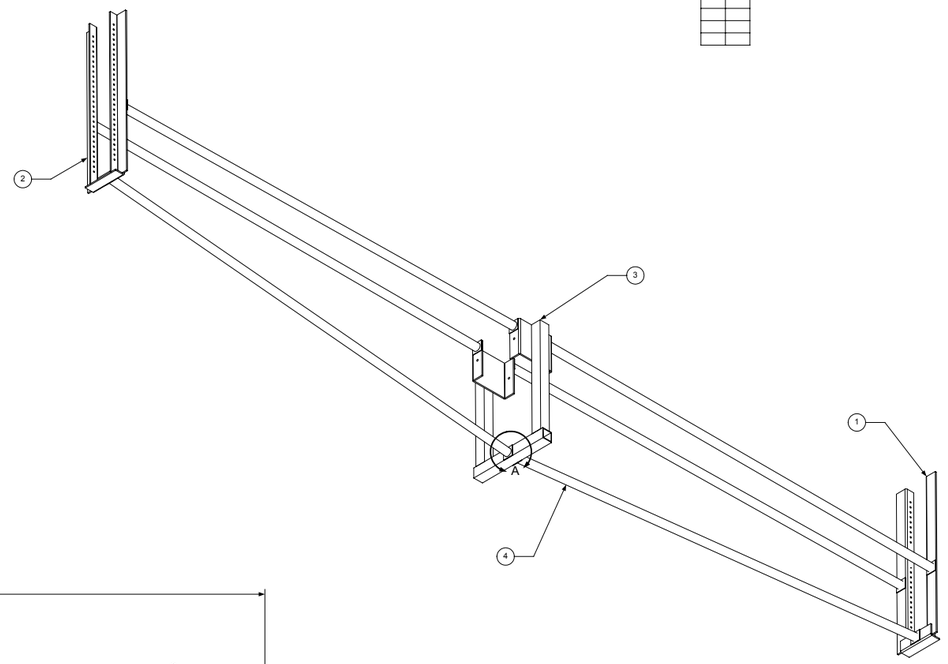

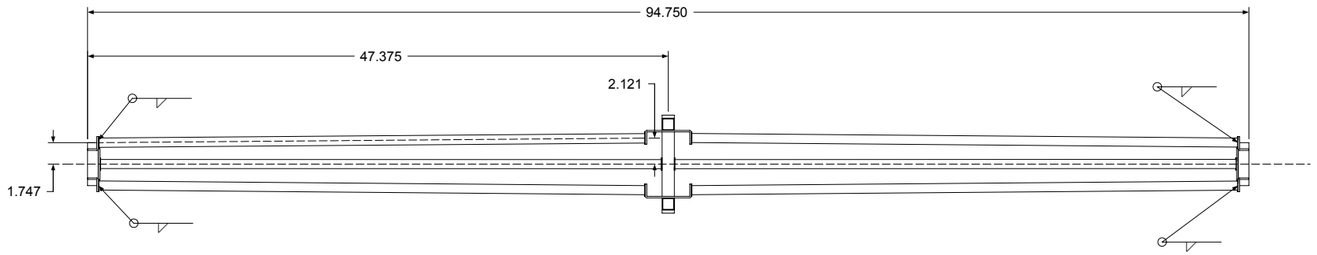

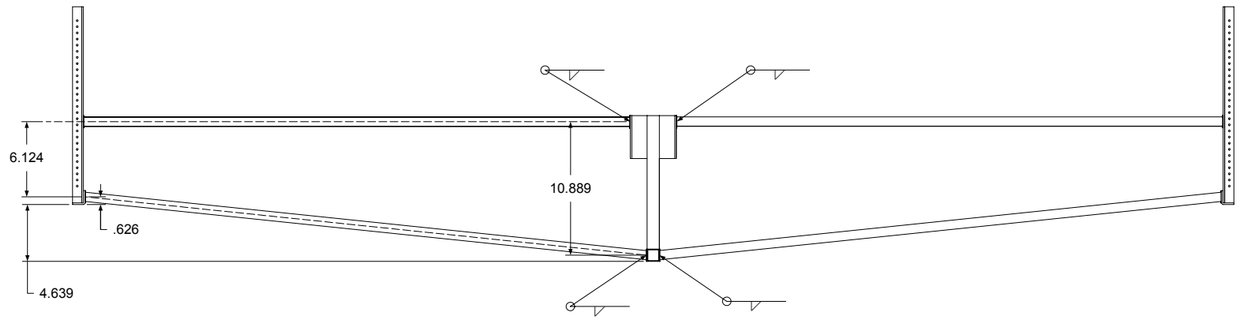

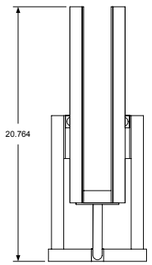

DRAWING NOT TO SCALE

Item No.	Part Number	Qty	Description
1	Height Adjust End Bracket	1	
2	Height Adjust End Bracket	1	
3	Pitch Frame Yaw Support	1	
4	6063-T6 3/4x .035 wall tube	6	Various lengths

UNLESS OTHERWISE SPECIFIED
DIM ARE IN INCHES
TOL ON ANGLE ± .5°
2 PL ± 020 3 PL .005
INTERPRET DIM AND TOL PER
ASME Y14.5M - 1994

THIRD ANGLE PROJECTION

NEXT ASSY | USED ON
APPLICATION

CAMERON KERR
46 NOVELLA ROAD, CONCORD, ONTARIO
L4K 5J9

TITLE
HELICOPTER IDP
PITCH FRAME ASSEMBLY

SIZE	CAGE CODE	DWG NO	REV
E		PITCH-04	A

SCALE 1:4 SHEET 1 OF 1

REVISION HISTORY			
REV	DESCRIPTION	DATE	APPROVED
A	INITIAL DWG.	FEB.16/02	
B	REVISED MOUNTING HOLE LOC'S	FEB.24/02	

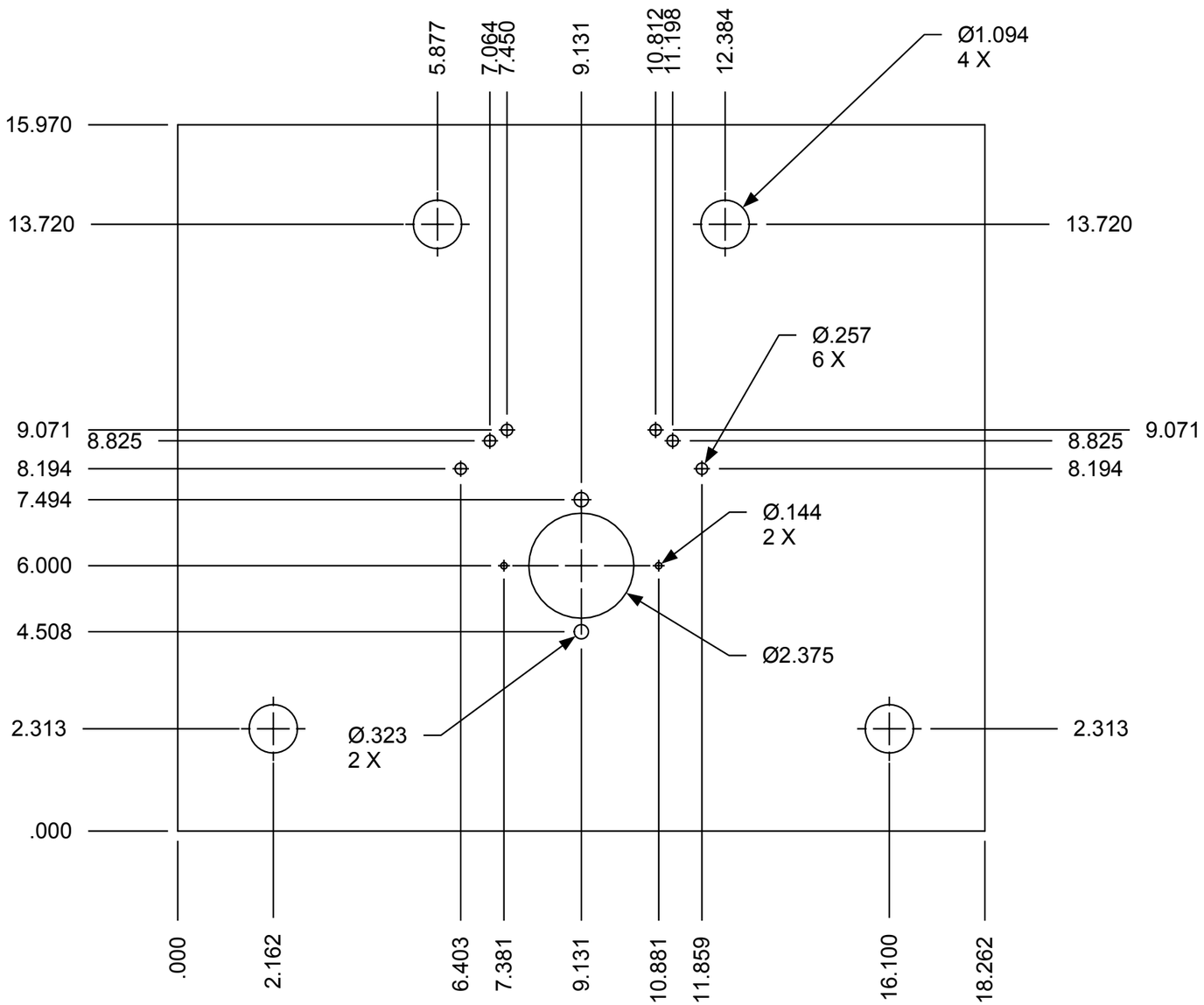

	REV
	SH

REV STATUS

NEXT ASSY	USED ON
APPLICATION	

MATERIAL:
0.250 ALUMINUM
6061-T6
FINISH: NONE

REMOVE BURRS AND SHARP EDGES

TOLERANCE +/-0.005

UNITS IN INCHES

CAMERON KERR
46 NOVELLA ROAD, CONCORD, ONTARIO
L4K 5J9

TITLE

HELICOPTER IDP
ENCODER PITCH BEARING SUPPORT A

SIZE	CAGE CODE	DWG NO	REV
B		PITCH-05	B

SCALE 1:3 | THIRD ANGLE PROJECTION | SHEET 1 OF 1

REVISION HISTORY			
REV	DESCRIPTION	DATE	APPROVED
A	INITIAL DWG.	FEB.16/02	
B	MOVED MOUNTING HOLE LOC'S	FEB.24/02	

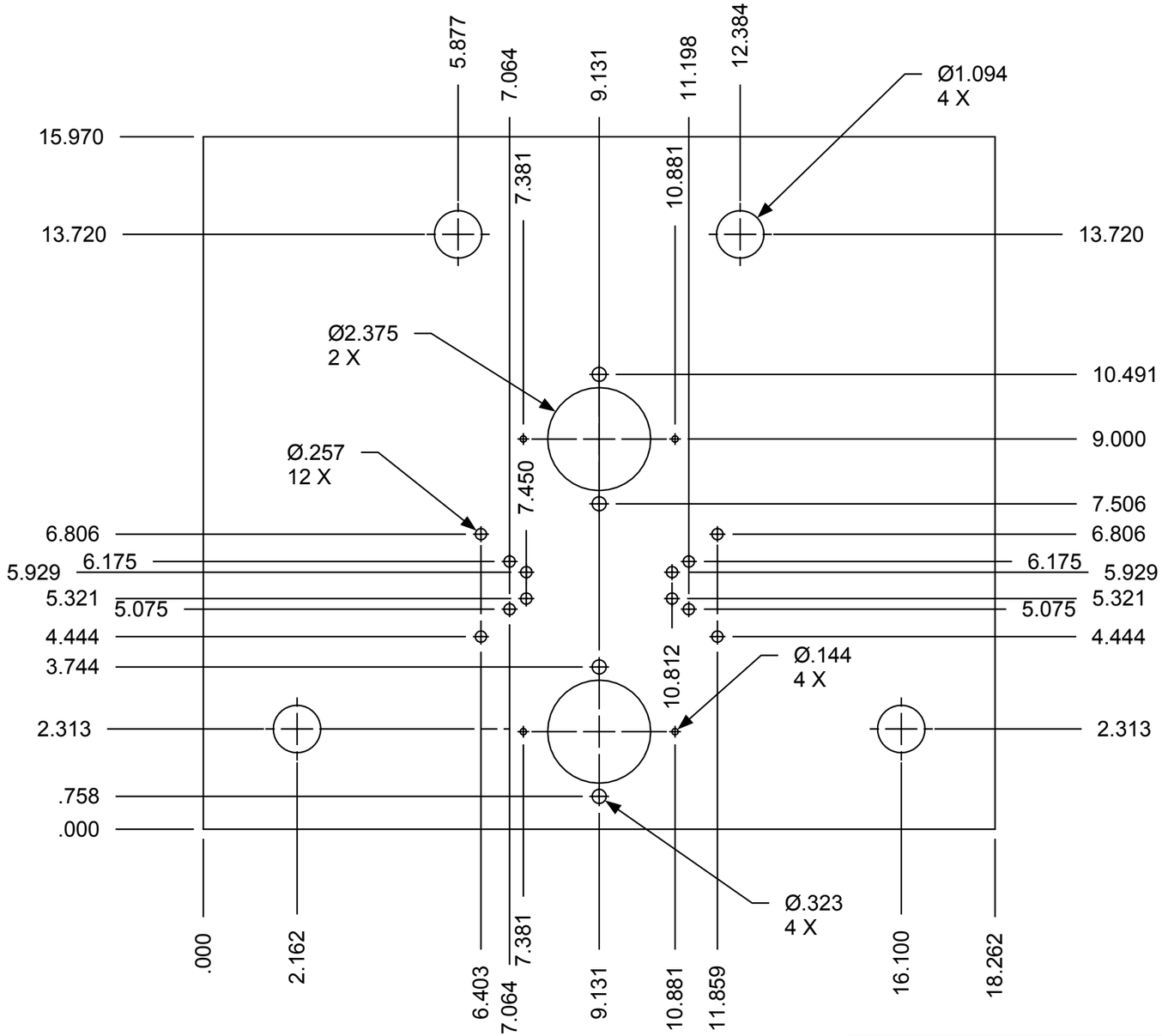

	REV	REV STATUS
	SH	

		MATERIAL: 0.250 ALUMINUM 6061-T6 FINISH: NONE REMOVE BURRS AND SHARP EDGES	CAMERON KERR 46 NOVELLA ROAD, CONCORD, ONTARIO L4K 5J9
NEXT ASSY	USED ON	TOLERANCE +/-0.005	TITLE HELICOPTER IDP ENCODER PITCH BEARING SUPPORT B
APPLICATION		UNITS IN INCHES	SIZE B · CAGE CODE · DWG NO PITCH-06 · REV B SCALE 1:3 · THIRD ANGLE PROJECTION · SHEET 1 OF 1

REVISION HISTORY			
REV	DESCRIPTION	DATE	APPROVED
A	INITIAL DWG.	FEB.16/02	
B	MOVED MOUNTING HOLE LOC'S	FEB.24/02	

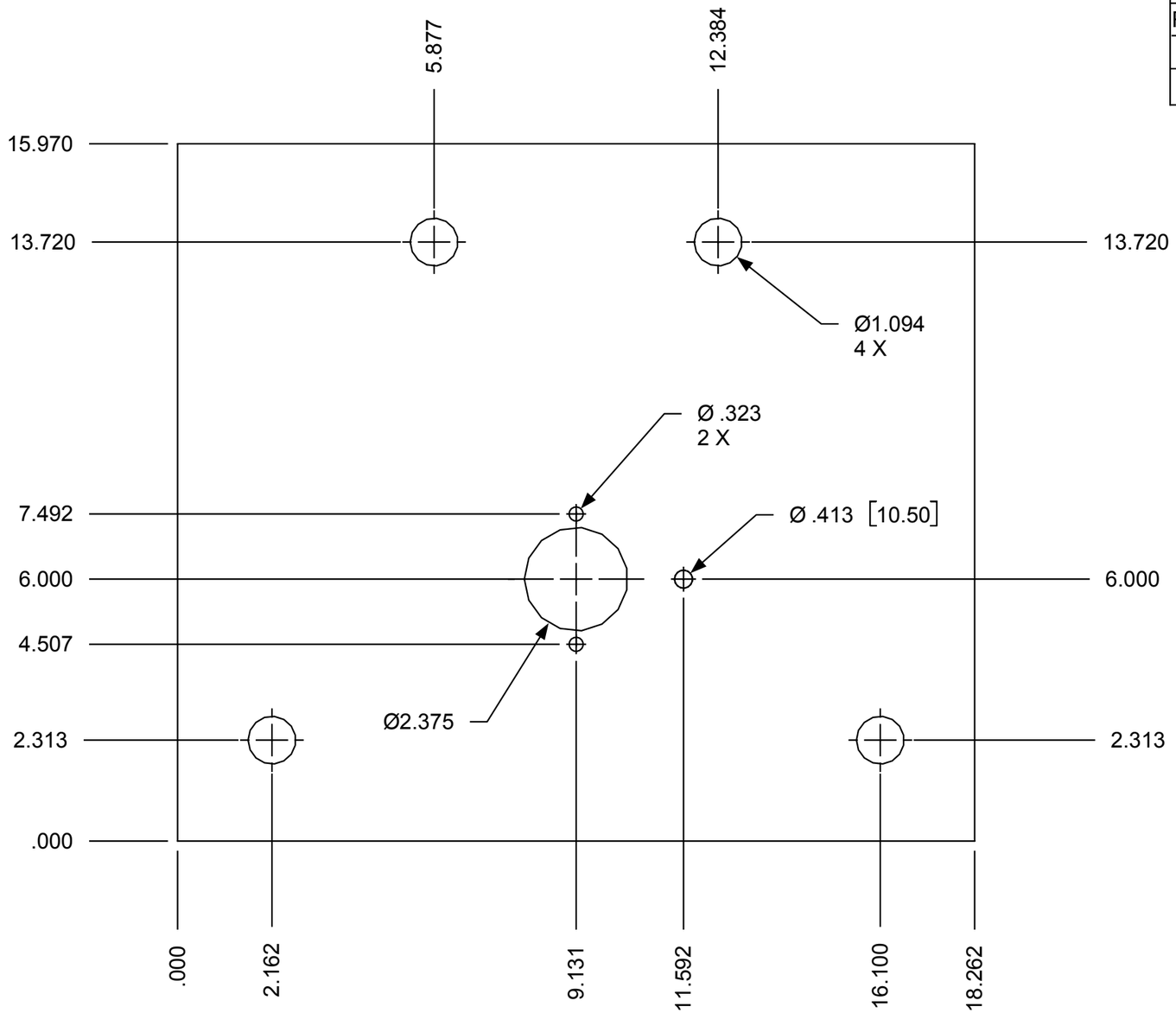

					REV	REV STATUS
					SH	

		MATERIAL: 0.250 ALUMINUM 6061-T6 FINISH: NONE REMOVE BURRS AND SHARP EDGES	CAMERON KERR 46 NOVELLA ROAD, CONCORD, ONTARIO L4K 5J9
			TITLE HELICOPTER IDP SLIPRING PITCH BEARING SUPPORT A
NEXT ASSY	USED ON	TOLERANCE +/-0.005	SIZE B | CAGE CODE | DWG NO PITCH-07 | REV B
APPLICATION		UNITS IN INCHES [MM]	SCALE 1:3 | THIRD ANGLE PROJECTION | SHEET 1 OF 1

REVISION HISTORY			
REV	DESCRIPTION	DATE	APPROVED
A	INITIAL DWG.	FEB.16/02	
B	MOVED MOUNTING HOLE LOC'S	FEB.24/02	

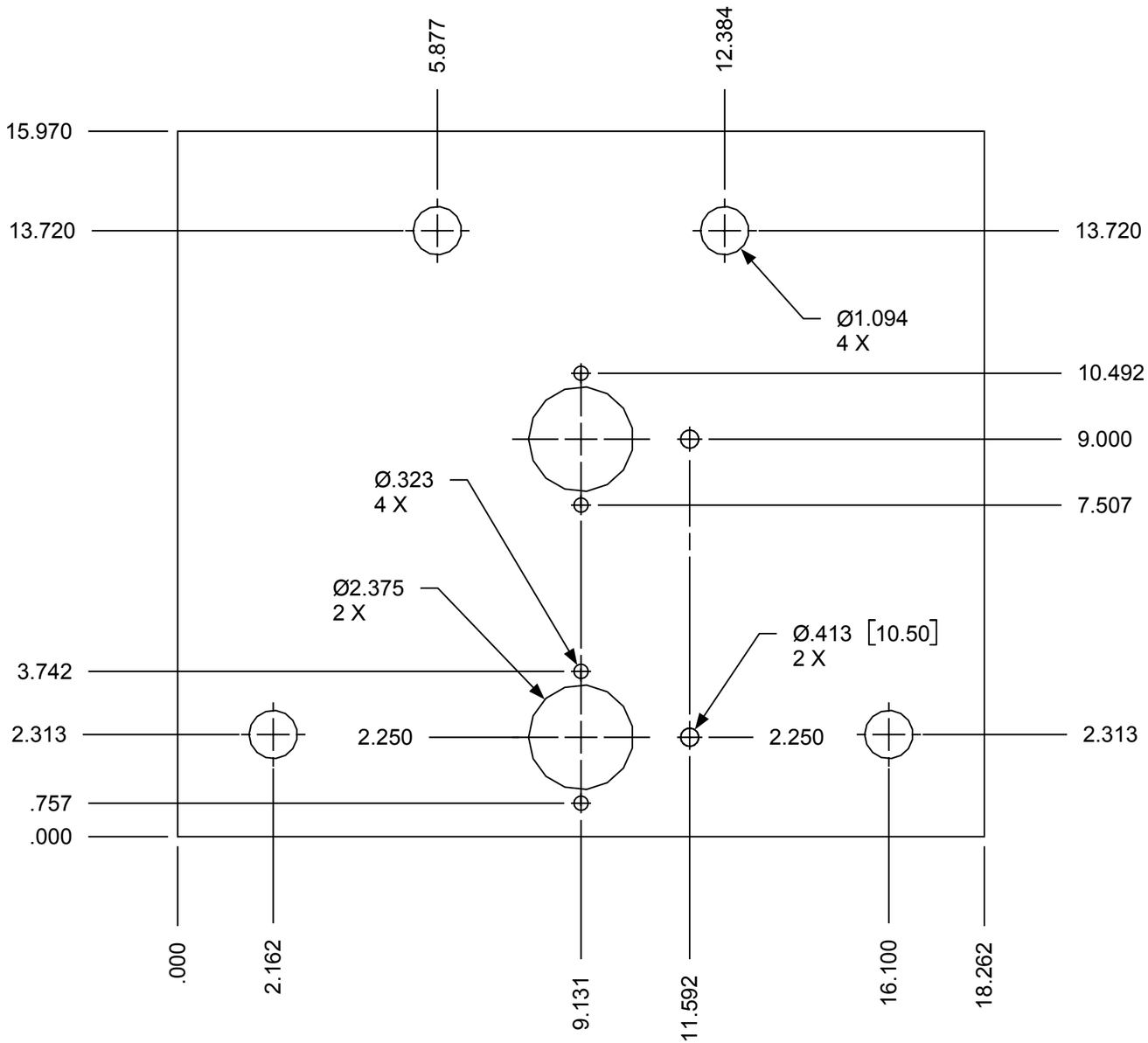

	REV
	SH

REV STATUS

NEXT ASSY	USED ON
APPLICATION	

MATERIAL:
0.250 ALUMINUM
6061-T6
FINISH: NONE

REMOVE BURRS AND SHARP EDGES

TOLERANCE +/-0.005

UNITS IN INCHES [MM]

CAMERON KERR
46 NOVELLA ROAD, CONCORD, ONTARIO
L4K 5J9

TITLE

HELICOPTER IDP
SLIPRING PITCH BEARING SUPPORT B

SIZE	CAGE CODE	DWG NO	REV
B		PITCH-08	B

SCALE 1:3 | THIRD ANGLE PROJECTION | SHEET 1 OF 1

REVISION HISTORY			
REV	DESCRIPTION	DATE	APPROVED
A	INITIAL DWG.	DEC.16/01	

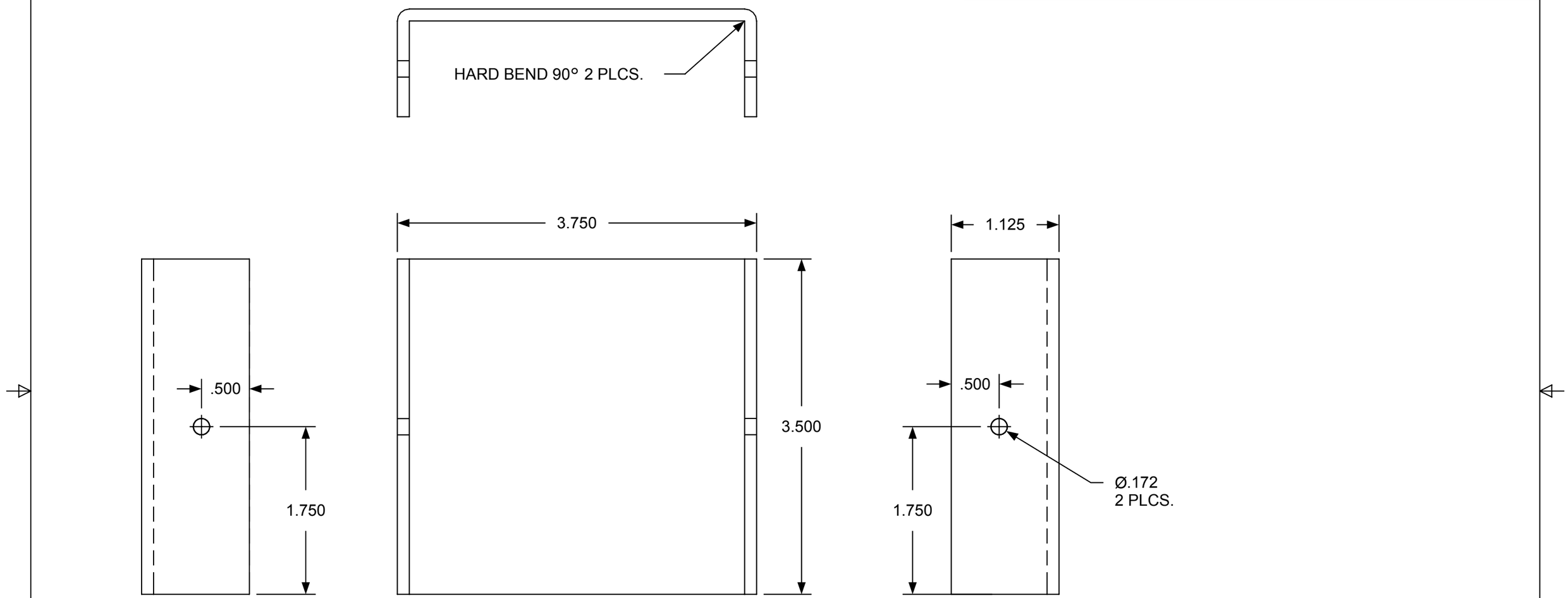

					REV	REV STATUS
					SH	

		MATERIAL: 0.125 ALUMINUM 5052 H32 FINISH: NONE REMOVE BURRS AND SHARP EDGES	CAMERON KERR 46 NOVELLA ROAD, CONCORD, ONTARIO L4K 5J9
			TITLE HELICOPTER IDP PITCH FRAME ADAPTER PLATE
NEXT ASSY	USED ON	TOLERANCE +/-0.005	SIZE B | CAGE CODE | DWG NO PITCH-09 | REV A
APPLICATION		UNITS IN INCHES	SCALE 1:2 | THIRD ANGLE PROJECTION | SHEET 1 OF 1

REV STATUS		REVISION HISTORY			
REV	SH	REV	DESCRIPTION	DATE	APPROVED
		A	INITIAL DWG.	JAN.09/02	

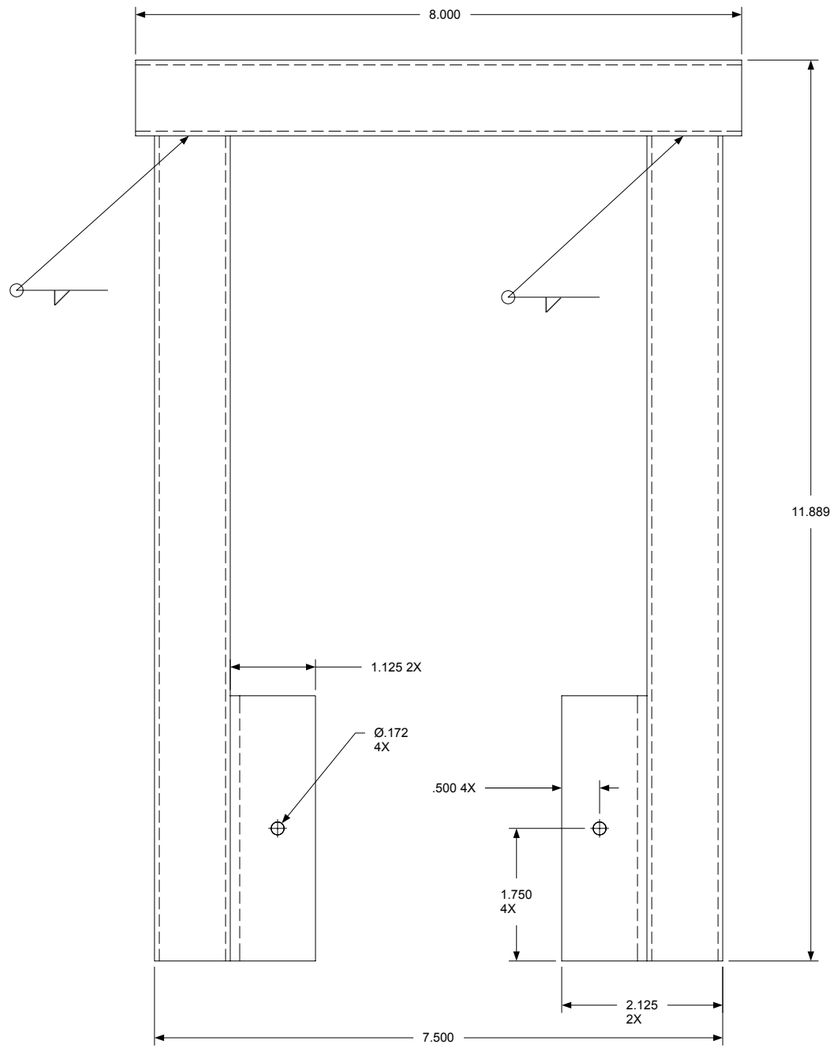

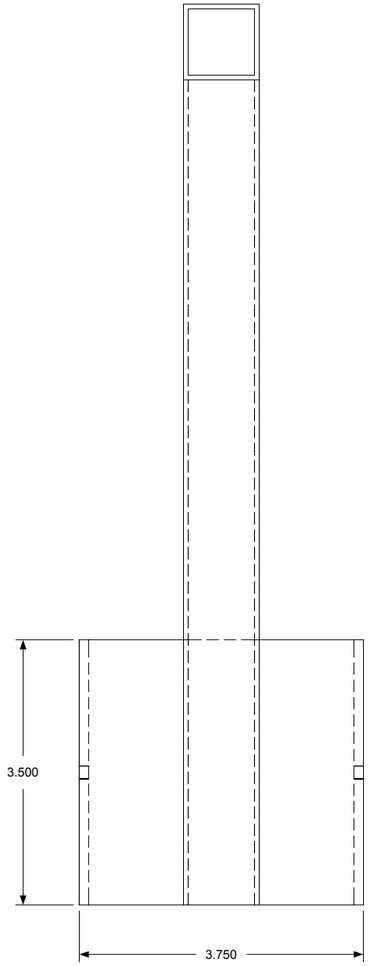

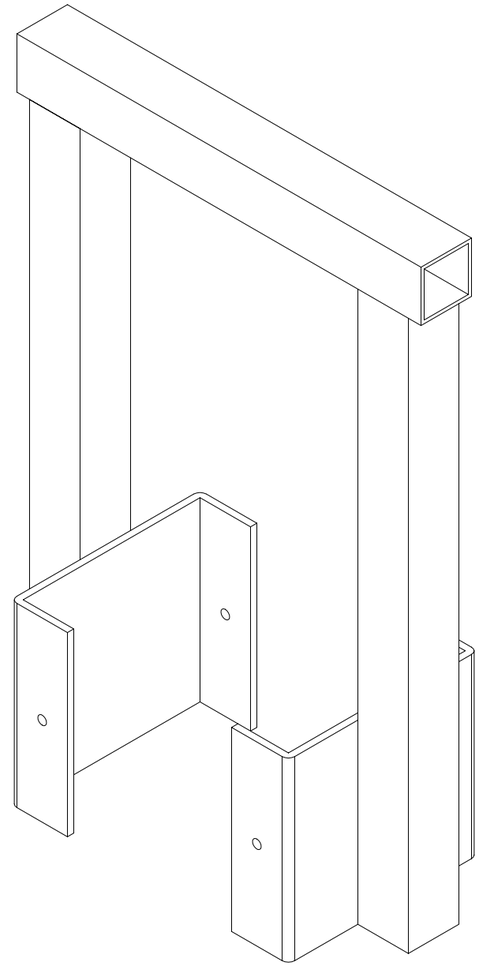

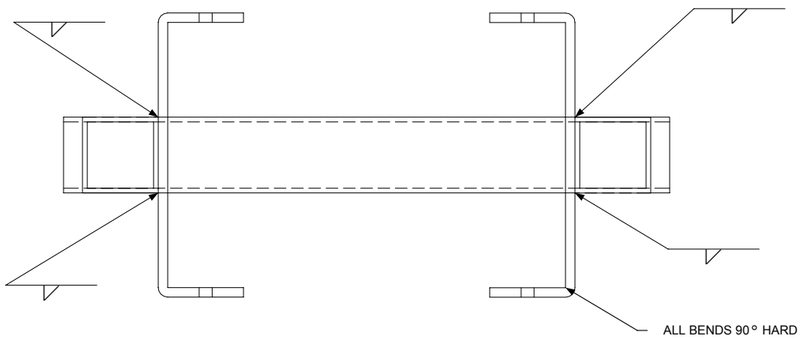

DRAWING NOT TO SCALE

NEXT ASSY	USED ON
APPLICATION	

UNLESS OTHERWISE SPECIFIED
DIM ARE IN INCHES
TOL ON ANGLE ± .5°
2 PL ± .02 3 PL .005
INTERPRET DIM AND TOL PER
ASME Y14.5M - 1994

THIRD ANGLE PROJECTION

MATERIALS:

.062 WALL, 1"X1" ALUMINUM SQUARE SECTION TUBE

5052 H32 .125" ALUMINUM

FINISH: NONE

REMOVE ALL BURRS AND SHARP EDGES

CAMERON KERR
46 NOVELLA ROAD, CONCORD, ONTARIO
L4K 5J9

TITLE

HELICOPTER IDP
PITCH FRAME YAW ASSEMBLY

SIZE	CAGE CODE	DWG NO	REV
D		PITCH-10	A

SCALE 1:1 SHEET 1 OF 1

REVISION HISTORY			
REV	DESCRIPTION	DATE	APPROVED
A	INITIAL DWG.	OCT.24/01	
B	HEIGHT INCREASED TO 16"	NOV.19/01	

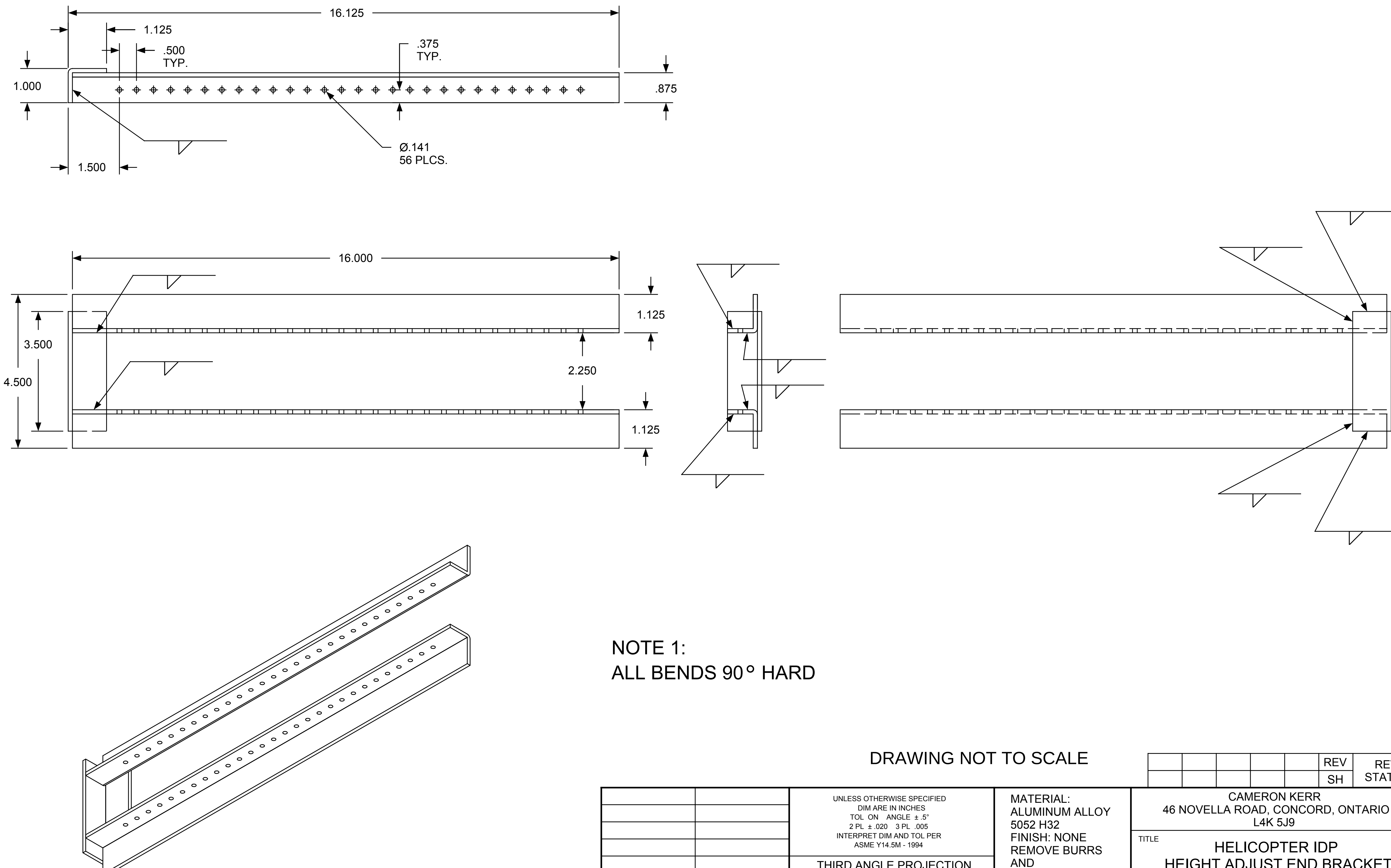

NOTE 1:
ALL BENDS 90° HARD

DRAWING NOT TO SCALE

					REV	REV STATUS
					SH	

		UNLESS OTHERWISE SPECIFIED DIM ARE IN INCHES TOL ON ANGLE ± .5° 2 PL ± .020 3 PL .005 INTERPRET DIM AND TOL PER ASME Y14.5M - 1994	MATERIAL: ALUMINUM ALLOY 5052 H32 FINISH: NONE REMOVE BURRS AND SHARP EDGES	CAMERON KERR 46 NOVELLA ROAD, CONCORD, ONTARIO L4K 5J9
		THIRD ANGLE PROJECTION		TITLE HELICOPTER IDP HEIGHT ADJUST END BRACKET
NEXT ASSY	USED ON			SIZE C / CAGE CODE / DWG NO PITCH-11 / REV B
APPLICATION				SCALE 1:2 / SHEET 1 OF 1

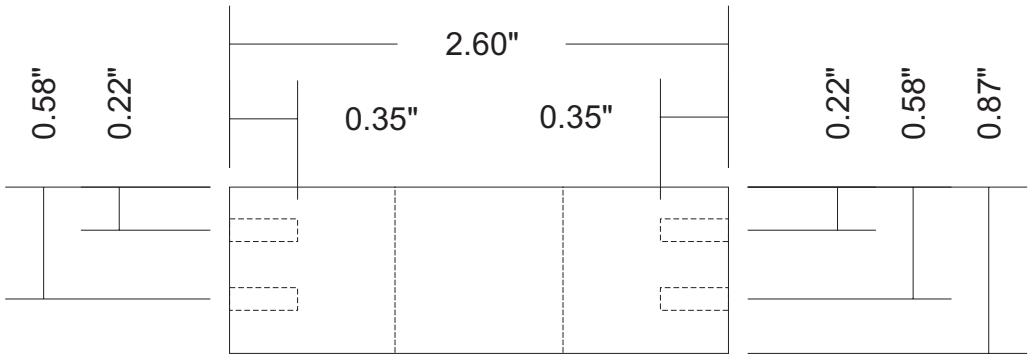

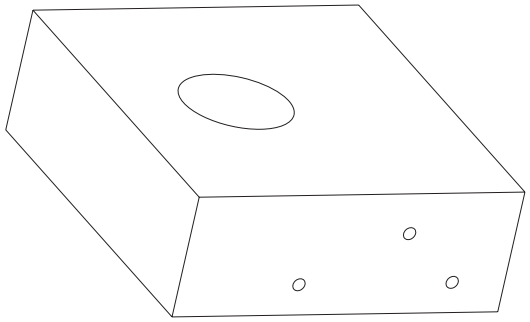

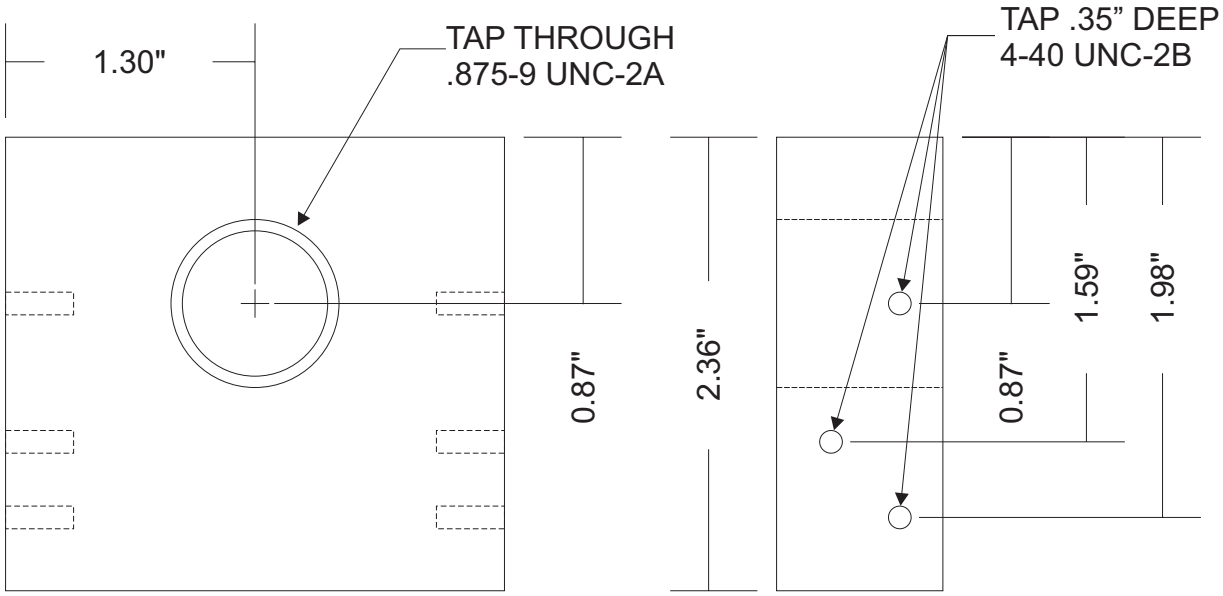

MATERIAL 7075-T6
ALUMINUM

HELICOPTER IDENTIFICATION PROJECT CONTROL GROUP UNIVERSITY OF TORONTO	TITLE: HELICOPTER MOUNTING BLOCK	NO: MOUNT-1
	DATE: JUNE 18, 2001	BY: C.L.

REVISION HISTORY			
REV	DESCRIPTION	DATE	APPROVED
A	INITIAL DWG.	FEB.10/01	

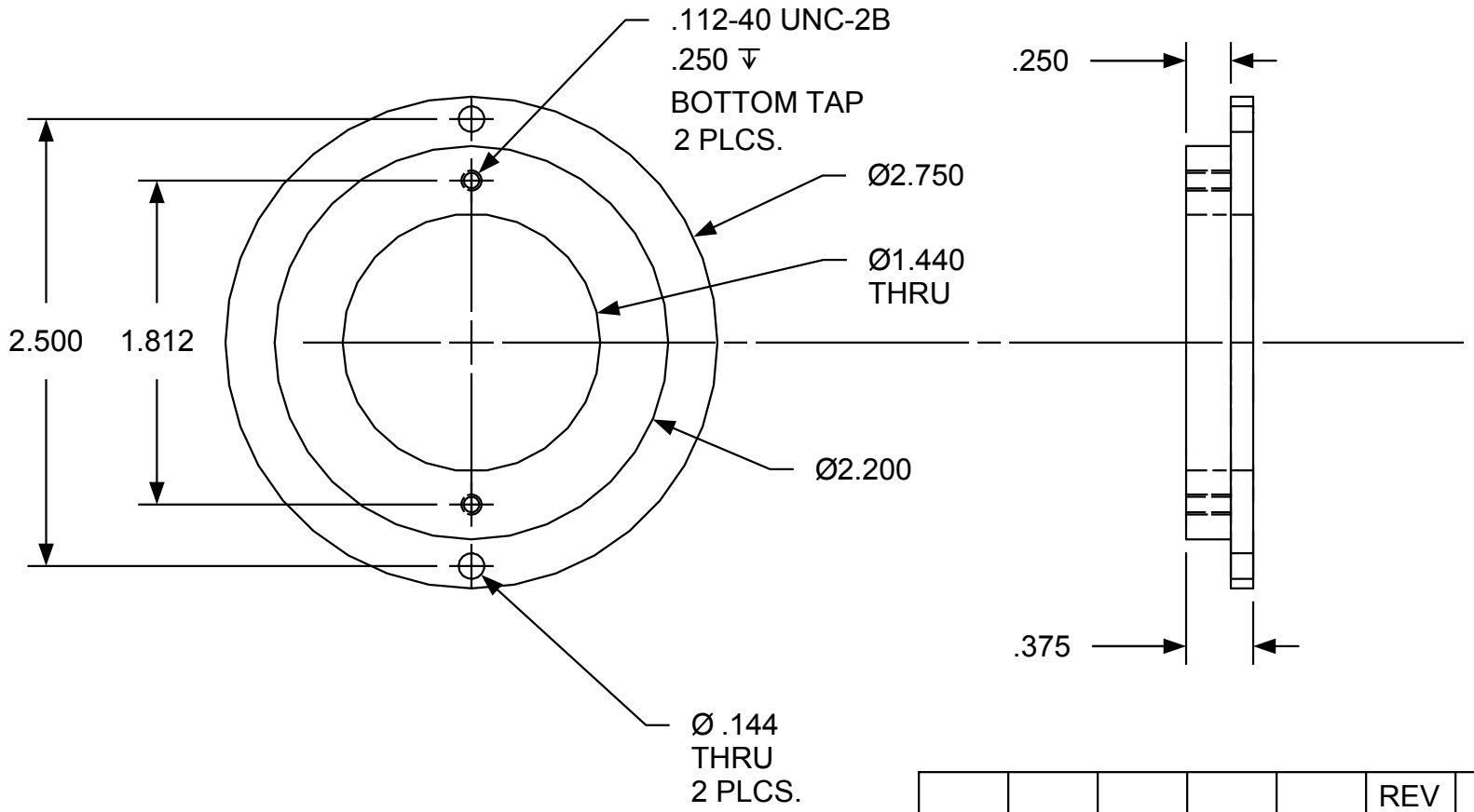

					REV	REV STATUS
					SH	

NEXT ASSY	USED ON
APPLICATION	

MATERIAL

ALUMINUM ALLOY
7075-T6
REMOVE ALL BURRS
AND SHARP EDGES

TOLERANCE +/-0.004
UNLESS OTHERWISE NOTED

UNITS IN INCHES

CAMERON KERR
179 CHISHOLM AVENUE, TORONTO ONTARIO
M4C 4V9

TITLE

LOWER SHAFT COVER
TEST CELL YAW ASS'Y

SIZE	CAGE CODE	DWG NO	REV
A		YAW-04	A

SCALE 1:1 | THIRD ANGLE PROJECTION | SHEET 1 OF 1

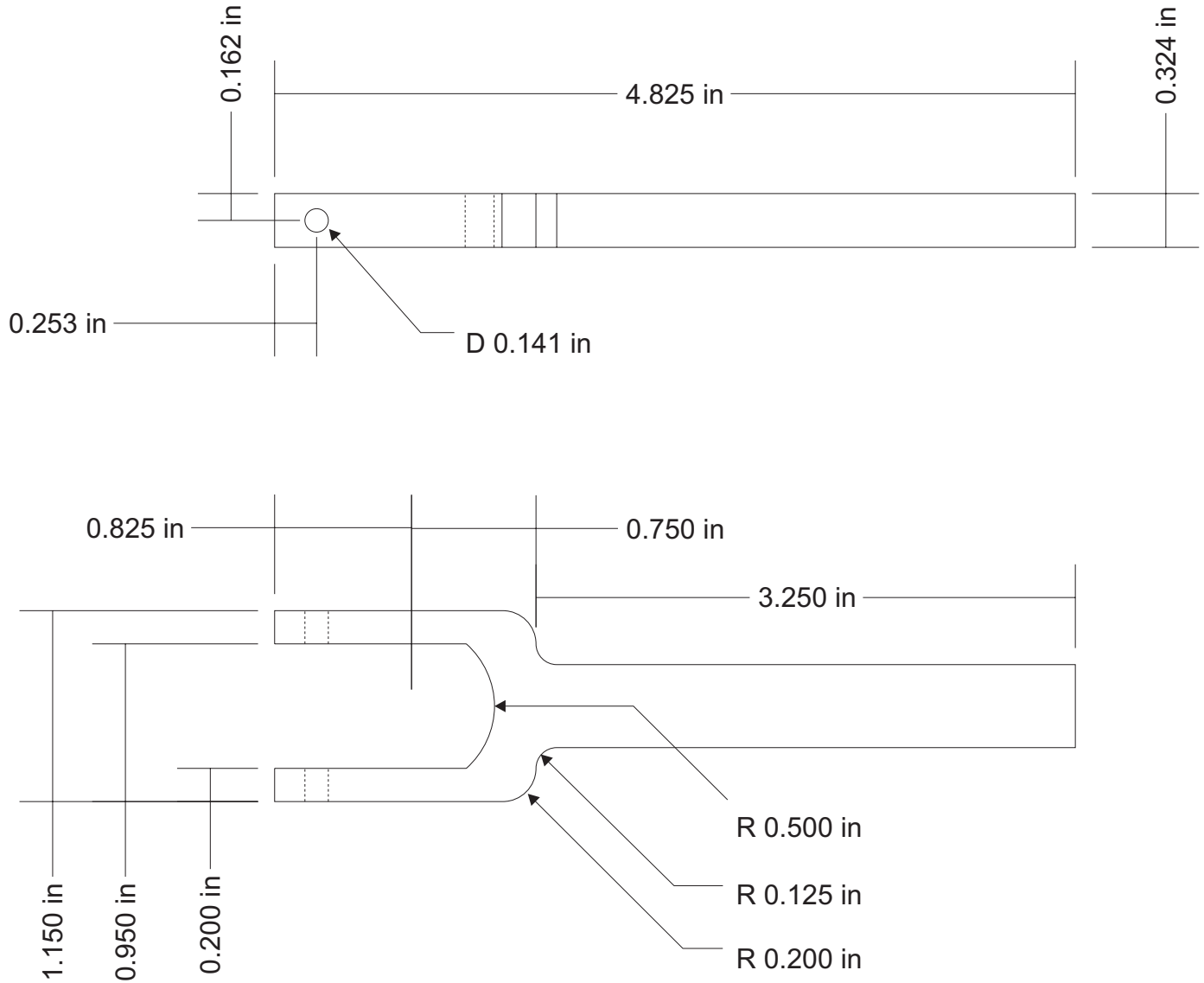

HELICOPTER IDENTIFICATION PROJECT CONTROL GROUP UNIVERSITY OF TORONTO	TITLE: PITCH LIMITER	NO: PITCH-12
	DATE: DECEMBER 17, 2001	BY: C.L.

DO NOT BUILD
FROM THIS DWG.
FOR REFERENCE
ONLY

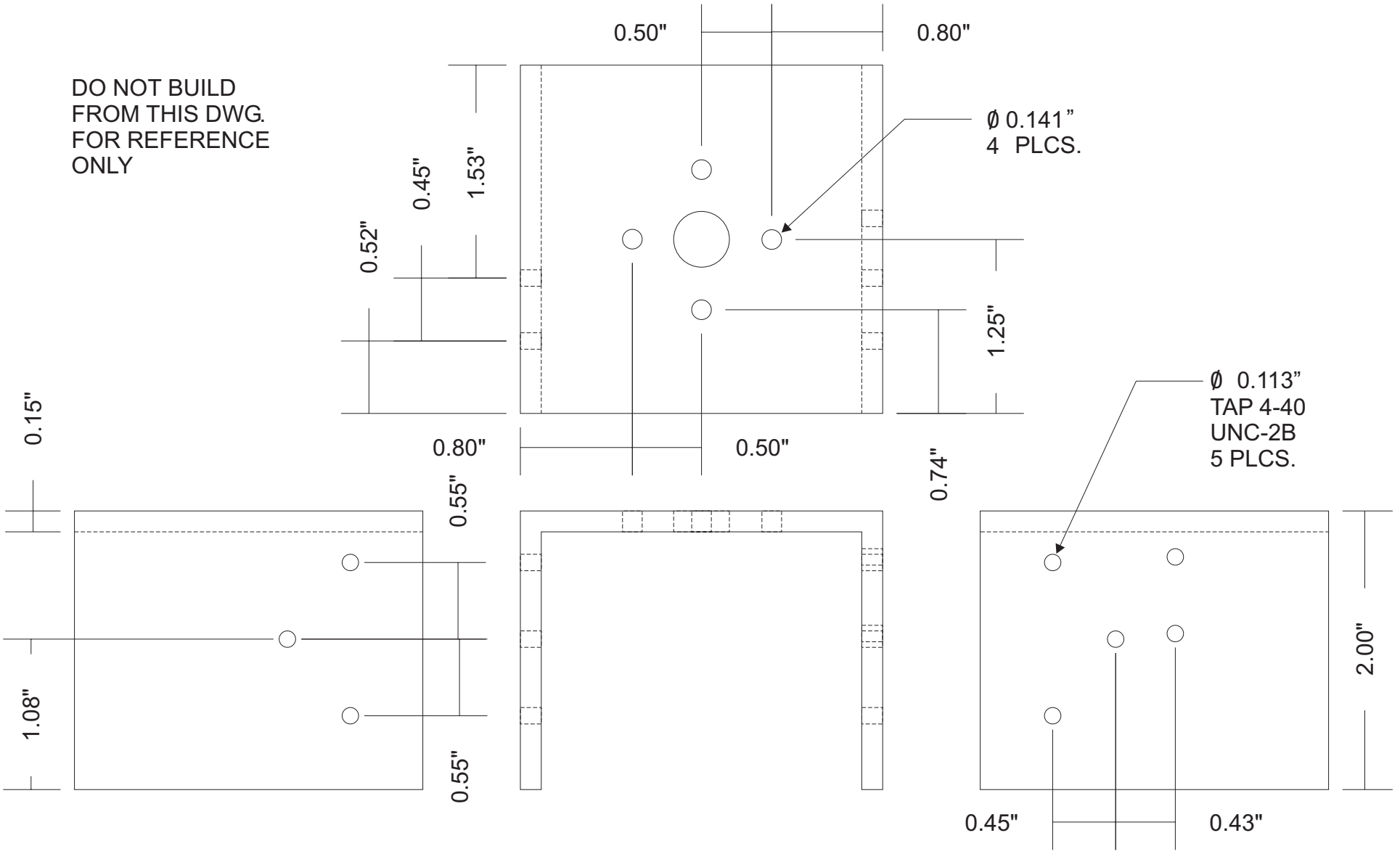

HELICOPTER IDENTIFICATION PROJECT CONTROL GROUP UNIVERSITY OF TORONTO	TITLE: ELECTRIC MOTOR MOUNT	NO:
	DATE: JANUARY 12, 2003	BY: C.L.

Appendix C

Notes on Improvements

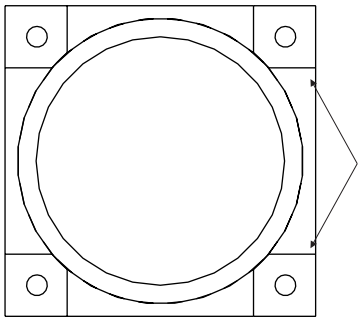

LOCKING FEATURE
ON END TBD.
4 PLCS.

BEARING SEAT

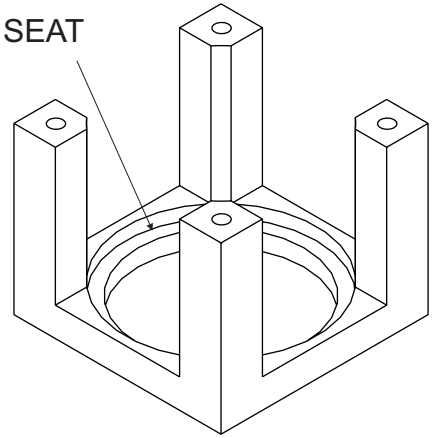

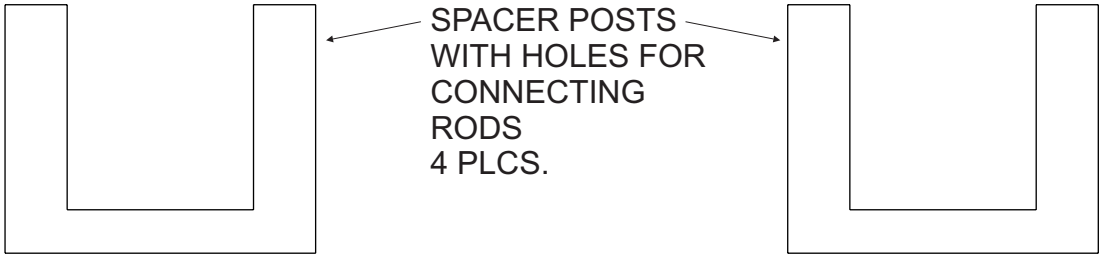

SPACER POSTS
WITH HOLES FOR
CONNECTING
RODS
4 PLCS.

Alternate Bearing Housing

The bearing housing does not need to be sealed, which can lead to substantial weight savings.

This would be machined from a solid block.

Sized to work with same bearings, shaft, and support brakets (YAW-05) as existing design

Matching upper and lower housings as in existing design.

MATERIAL 7075-T6
ALUMINUM

HELICOPTER IDENTIFICATION PROJECT CONTROL GROUP UNIVERSITY OF TORONTO	TITLE: BEARING HOUSINGS		NO:
	DATE: JANUARY 12, 2003	BY: C.L.	

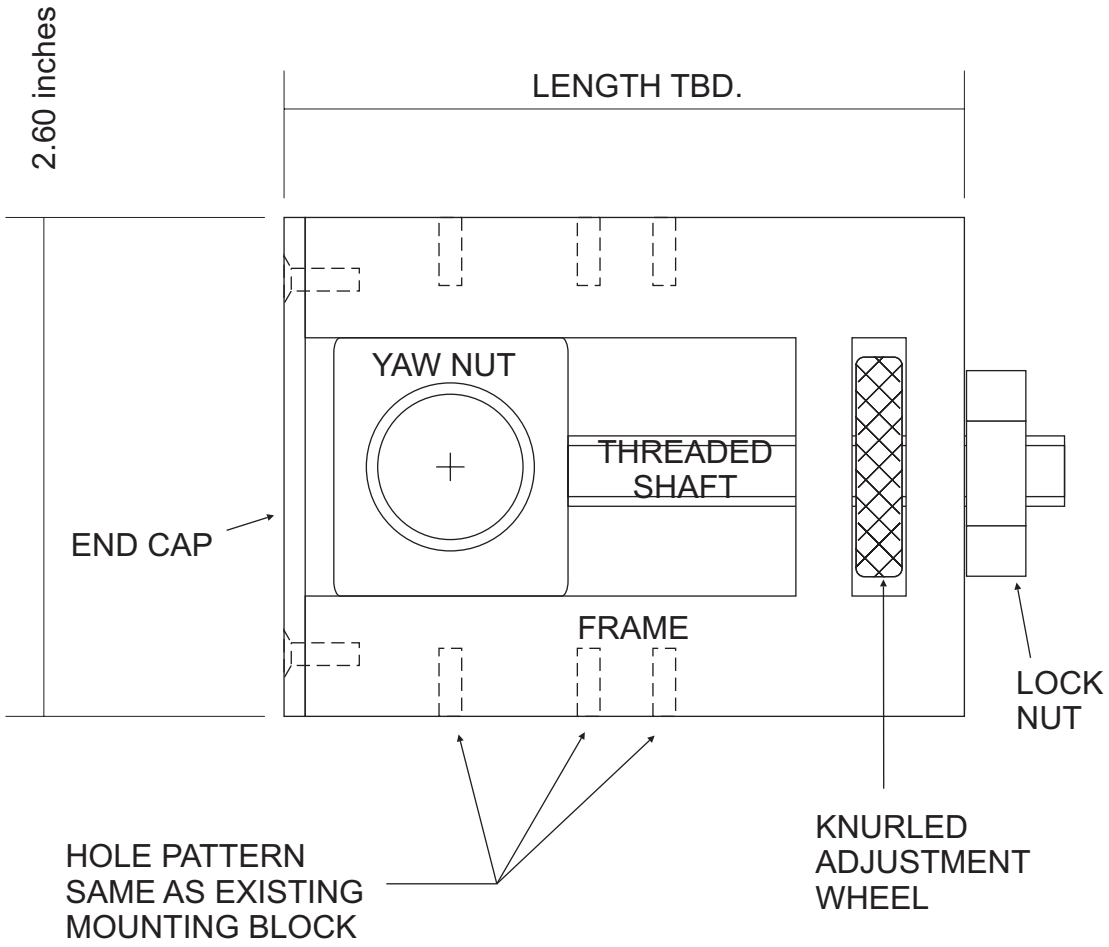

The YAW NUT accepts the yaw shaft from the test stand.

The yaw nut can slide back and forth along rails (not drawn) in the FRAME.

The THREADED SHAFT is fixed to the yaw nut.

The KNURLED WHEEL is turned to adjust the yaw nut's position in the frame.

The LOCK NUT is tightened when adjustments are finished to lock the yaw nut in place.

The END CAP prevents the yaw nut from falling out of the frame.

MATERIAL 7075-T6
ALUMINUM

HELICOPTER IDENTIFICATION PROJECT CONTROL GROUP UNIVERSITY OF TORONTO	HELICOPTER MOUNT WITH ADJUSTMENT	NO:
	DATE: JANUARY 10, 2003	BY: C.L.

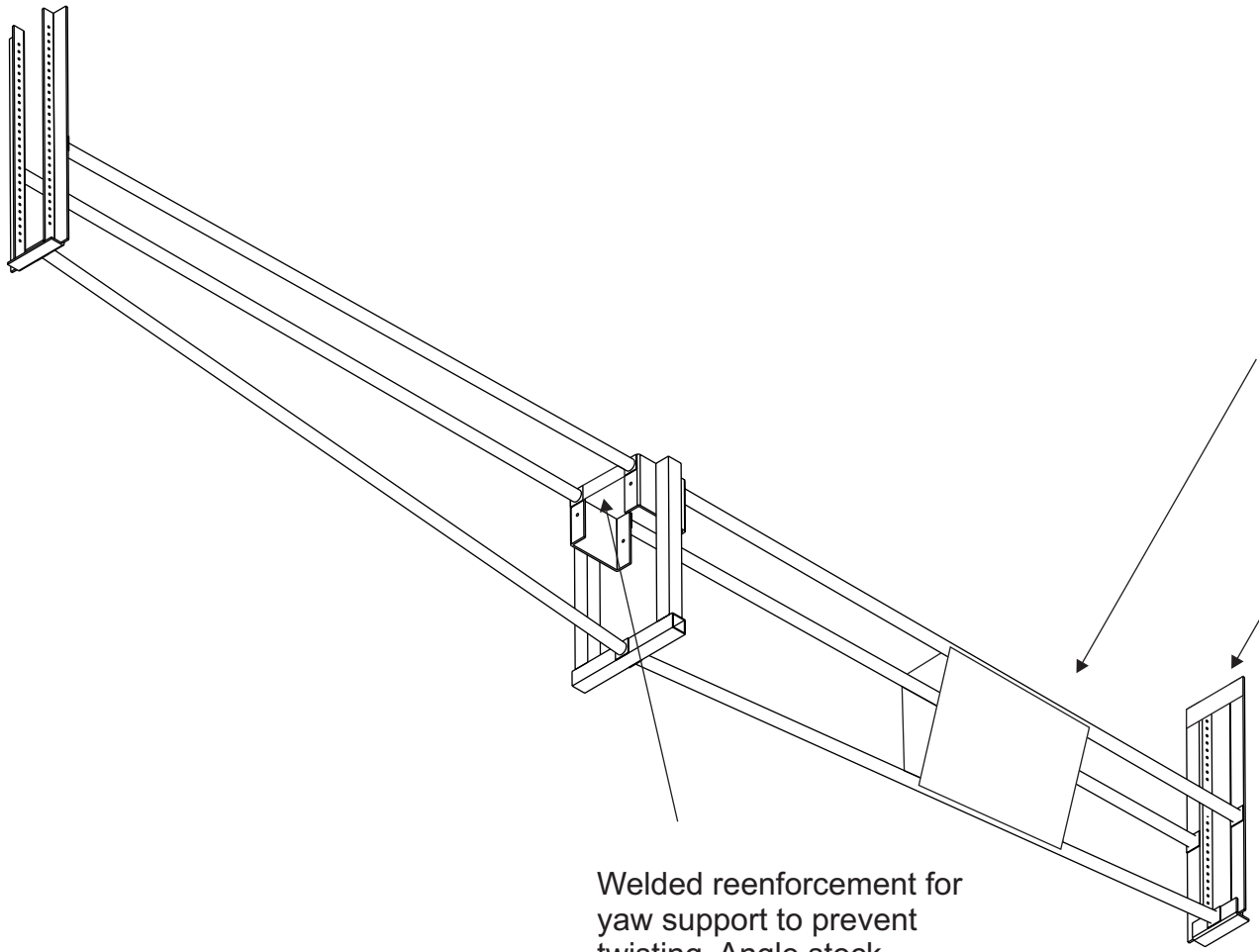

Weld sheet metal to horizontal members to increase stiffness.

Avoid area under rotor downwash.

Thickness should be under 0.04” to minimize weight.

Welded reenforcement for end brackets to prevent twisting. Angle stock.

Welded reenforcement for yaw support to prevent twisting. Angle stock.

HELICOPTER IDENTIFICATION PROJECT CONTROL GROUP UNIVERSITY OF TORONTO	TITLE: PITCH FRAME STIFFENING		NO:
	DATE: JANUARY 12, 2003	BY: C.L.	

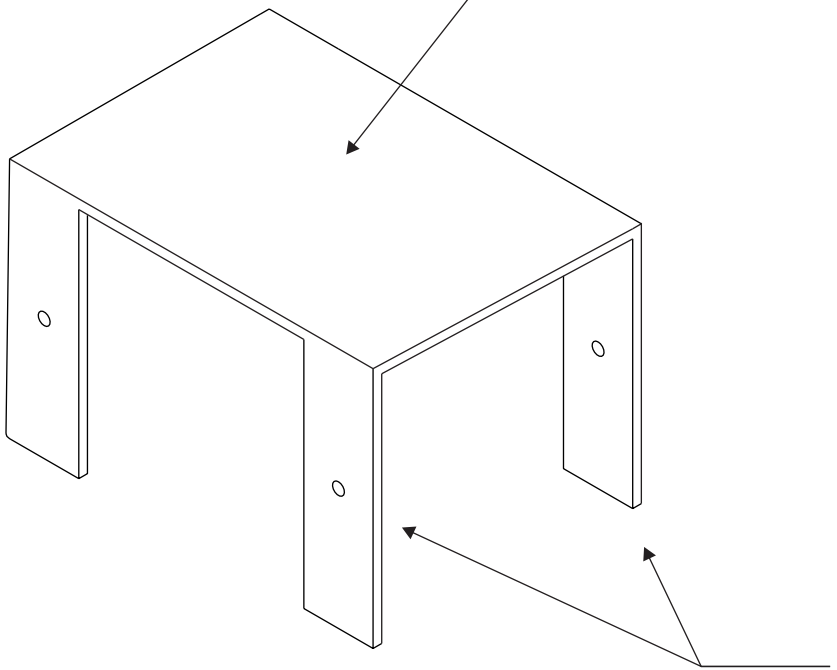

MATERIAL:
FOLDED SHEET METAL
ALUMINUM 0.100”

HELICOPTER IDENTIFICATION PROJECT CONTROL GROUP UNIVERSITY OF TORONTO	TITLE: YAW BEARING ELIMENATOR		NO:
	DATE: JANUARY 12, 2003	BY: C.L.	

DO NOT BUILD
FROM THIS DWG.
FOR REFERENCE
ONLY

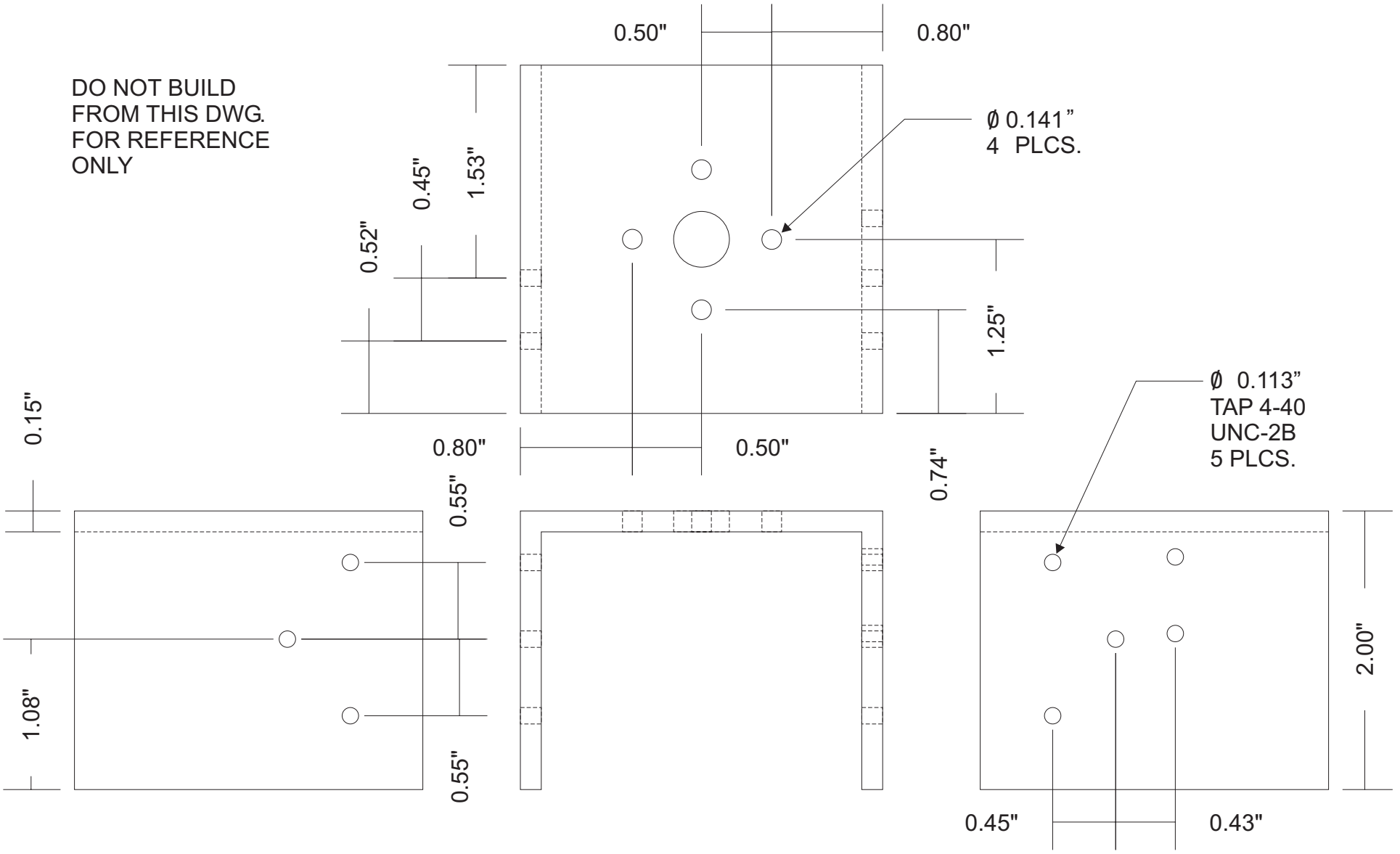

HELICOPTER IDENTIFICATION PROJECT CONTROL GROUP UNIVERSITY OF TORONTO	TITLE: ELECTRIC MOTOR MOUNT	NO:
	DATE: JANUARY 12, 2003	BY: C.L.

Appendix D

Schematics

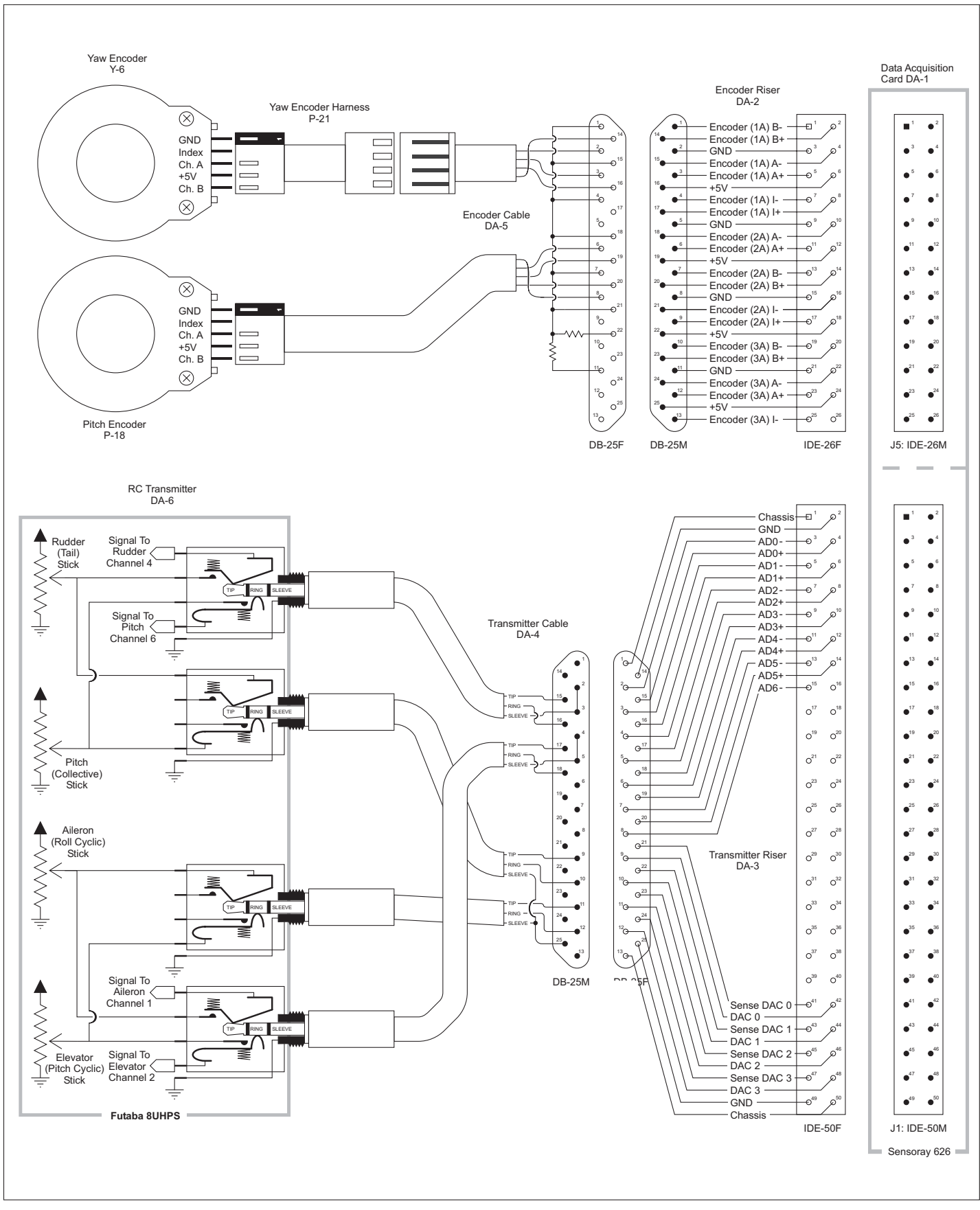
Yaw Encoder
Y-6
Yaw Encoder Harness
P-21
GND
Index
Ch. A
+5V
Ch. B
Encoder Cable
DA-5
Pitch Encoder
P-18
DB-25F
Encoder Riser
DA-2
Encoder (1A) B-
Encoder (1A) B+
GND
Encoder (1A) A-
Encoder (1A) A+
+5V
Encoder (1A) I-
Encoder (1A) I+
GND
Encoder (2A) A-
Encoder (2A) A+
+5V
Encoder (2A) B-
Encoder (2A) B+
GND
Encoder (2A) I-
Encoder (2A) I+
+5V
Encoder (3A) B-
Encoder (3A) B+
GND
Encoder (3A) A-
Encoder (3A) A+
+5V
Encoder (3A) I-
DB-25M
IDE-26F
Data Acquisition
Card DA-1
J5: IDE-26M
RC Transmitter
DA-6
Rudder
(Tail)
Stick
Signal To
Rudder
Channel 4
Signal To
Pitch
Channel 6
Pitch
(Collective)
Stick
Aileron
(Roll Cyclic)
Stick
Signal To
Aileron
Channel 1
Elevator
(Pitch Cyclic)
Stick
Signal To
Elevator
Channel 2
TIP
RING
SLEEVE
Futaba 8UHPS
Transmitter Cable
DA-4
DB-25M
Transmitter Riser
DA-3
Chassis
GND
AD0-
AD0+
AD1-
AD1+
AD2-
AD2+
AD3-
AD3+
AD4-
AD4+
AD5-
AD5+
AD6-
Sense DAC 0
DAC 0
Sense DAC 1
DAC 1
Sense DAC 2
DAC 2
Sense DAC 3
DAC 3
GND
Chassis
IDE-50F
J1: IDE-50M
Sensoray 626

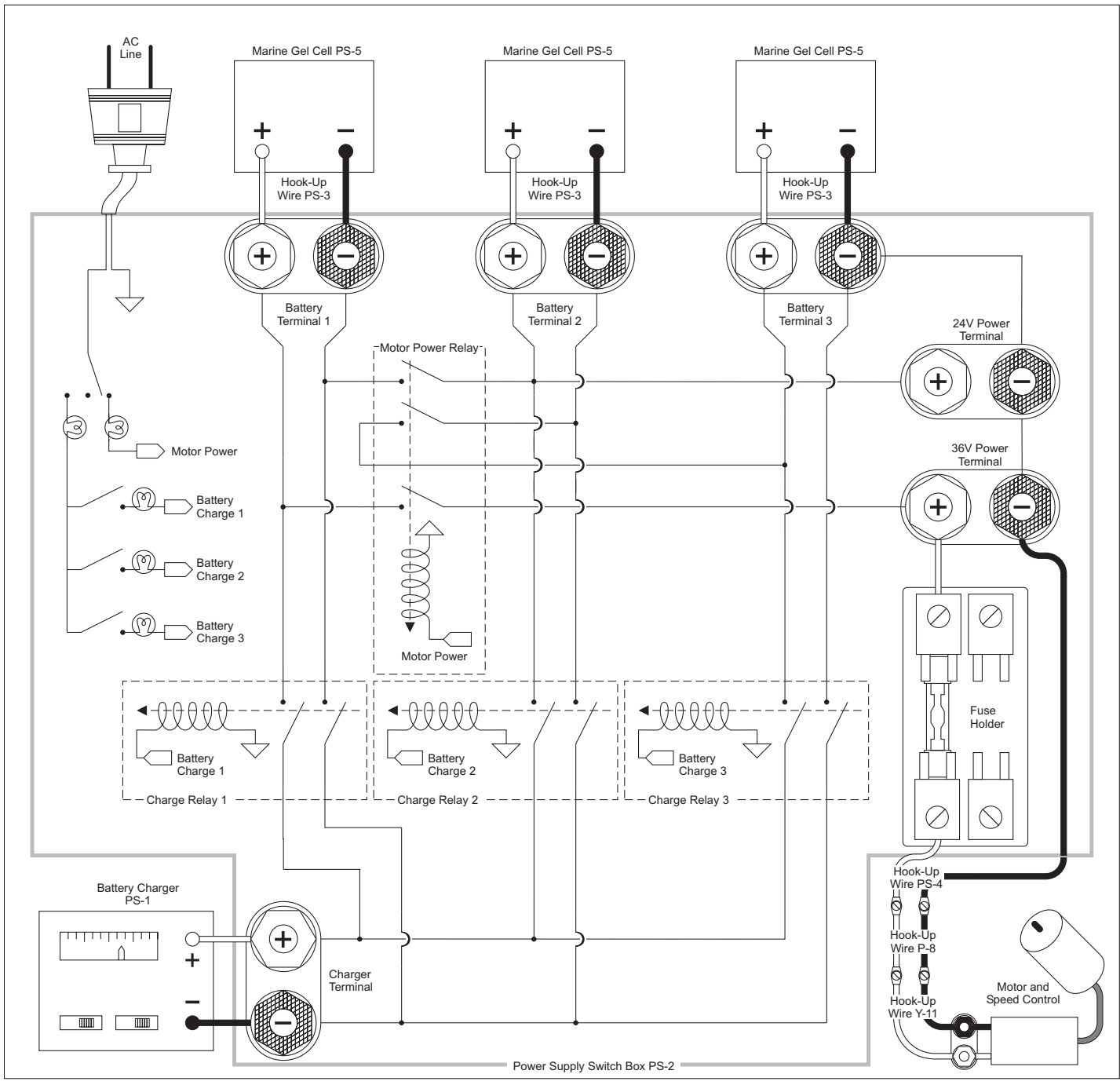
AC Line
Marine Gel Cell PS-5
Marine Gel Cell PS-5
Marine Gel Cell PS-5
Hook-Up Wire PS-3
Hook-Up Wire PS-3
Hook-Up Wire PS-3
Battery Terminal 1
Battery Terminal 2
Battery Terminal 3
24V Power Terminal
36V Power Terminal
Motor Power Relay
Motor Power
Battery Charge 1
Battery Charge 2
Battery Charge 3
Motor Power
Battery Charge 1
Battery Charge 2
Battery Charge 3
Charge Relay 1
Charge Relay 2
Charge Relay 3
Fuse Holder
Battery Charger PS-1
Charger Terminal
Hook-Up Wire PS-4
Hook-Up Wire P-8
Hook-Up Wire Y-11
Motor and Speed Control
Power Supply Switch Box PS-2

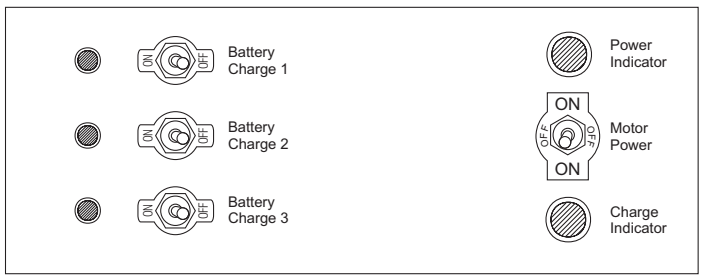
Battery Charge 1
Battery Charge 2
Battery Charge 3
Power Indicator
Motor Power
Charge Indicator
ON
OFF

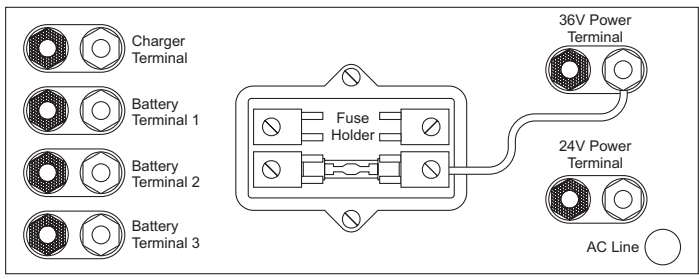
Charger Terminal
Battery Terminal 1
Battery Terminal 2
Battery Terminal 3
Fuse Holder
36V Power Terminal
24V Power Terminal
AC Line

References

[1] S. A. Bortoff, "The University of Toronto RC helicopter: a test bed for nonlinear control," in Proc. IEEE International Conference on Control Applications, 1999, vol. 1, pp. 333-338.

[2] S. K. Kim and D. M. Tilbury, "Mathematical modeling and experimental identification of a model helicopter," Paper AAIA-98-4357, presented at the AIAA Modeling and Simulation Technologies Conference and Exhibit, Boston, MA, 1998.

[3] J. C. Morris, M. van Nieuwstadt and P. Bendotti, “Identification and control of a model helicopter in hover,” in Proc. American Control Conference Control, 1994, pp. 1238-1242.

[4] M. Sugeno, I. Hirano, S. Nakamura, "Development of an intelligent unmanned helicopter," in Proc. IEEE International Conference on Fuzzy Systems, 1995, vol. 5, pp. 33-34.

[5] A. R. Conway, “Autonomous control of an unstable model helicopter using carrier phase GPS only,” Ph.D thesis, Dept. of Electrical Engineering, Standford University, Standford, CA, USA, 1995.

[6] H. Shim, T. J. Koo, F. Hoffmann and S. Sastry, "A comprehensive study of control design for an autonomous helicopter," in Proc. IEEE Conference on Decision and Control, 1998, pp. 3653-3658.

[7] M. F. Weilenmann and H. P. Geering, "Test Bench for Rotorcraft Hover Control," Journal of Guidance, Control, and Dynamics, vol. 17, pp. 729-736, Jul.-Aug. 1994.

[8] S. Sastri, “Robust rotation estimation from three orthogonally-oriented cameras,” M.A.Sc. thesis, Dept. of Electrical and Computer Engineering, University of Toronto, Toronto, ON, Canada, 2003.

[9] W. Johnson, Helicopter Theory, Mineola, NY: Dover, 1994.

[10] R. W. Prouty, Helicopter Performance, Stability and Control, Boston, MA: PWS Engineering, 1986.

[11] TSK, TSK Original R/C Helicopter - My Star 60 - Instruction Manual, 4th ed., Japan: TSK, Jul. 1996.

[12] R. Hostetler, Ray's Complete Helicopter Manual, 3rd ed., Sierra Madre, CA: R/C Modeler Corp., 1991.

[13] The SKF Group, "Bearing arrangement," [Online], Available: http://iec.skf.com/skf_en/1/1_0/1_0_71.htm

[14] US Digital Corp., US Digital E3 Series Optical Kit Encoder - Datasheet, Technical Data Rev. 12.04.01, Vancouver, WA: US Digital Corp., Dec. 2001.

[15] L. Ljung, System Identification: Theory for the User, 2nd ed., Upper Saddle River, N.J.: Prentice Hall, 1999.

[16] W. Z. Stepniewski and C. N. Keys, Rotary-Wing Aerodynamics, Mineola, NY: Dover, 1984.

[17] S. K. Kim and D. M. Tilbury. (2000, Aug 31). Mathematical modeling and experimental identification of a model helicopter. [Online] Available: http://www-personal.engin.umich.edu/~tilbury/papers/kt00jgcd.pdf

[18] E. Hallberg, I. Kaminer and A. Pascoal, "Development of a flight test system for unmanned air vehicles," IEEE Control Systems Magazine, vol. 19, no. 1, pp. 55-65, Feb. 1999.

[19] M. Sugeno, I. Hirano, S. Nakamura and S. Kotsu, "Development of an intelligent unmanned helicopter," in Proc. IEEE International Conference on Fuzzy Systems, 1995, vol. 5, pp. 20-24.

[20] E. N. Johnson, P. A. DeBitetto, C. A. Trott and M. C. Bosse, "The 1996 MIT/Boston University/Draper Laboratory autonomous helicopter system," presented at the 15th AIAA/IEEE Digital Avionics Systems Conference, Atlanta, GA, USA, 1996.

[21] A. H. Fagg, M. A. Lewis, J. F. Montgomery and G. A. Bekey, "The USC autonomous flying vehicle: an experiment in real-time behaviour-based control," in Proc. IEEE/RSJ International Conference on Intelligent Robots and Systems, 1993, vol. 2, pp. 1173-1180.

[22] J. C. Morris and M. van Nieuwstadt, "Experimental platform for real-time control," in Proc. ASEE Annual Conference, 1994, pp. 885-888.

[23] M. van Nieuwstadt and J. C. Morris, "Control of rotorspeed for a model helicopter: a design cycle," presented at the 14th American Control Conference, Seattle, Washington, USA, 1995.

[24] A. K. Mallik, A. Ghosh and G. Dittrich, Kinematic Analysis and Synthesis of Mechanisms, Boca Raton, FL: CRC Press, 1994.

[25] J. J. Craig, Introduction to Robotics: Mechanics and Control, 2nd ed., Reading, MA: Addison-Wesley, 1989.

[26] K. Kozlowski, Modelling and Identification in Robotics, New York: Springer, 1998.

[27] H. Baruh, Analytical Dynamics, Boston, MA: WCB/McGraw-Hill, 1999.

[28] J. S. Török, Analytical Mechanics: with an Introduction to Dynamical Systems, New York: Wiley, 2000.

[29] D. H. Shim, E. H. Lee, H. Park, and K. I. Lee, "Design of hovering attitude controller for a model helicopter", in Proc. Society of Instrument and Control Engineers, Kanazawa, Japan, 1993.

[30] T. J. Koo, D. H. Shim, O. Shakernia, B. Sinopoli, Y. Ma, F. Hoffmann and S. Sastry, "Hierarchical Hybrid System Design on Berkeley UAV", presented at the International Aerial Robotics Competition, Richland, Washington, USA, 1998.

[31] L. Ljung, System Identification Toolbox – for Use with MATLAB – User's Guide, Natick, MA: The MathWorks Inc., 1987.

[32] W. von Grünhagen, G. Bouwer, H. J. Pausder, F. Henschel and J. Kaletka, "A high bandwidth control system for a helicopter in-flight simulator", Int. J. Control, vol. 59, no. 1, pp. 239-261, 1994.

[33] G. L. Hataway, "Development of a ground control system for autonomous flight of a radio controlled scale helicopter," M.Sc. thesis, Dept. of Aerospace Engineering, Mississippi State University, Mississippi State, MS, USA, 1996.

[34] R. Emami, "Robot Kinematics and Dynamics," MIE 1062F Course Notes, Dept. of Electrical and Computer Engineering, University of Toronto, Toronto, ON, Canada, 1999.

[35] Sensoray Co. Inc., Sensory Model 626 - PCI Multifunction I/O Board - Instruction Manual, Revision B, Tigard, OR: Sensoray Co. Inc., May 11, 1999.

[36] Featherlite Industries Ltd., Jaws Ladder™ Telescopic Climbing System - Operation & Safety Manual/Guide, Aurora, ON: Featherlite Industries Ltd., n.d.

[37] Futaba, Futaba 8Usuper Series Digital Proportional R/C System 8UHPS/8UHFS - Instruction Manual, Futaba, n.d.

[38] Futaba, Futaba GV-1 Governor for Model Helicopter - Instruction Manual, Futaba, Mar. 1999.